universität wien

# DIPLOMARBEIT / DIPLOMA THESIS

Titel der Diplomarbeit / Title of the Diploma Thesis

"Optimization of breast cancer cell spheroids for co-culture with archaea"

verfasst von / submitted by

Lara Lang

angestrebter akademischer Grad / in partial fulfilment of the requirements for the degree of

Magistra der Pharmazie (Mag. pharm.)

Wien, 2021 / Vienna, 2021

| | |
|---|---|
| Studienkennzahl lt. Studienblatt / degree programme code as it appears on the student record sheet: | UA 449 |
| Studienrichtung lt. Studienblatt / degree programme as it appears on the student record sheet: | Diplomstudium Pharmazie |
| Betreut von / Supervisor: | Univ. Prof. Dipl. Ing. Dr. Manfred Ogris |
| Mitbetreut von / Co-Supervisor: | Dr. Haider Sami |

# *ACKNOWLEDGMENT/DANKSAGUNG*

*Ich möchte mich bei Prof. Manfred Ogris für die spontane Einladung zu diesem spannenden und durchaus außergewöhnlichen Projekt, durch das ich unglaublich viel lernen durfte und das mir auch sehr viel Spaß gemacht hat, bedanken. Durch Ihre entspannte und humorvolle Art schaffen Sie eine warme, familiäre Atmosphäre für Ihre MMCT-Familie!*

*Ein großes Dankeschön möchte ich an Dr. Haider Sami richten, der mich während meiner Zeit im MMCT und auch während des Schreibens dieser Diplomarbeit mit viel Geduld und mit großem Vertrauen unterstützt hat. Durch dich habe ich gelernt, wie wichtig genaues Arbeiten ist und auch Verantwortung für meine Schritte zu übernehmen. Danke für dein offenes Ohr für meine vielen Fragen!*

*Auch bei Thi Ngoc Le möchte ich mich für die lustige Zusammenarbeit im MMCT und die große Unterstützung im Studium bedanken. Ich freue mich, dass wir am gleichen Projekt gearbeitet und uns dadurch kennengelernt haben!*

*Meinen lieben Eltern - Heinz & Silke - möchte ich besonders großen Dank aussprechen. Danke für eure unendliche Liebe und (finanzielle) Hilfe während des gesamten Studiums und für eure Offenheit und euren Wohlwollen bezüglich meiner immer wieder etwas ungewöhnlichen Lebenspläne. Danke auch an meine vier lieben Geschwister - Florian, Julia, Leonie, Valerie - und deren Familien, die mir immer den Rücken gestärkt haben!*

*Nicht zuletzt möchte ich mich auch bei meinen lieben FreundInnen - Valentina, Hannah, Emily, Tanja, Lisa, Elisa, Stella, Sarah, Verena, Michelle und Filip - bedanken. Danke für die gute Zeit mit jedem/r von euch, die wir abseits vom Studium miteinander verbracht haben. Ohne euch hätte ich es wohl nicht geschafft, immer wieder die Energie aufzuwenden und mich den Lern-Marathons hinzugeben!*

# Table of Contents

# 1 Abstract – English

Conventional anticancer therapies, such as antineoplastic chemotherapy, surgical resection or radiotherapy, are frequently followed by relapse and the occurrence of resistance in cancer patients. The introduction of exogenous therapeutic genetic material into target cells represents a novel approach to tackle cancer more specifically. To enable transfer to desired sites and to provide protection against enzymatic degradation, efficient vector mediated transportation is required. Several investigations on anaerobic bacteria as tumor-targeting gene delivery vectors have been conducted *in vitro* as well as through animal experimentations in the past.

In the course of this thesis, three-dimensional multicellular tumor spheroids (MCTS) were generated from 4T1 cells (murine mammary cancer cell line) and optimized in order to display relevant main features of natural tumors. For the formation of reproducible MCTS, several operating procedures including cell seeding in specialized well plates, harvesting, cryostat sectioning, and fixation were established and improved. Spheroids of different seeded cell numbers (20,000 | 10,000 | 5,000 | 1,000 | 500 | 200 cells) were compared with regard to various parameters, such as mechanical stability, reproducibility, consistent morphological shape, steady growth, and development of a necrotic core. Said properties were assessed through the harvesting of MCTS at different times and the subsequent preparation of thin sections. MCTS initially comprising of 5,000 or 10,000 cells were considered the models with the most favorable features and were hence selected for final experiments.

Furthermore, MCTS were investigated for their suitability as *in vitro* tumor model systems for co-culture studies with the anaerobic methanogenic archaea strain *Methanococcus maripaludis* S0001. As part of the experiment, optimized MCTS (5k and 10k) were incubated with different concentrations of archaea per spheroid ($3.6x10^7$ or $3.2x10^5$) for various periods of time (24 h, 48 h, 96 h, 120 h, 168 h) during which archaea's colonization patterns were observed. To visualize the microorganisms among cancer cells, different dyes (HOECHST, DAPI, Alexa Fluor 488) were tested for their applicability to label the used archaea strain. During co-culture experiments, the ability of *M. maripaludis* to infiltrate inner spheroid zones (hypoxic/necrotic regions) was assessed.

The results obtained from fluorescence microscopy suggest that, within a distinct setup, MCTS could represent appropriate models for the investigation of archaeal infiltration of hypoxic regions of tissues *in vitro*. Moreover, the collected data indicates that *M. maripaludis* S0001 is capable of spontaneously proceeding towards inner layers of MCTS over time, suggesting that hypoxia/anoxia within spheroids might have a “pulling effect” on the microorganism.

# 2 Zusammenfassung – Deutsch

Nach konventionellen Krebstherapien, wie beispielsweise der antineoplastischen Chemotherapie, der chirurgischen Tumorresektion oder der Radiotherapie, treten oft Rezidive oder Resistenzen bei Krebspatienten auf. Ein innovativer Therapieansatz, um den Krebs spezifischer zu bekämpfen, bedient sich der Einschleusung von therapeutisch wirksamem Genmaterial in Krebszellen. Um den Transfer der hochpolaren Substanzen zum Zielort zu ermöglichen und Schutz vor enzymatischem Abbau zu bieten, ist ein effizienter Vektor-vermittelter Transport erforderlich. In einigen präklinischen Studien, *in vitro* aber auch anhand von Tierversuchen, wurde bereits die Fähigkeit von anaeroben Bakterien, spezifisch Tumore zu besiedeln, untersucht.

Im Rahmen dieser Diplomarbeit wurde die Kultur dreidimensionaler Tumorsphäroide (MCTS) aus 4T1-Zellen (murine Brustkrebszelllinie) für die Darstellung einiger wichtiger Hauptmerkmale solider Tumore optimiert. Um reproduzierbare MCTS erstellen zu können, wurden mehrere Arbeitsverfahren etabliert und verbessert. Diese umfassten das Aussäen der Zellen in Spezial-Mikrotiterplatten, die Ernte der Sphäroide, das Anfertigen von Cryostat-Dünnschnitten und die Fixierung der Sphäroide. MCTS, die aus unterschiedlichen Zellzahlen (20,000 | 10,000 | 5,000 | 1,000 | 500 | 200 Zellen) generiert worden waren, wurden hinsichtlich ihrer mechanischen Festigkeit, ihrer Reproduzierbarkeit, ihrer Morphologie, ihres Wachstums und der etwaigen Entwicklung eines nekrotischen Kerns untersucht. Dafür wurden die Sphäroide zu verschiedenen Zeiten geerntet und genannte Parameter anhand von Dünnschnitten beurteilt. Jene Sphäroide, die aus 5.000 oder 10.000 Zellen kultiviert worden waren, wiesen die günstigsten Eigenschaften auf und wurden daher für finale Experimente ausgewählt.

Darüber hinaus sollte untersucht werden, ob die generierten Sphäroide geeignete *in vitro* Tumormodelle für Co-Kultur-Experimente mit der anaeroben, methanogenen Archchaeen-Spezies *Methanococcus maripaludis* S0001 darstellten. Hierfür wurden die optimierten MCTS (5k und 10k) zunächst mit verschiedenen Archaeen-Konzentrationen ($3.6x10^7$ oder $3.2x10^5$) unterschiedlich lange (24 h, 48 h, 96 h, 120 h, 168 h) inkubiert und währenddessen das Kolonisierungsmuster der Archaeen beobachtet. Um die Mikroorganismen im Tumorsphäroid mikroskopisch identifizieren

zu können, wurden verschiedene Farbstoffe (HOECHST, DAPI, Alexa Fluor 488) für die Färbung der verwendeten Archaeen-Spezies getestet. Im Zuge der Co-Kultur-Experimente wurden *M. maripaludis* auf ihre Fähigkeit, innere Schichten (hypoxische/nekrotische Bereiche) der Sphäroide zu infiltrieren, untersucht.

Die Ergebnisse der Fluoreszenz-Mikroskopie deuten darauf hin, dass ausgewählte Sphäroide durchaus geeignete *in vitro* Modelle für die Erforschung der Eigenschaft von Archaeen, sich in Richtung hypoxischer Umgebung zu bewegen, darstellen könnten. Außerdem konnte gezeigt werden, dass *M. maripaludis* S0001 in der Lage ist, sich in Abhängigkeit von der Zeit spontan in Richtung innerer Schichten der Sphäroide zu bewegen. Dies lässt vermuten, dass Hypoxie/Anoxie innerhalb der MCTS einen Effekt auf die Migrationsrichtung dieser Mikroorganismen haben könnte.

# 3 Introduction

## 3.1 Cancer

Cancer represents an increasing threat to human life throughout all regions of the world and hence, a great focus lies on the development of new therapeutic approaches towards this disease. [1,2] Due to the current treatment methods, such as surgical resection, radiotherapy and antineoplastic chemotherapy, the mortality rate for cancer has remained stable or declined slightly in high-income countries over the past decade. On the contrary, the incidence rates for many types of cancer were observed to be relatively high in the recent years. [3,4] Moreover, targeted therapy, such as monoclonal antibody therapy (immunotherapy) and hormonal therapy are being applied for certain cancers. [4]

However, there is a frequent lack of response to the aforementioned anticancer therapies in numerous cancer patients. Besides that, patients are suffering relapse quite commonly, even after initially responding to the treatment. [4,5] Due to unspecific effects of traditional anticancer treatments, healthy tissue is often equally damaged as pathogenic tissue. Unsurprisingly, conventionally treated cancer patients suffer several major side effects. [6]

The deficiencies of conventional cancer treatments are due to (multidrug-) resistance to chemo- and radiotherapy, metastasis, heterogeneity, recurrence, and others and might as well be associated with the unsuccessful eradication of cancer stem cells. Research on innovative strategies to fight cancer is hence, among others, targeted on the extermination of cancer stem cells to a great extent. [4,5,7]

In response to the outlined downsides of conventional strategies to treat cancer, extensive research efforts are currently devoted to the field of gene therapy. In the context of this novel approach, nucleic acids are introduced into cells utilizing viral or non-viral vectors as vehicles. A prospective direction of cancer therapy could consist of a combination of conventional therapy and novel approaches, and thereby result in a more effective tumor elimination. [8,9] Before being approved for admission in persons/patients in clinical trials, all new drug candidates must undergo preclinical

testing in *in vitro* cell culture and subsequently in preclinical *in vivo* experiments (animal trials). [10,11]

## 3.2 Tumor models

The use of tumor model systems aims to reflect the complexity of human cancer disease and represents a critical stage in preclinical cancer research. Currently, various concepts to model native tumors are being applied (*Figure 1*): (i) two-dimensional (2D) cell cultures (discussed in detail hereafter); (ii) organ-on-a-chip technologies where cells are cultured on 3D multichannel microfluidic cell culture chips, aiming to obtain artificial organs; three-dimensional (3D) cell models, such as (iii) organoids (generated from tumor-derived tissue or stem cells) or (iv) spheroids (discussed in detail hereafter); and (v) animal experimentations where *in vivo* tumor development is induced by drugs, viruses or radiation. [12–14]

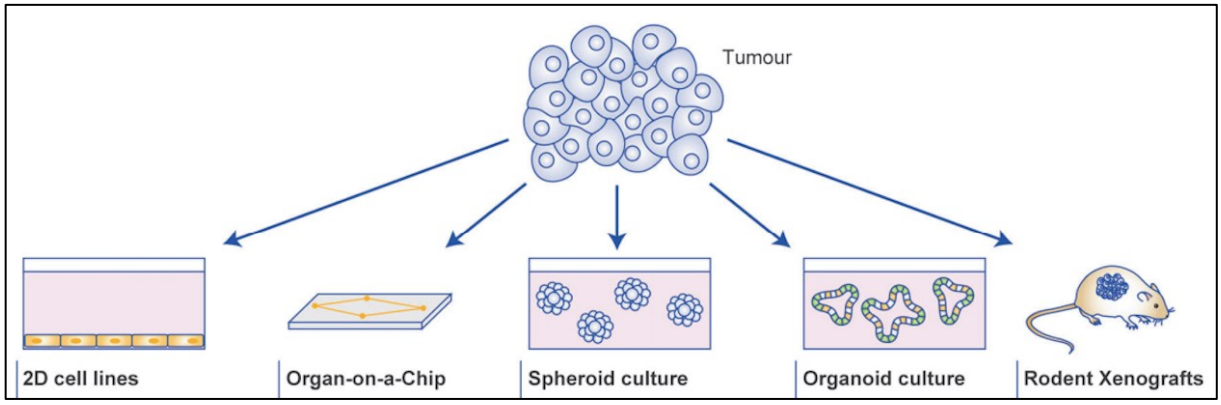


*Figure 1. Currently employed tumor model systems to study cancer. (Illustration from Porter et al. [13])*

Animal models (mainly rodents) are highly relevant for studying tumorigenesis as well as drug functionality. Encouragingly, preclinical outcomes derived from animal testing frequently do not correlate with the clinic due to unequal physiological characteristics of rodents when compared to humans. Thus, to further improve the translational success, human tissue or cells are being transplanted into humanized animals (xenografts). [12–14]

The outlined *in vitro* and *in vivo* approaches are of great value to study and understand cancer biology. However, novel *in vitro* methodologies in particular, such as spheroids

and organoids have the potential to substantially contribute to more dependable predictions from preclinical testing to the bedside. [12,13]

### 3.2.1 2D *in vitro* cell culture

Traditionally, research on potential therapeutic candidates to evaluate their efficacy and toxicity is performed utilizing 2D monolayer cell models. [11] The cell cultures are grown from primary or immortalized cell lines. [13] Given its cost-efficiency, convenience and reproducibility, those models remain the most employed methodologies for preclinical *in vitro* analyses. [10] Monolayer cell models are in use for the investigation of various parameters in the early stages of drug development, however the determined results can deviate considerably from those obtained in subsequently conducted animal trials or clinical findings. [11]

These inconsistencies are derived from insufficient representation of *in vivo* (native) tissues by flat two-dimensional cell models. [11,15,16] Breslin and O'Driscoll [13] reported in 2016 that cells in a monolayer culture, where cells grow attached to the polystyrene surface of the culture flask exhibit fundamentally different morphologies than cells in a three-dimensional organization. [17] With regard to oncology research, it is known that solid tumors naturally arrange in a three-dimensional manner and display a complex tumor microenvironment (TME), which has a major impact on the response to investigated therapeutics. [11,15] When cells are cultured in monolayers, important characteristics of native tumors, such as the inter- and intracellular communication and organization through cell closeness or the oxygen gradient cannot be taken into account (for further details please refer to chapter 3.2.2). [15,18]

In 1990, Teicher *et al.* [19] discovered that murine breast cancer cell sublines acquired resistance to alkylating drugs after repeatedly being treated with various alkylating cancer therapeutics *in vivo*. When these cells were cultivated in monolayer cell culture *in vitro* they lost their resistance to the alkylating agents. After reimplanting the same cells into mice, the resistance to the alkylating treatments was observed to be restored just as before the excision. [20] In 1993, Kobayashi *et al.* [21] demonstrated that three-dimensional tumor models (e.g. spheroids) could fully mirror drug resistance patterns of native tumors, and hence suggest to possess more predictive accuracy regarding drug responses *in vivo*. [20]

Essentially, due to the aforementioned deviations monolayer cell culture models do not represent satisfactory systems for the investigation of different cancer therapies. [11,16] To overcome those discrepancies between *in vitro* cancer research models and *in vivo* solid tumors it is of critical importance to further study and optimize three-dimensional cancer cell models. [17]

### 3.2.2 3D *in vitro* cell culture

Three-dimensional cell culture models have proven to be an attractive methodology for the early stage drug discovery, drug screening [22] and drug development. [10,23] In 1970, Sutherland *et al.* [24] initially introduced multicellular tumor spheroids (MCTS) for the utilization as tumor models. [14] Specific significance of these systems applies to the field of oncology research, where several parameters, such as anticancer drug efficacy [25], (multidrug-) resistance [14], metabolism [18], toxicity and safety [18] are being investigated. Given the capability to mimic the main features of human tumors *in vivo*, 3D tumor models represent a valuable research model for the prediction of *in vivo* treatment effects. [10,18] An increased use of three-dimensional cell culture systems could, hence, promote a reduction of laboratory animal testing due to a more dependable translation from *in vitro* investigations to clinical use in human tumors. [14] Given the discrepancies between traditional *in vitro* (2D cell cultures) and *in vivo* (animal testing) experimentation outcomes, the approval rate for new therapeutics is, and remains, low. Thus, the promotion of three-dimensional cell culture models could substantially enhance drug registration to the market. [25] The utilization of 3D methodologies can be considered as a bridging between 2D cell cultures and animal experimentation *in vivo*. [10,23]

**Microenvironment of solid tumors**

Solid tumors thrive within a diverse microenvironment, which displays a complex organization and cooperation of multiple types of cells, such as stromal cells (e.g. fibroblasts, adipocytes), cancer cells, immune cells, vascular and lymphatic endothelial cells and pericytes. [10,15,26] Part of the complex tumor architecture is the spontaneous development of an extracellular matrix (ECM, primarily consisting of proteoglycans and fibrous proteins [23]), which is found to embed the cells. Spatial cell-cell interactions as well as interactions between cells and the ECM are substantially responsible for the properties of solid tumors. Hence, the behavior of cells, such as signaling between

distinct cells, gene expression, growth process, drug response and resistance and cell function can diverge within tumors. [11,17,27]

Furthermore, native tumors possess particular characteristics due to a progressive decrease of vascularization from tumor border to tumor core. The declining presence of oxygen towards the core eventually results in hypoxic or even anoxic areas in the tumor center, which renders cells increasingly resistant to chemo- and radiotherapy. [28] Consequently, the diffusional supply with soluble factors [20], such as growth factors [29], cytokines [17], nutrients and metabolites [30] towards the inner zones of the tumor mass becomes more and more aggravated. [15] Accordingly, as the consumption of nutrients is facilitated in peripheral layers, cells located in this area are found to be proliferating. [15] The increasing hypoxia, decreasing nutrient supply as well as accumulating metabolic waste towards the core entail non-proliferating, quiescent or senescent [10], apoptotic, and eventually necrotic cells. [23,31] Noteworthy, the development of hypoxic and necrotic regions can also be observed in *in vitro* tumor spheroids with diameters above 400-500 µm. [31] Consequently, tumor cells residing in inner zones of the tumor generate their energy through anaerobic glucose degradation, which, through the conversion of pyruvate, leads to an accumulation of lactate (Warburg-effect) [27]. The increasing lactate concentration results in the acidification of the tumor core. [10] Eventually, the above delineated features of solid tumors contribute to enhanced resistance to anticancer drugs. This is due to various biochemical modifications within the TME which lead to attenuated or failed drug efficacy. Also, the spatial cell-cell and cell-ECM linkage was found to physically obstruct drug penetration into the tumor mass. [10,23]

**3D tumor models *in vitro***

To achieve a more realistic prediction of drug efficacy in *in vivo* experimentations, three-dimensional tumor models function to recapitulate the characteristic architecture of native tumors *in vitro*. [15] Different 3D in vitro cell culture technologies have been established to date, which can be subdivided into three major groups: (i) scaffold/hydrogel models based on porous matrices of various compositions (mimicking the ECM) which allow cell-ECM interactions from the onset (e.g. organ-on-a-chip); (ii) non-scaffold models which promote the assembly of cells under adherence-

free conditions; (iii) hybrid models which represent a combination of the two aforementioned methodologies (e.g. microparticles or microencapsulations). [14,32]

With regard to scaffold-free technologies three approaches of 3D model cultivation can be defined: (i) multicellular tumor spheroids (MCTS); (ii) organ-derived multicellular spheroids established through cultivation of fragmented tumor material; (iii) tissue spheres derived by fractional enzymatic/mechanical disintegration of tumor tissues. [32]

**Properties of multicellular tumor spheroids (MCTS)**

In this project particular focus was placed on the generation of scaffold-free multicellular tumor spheroids (MCTS). MCTS allow the reproduction of the main hallmarks of solid tumors (as described extensively previously), such as cellular heterogeneity, architecture of cell layers, cell-cell and cell-ECM interactions, deposition of extracellular matrix, expression of specific genes, growth kinetics and drug resistance. [17,32]

The composition of three-dimensional spheroids can vary, depending on the selected starting cells. MCTS assembled solely of cancer cells can be referred to as “homotypic”, whereas “heterotypic” describes MCTS incorporating a variety of cells, such as cancer cells, fibroblasts, immune cells or endothelial cells. [15,17] All involved cells communicate via cellular signaling pathways (e.g. cytokines, growth factors) just as it is observed in solid tumors (*Figure 2A*). [17]

The formation of altering cell zones starts to develop when spheroids reach diameters of 200-500 µm with concomitantly emerging chemical gradients, such as nutrient, oxygen and metabolic waste gradients. [30] The secondary generation of a necrotic core occurs in spheroids exceeding 500 µm in diameter (*Figure 2B*). [10,30,33]

Cells of 3D MCTS deposit extracellular matrix (e.g. collagen) over time during their growth process just like solid tumors, as discussed earlier. The consequent cell-cell and cell-ECM junctions create physical barriers for the permeation and distribution of anticancer agents into the tumor tissue (“limited mass transport”) (*Figure 2C*). Additionally, spheroid density is increased through close physical contacts between cells and ECM. [17,31,34]

Solid tumors show specific growth characteristics with an initial exponential increase of volume (avascular phase), followed by a plateau phase and a subsequent vascular growth period in which cancer cells obtain invasive and metastatic capacities. Similar to in vivo tumors, 3D MCTS demonstrate an early accelerated growth leading to a consecutive plateau phase (Figure 2*D*). [17]

The gene expression profile of 3D MCTS resembles that of in vivo tumors to a high degree. Several genes encoding molecules for cell-adhesion, chemokines and pro-angiogenic factors were evaluated and compared by Ghosh *et al.* [35]. The study group revealed that several genes that are associated with the development of melanoma were also upregulated in three-dimensional MCTS as opposed to two-dimensional cell cultures (*Figure 2E*). [17,35]

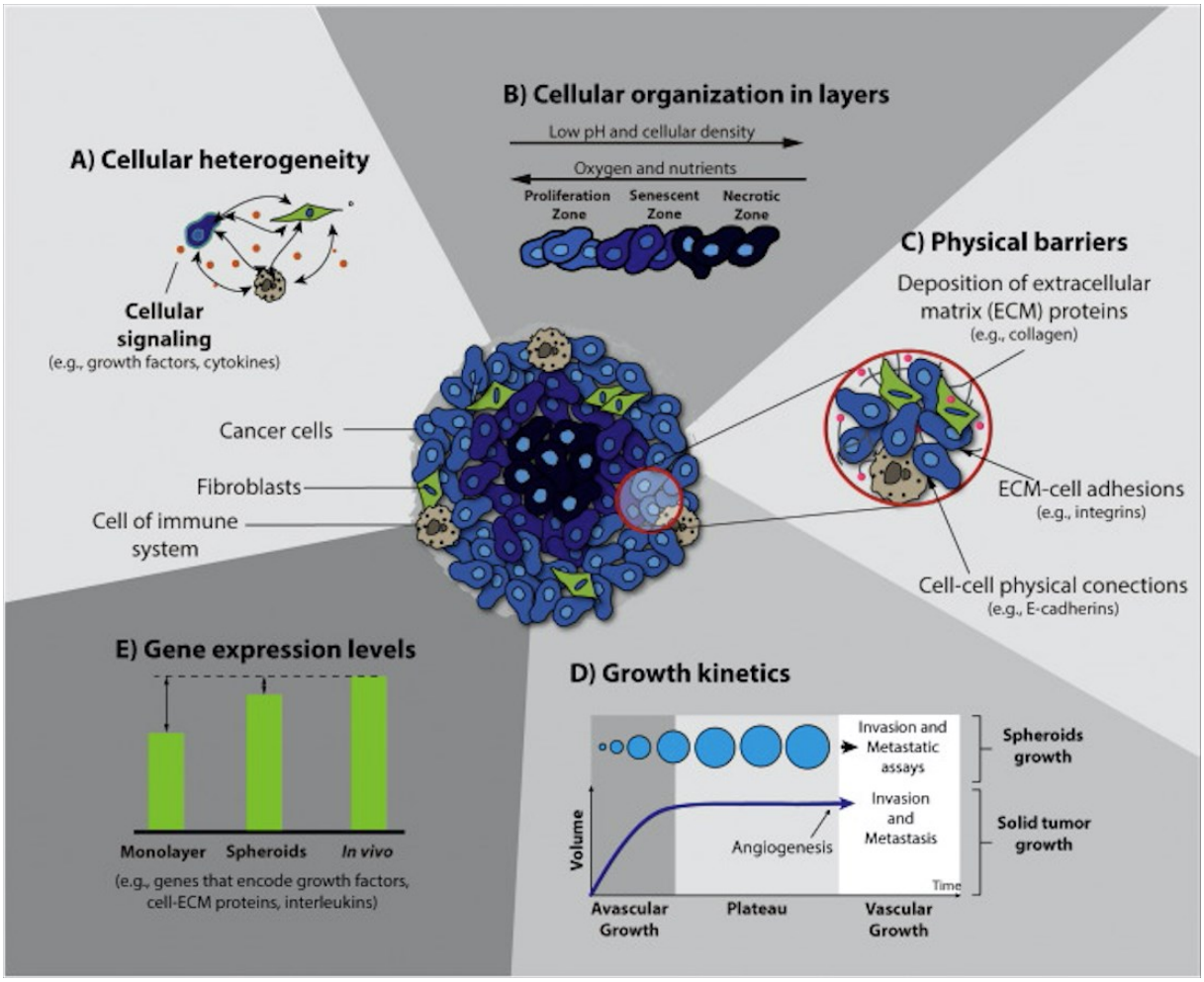


*Figure 2. Representational illustration of essential features of 3D spheroids utilized for the investigation of anticancer treatments. A) Heterogenic cellular constitution (cancer cells, stromal cells).* [10,17] *B) Arrangement of different cell stages in layers due to oxygen, nutrient and metabolic waste gradients.* [30] *The deteriorating supply with oxygen and soluble factors renders cells less and less viable towards the center. As a result, 3D spheroids encompass an outer layer of proliferative cells, an adjacent senescent/quiescent zone and eventually necrotic regions within the core which exhibits low pH and high cell density.* [10,17] *C) The manifestation of physical barriers is induced through cell-cell and cell-ECM interactions.* [17,31] *D) Comparison of growth kinetics of 3D spheroids with that of solid tumors. In either case an initial augmented gain of size followed by a plateau phase can be observed.* [17] *E) Correlation of gene expression levels of 2D, 3D cell cultures and native tumors in vivo.* [17] *(Figure from Costa et al.* [17]*)*

**Methodologies for MCTS formation**

The establishment of scaffold-free tumor models is based on cell-cell self-adhesion and -aggregation [32], resulting in the formation of 3D spheroids. [14] Fundamentally, spheroid formation strategies can be subdivided in two different approaches: (a) immobile, static cell culture conditions and (b) dynamic, agitation-based cell culture technologies. [32] The former methodology includes the (i) “liquid overlay technique”, the

(ii) “hanging drop technique” [10] and the (iii) “patterned surface technique”. [23] The latter incorporates (iv) “microgravity bioreactors” [32], (v) “spinner flasks” [14], (vi) “microfluidic devices” [23] and (vii) “gyratory shakers”. [10]

As for the “liquid overlay” [10] (also termed “forced-floating” [32]) method, spheroid formation is induced by seeding cells in multiwell plates coated with super-hydrophobic surfaces. The special well plates are obtained through agarose or poly-2-hydroxyethyl methacrylate (pHEMA) coating. [32] Essentially, spherical cell mass emerges through intercellular self-assembly [18] which is facilitated by the attachment-resistant plate coating but also through explicit well geometry (u-, v- or conical shaped wells). [14] The cells in suspension are prevented to adhere to the non-adhesive plate material and are thus promoted to attach to one another. By seeding defined numbers of cells, spheroid sizes can be precisely adjusted. [23] Subsequently, the forming MCTS start to deposit ECM, which contributes to an increase of density and a reduction of size, which progressively renders the spheroid’s structure closer to that of solid tumors. [32] The liquid overlay technology represents an applicable method for various high-throughput analyses due to its simple handling and the production of large amounts of spheroids. [23]

Another static-based technology for spheroid cultivation is referred to as the “hanging-drop technique”. [10] Just like the liquid overlay methodology this technique is based on the forced intercellular adhesion and aggregation instead of the cell’s attachment to the container wall. [32,36] For the formation of spherical clusters, cells are suspended in media and dispensed onto particularly shaped hanging drop well plates exhibiting apertures on the bottoms of the wells. Consequently, distinct droplets of cell suspension are being formed below the perforations. [14] Moreover, hanging drops can be generated on the bottom side of a petri dish lid. [36] Both approaches function due to surface tension which allows the droplets to remain in position. Through gravitational effects, cells within the droplets accumulate at the liquid-air boundary layer and rapidly aggregate to form spheroids. [23]

A more recent development is the formation of spheroids on flat micro- or nanopatterned substrates. [14] This technology resembles the liquid overlay technique to a certain extent but requires specific culture plates comprising much higher numbers

of wells. These wells are within the nano- or micrometer scale and are imprinted onto polyacrylamide or agarose gel. Spheroid formation is achieved by adding the suspended cells onto the plate and allowing them to migrate into the microwell array by shaking the plate. Consequently, MCTS are generated through cell-cell clustering and intercellular aggregation. [37]

Dynamic methodologies for the production of MCTS (e.g. microgravity bioreactors, gyratory shakers [10] or spinner flasks [14]) are based on the spinning agitation of cell suspensions. [23,32] The rotational motion of the liquid is either driven by stirring effects by means of blade systems or by spinning the container. Consequently, cells are forced to remain in suspension which results in preferential intercellular adhesion and aggregation and an impeded attachment to the container surface. The application of dynamic technologies allows large-scale production of MCTS due to facilitated culture medium exchange. However, in comparison to static-based approaches, spheroids obtained from agitation-based methods commonly display non-uniform sizes and morphologies due to the rather uncontrollable culture conditions. [32]

Moreover, “microfluidic devices” [23] represent a complex spheroid culturing system composed of channels and chambers in the micrometer range. [10,23] The suspended cells are being trapped in respective compartments, and consequently assemble to form numerous spheroids. [37] The low amounts of medium, cells, and substrates and the possibility to directly investigate treatments within the system renders this technology suitable for high-throughput drug screenings. [23,37] However, the unfeasible retrospective characterization of the obtained MCTS represents a drawback of this methodology. [23]

*Table 1. Comparison of some widely used techniques for the generation of tumor spheroids and their main benefits and downsides. HTS = High Throughput Screening*

| Technique | Advantages | Disadvantages |
|---|---|---|
| *Liquid overlay technique* | · Uniformity of spheroid diameter<br>· Easy scaling-up of spheroid production<br>· Easy handling<br>· Spheroid formation in separated compartments<br>· No need for specialized materials<br>· HTS compatibility<br>· High versatility<br>· Low cost | · Non-uniformity of spheroid shape<br>· Uncontrollability of spheroid size<br>· Laborious plate fabrication |
| *Hanging drop technique* | · Uniformity of spheroid diameter<br>· Easy handling<br>· Spheroid formation in separated compartments<br>· HTS compatibility<br>· Array production<br>· High versatility<br>· Low cost | · Instability<br>· Short time culture<br>· Challenging media change<br>· Laborious<br>· Challenging scaling-up of spheroid production, drug-screenings and HTS performance<br>· Costly special plates |
| *Patterned surface technique* | · Control of spheroid structure and size<br>· Easy handling<br>· Array production<br>· HTS production<br>· High efficiency | · Problematic long-term cultures<br>· Potential incompatibility with drugs<br>· Low reproducibility without automation<br>· Challenging sample retrieval<br>· Costly equipment |
| *Agitation-based techniques* | · Easy handling<br>· Possible scaling-up of spheroid production<br>· Control of nutrient and gas exchange<br>· Good accessibility of spheroids | · Challenging control of spheroid size and shape<br>· Requirement of specialized equipment<br>· Non-compatibility with HTS |

*(Table based on content from Zanoni et al. [36], Lin et al. [38], Velasco et al. [39], Nunes et al. [10], Lazzari et al. [23] and Mehta et al. [31])*

In this project, MCTS were developed by means of the liquid overlay technique. The intention was to establish three-dimensional tumor models exhibiting the typical architecture of different cell layers due to its high relevance for the archaea colonization of the tumor. The generated 3D MCTS were exclusively assembled of cancer cells, and hence can be defined as “homotypic” [17] spheroids. The engagement of stromal cells, such as immune cells and endothelial cells [36] was not taken into account. Nonetheless, the generation of 3D tumor models which mirror the *in vivo* settings to a higher extent was performed successfully by Upreti *et al.* in 2011 [40] by co-culturing cancer cells with endothelial cells. [40]

## 3.3 Cancer gene therapy

Since its introduction in the 1970s, gene therapy has made major advances towards the cure of recessive and dominant genetic defects, various cancers, cardiovascular disease and neurodegenerative disorders, which are inapproachable to conventional treatments. [41–43] While gene therapy for monogenic diseases aims at the restoration of the malfunctioning gene, cancer gene therapy is targeted on the elimination of cancer cells in a direct or indirect manner. [44] The evidence that the development of cancer is closely correlated with multiple genomic alterations renders gene therapy a promising concept to tackle cancer at the level of gene expression. [9,45] The genetic instability of tumor cells leads to persistent proliferative signaling, evasion of apoptosis, circumvention of tumor suppressor mechanisms, infinite replication, induction of angiogenesis, escape from immune defense, invasion and metastasis. These attributes maintain the tumor microenvironment (TME) which, in turn, determines tumor growth as well as efficacy and prognosis of chemotherapeutic treatment. Gene therapy can be defined as the “introduction of exogenous nucleic acids, such as genes, gene segments, oligonucleotides, miRNAs or siRNAs into cells” [46] with the aim to alter, down-regulate, silence, replace, or delete mutated gene(s), and concomitantly modify gene expression. Different strategies are currently being applied in the field of cancer gene therapy. [9,46–49] A selection of approaches will briefly be portrayed in the following.

The introduction of siRNA, miRNA and shRNA into tumor cells enables the silencing of oncogenes (e.g. cMYC, KRAS) as well as the multi-drug resistance 1 (MDR1) gene. Complementary sequences of specific mRNA transcripts are targeted which results in their subsequent degradation or the inhibition of protein synthesis (referred to as RNAi,

RNA interference). This allows the regulation of the translation of pathophysiological proteins that are associated with tumorigenesis, tumor progression and metastasis. Hence, gene silencing induces aggravation of cell growth and tumor regression. [9,46,47,49]

A further approach is to restore the expression of tumor suppressor genes (e.g. TP53, PTEN, P21) by replacing or correcting the mutated gene. Special focus is placed on the P53 protein, which plays a crucial role in the regulation of the cell cycle, initiation of apoptosis, DNA repair and senescence response. The world's first commercially available gene therapy product gendicine consists of a recombinant adenovirus armed with human P53 and was approved by the Chinese FDA in 2003. [46,48]

The methodology of suicide gene therapy describes the insertion of genetic material, which can induce two possible effects, into tumor cells. It either encodes cytotoxic proteins that are capable of killing tumor cells, or it effects the production of prodrug-converting enzymes which modify substances without biological toxicity into cytotoxic agents. [46,47]

Moreover, double stranded oligodeoxynucleotides (ODN) consisting of sequences that are recognized by oncogenic transcription factors represent another method for gene suppression. Said ODNs function as decoys for transcription factors (e.g. STAT3 or NF-KB) by competing with their binding sites, and hence inhibit gene expression modulated by the selected transcription factor. [46,47]

The overexpression of certain miRNAs (i.e. oncogenic miRNAs) as well as the reduced expression of other miRNAs (i.e. tumor suppressor miRNAs) are found to be associated with tumorigenesis, tumor growth and formation of metastasis, and hence represent a promising target for cancer therapy. The upregulation of miRNAs could be restored to physiological conditions similarly as for the RNAi oncogene silencing methodology by introducing antisense miRNA oligonucleotides into the cell. By contrast, downregulated tumor suppressor miRNA could be rebalanced by inserting exogenous miRNA mimics to reposition the miRNA levels. [46,47,50]

Gene editing technologies allow the alteration of genomic DNA by inserting, modifying, replacing or deleting sequences in a site-specific manner. Different endonucleases, such as “zinc-finger nuclease (ZFN), transcription activator-like effector nucleases (TALENs), or the clustered regulatory interspaced short palindromic repeats (CRISPR)/Cas (RNA-guide Cas9 nucleases) technology” [47] are utilized to achieve DNA double strand breaks for the subsequent repair of the mutation. [9,42,46,47,49]

The developing hypoxia in growing tumors entails the secretion of angiogenic factors, “such as vascular endothelial growth factor (VEGF) or fibroblast growth factor-2 (FGF-2)” [46] which enable the tumor’s access to oxygen and nutrients. [46] Current anti-angiogenesis methodologies employ the down-regulation of these angiogenesis promoting factors, and on the other hand, the enhancement of the expression of angiogenesis inhibitory factors (e.g. angiostatin, endostatin or TSP-1s). [8,46]

Tumor cells of various cancers have the capability to elude immune surveillance [44] by producing immunosuppressant cytokines. Immunomodulatory gene therapy in the field of oncology addresses the enhancement of the immune response towards cells of the tumor microenvironment (TME). [8,49] Currently, three major immunogenic approaches are pursued: (i) Cytokine gene therapy applies the introduction of cytokine genes with the subsequent production of particular interleukins, “including interleukin-2 (IL-2), IL-4, IL-6, IL-12, IL-24, interferon-alpha (IFN-α), IFN-γ, IFN-β or tumor necrosis factors (TNF) TNF-α and TNF-β” [46] with tumor combating capacities. [8,46] (ii) The methodology of tumor vaccination is based on the presentation of tumor-associated antigens (e.g. prostate specific antigen, PSA; glycoprotein 100, gp100; tumor-specific epitopes) to the immune system in order to stimulate the immune-mediated antigenicity against tumor cells. (iii) The chimeric antigen receptor T cell (CAR-T) therapy relies on the genetic engineering of patient- or donor-derived T lymphocytes to achieve the production of synthetic chimeric antigen receptors. Tumor-related antigens constitute a specific target to the genetically altered T cells, therefore antigen-carrying tumor cells can be attacked and destroyed. Two promising CAR-T cell based therapies for the treatment of particular B-cell cancers are tisagenlecleucel (Kymriah, Novartis) and axicabtagene ciloleucel (Yescarta, Gilead). [8,46]

### 3.3.1 Vectors for gene therapy

Nucleic acid therapeutics (transgenes) are highly polar, macromolecular substances which, as opposed to small molecule drugs, cannot permeate cell membranes by means of diffusion. Moreover, the systemic administration of naked nucleic acids does not lead to desired therapy outcomes due to rapid enzymatic degradation (endonucleases) and renal clearance, low cellular uptake and unspecific distribution. [9,45,47,49,51,52]

Apart from this, conventionally applied cancer therapies commonly fail because of the divergent conditions in the tumor vicinity compared to physiological tissue. The distribution of systemically administered chemotherapeutics to hypoxic and necrotic regions of tumors is found to be impaired due to irregularly organized blood vessels, which entails poor vascularization, and thus limits drug efficacy. Moreover, low oxygen levels in hypoxic and necrotic zones impede the efficacy of radiotherapy, which mainly depends on the presence of oxygen in tissues. [53–55] Hence, in order to protect the genetic material and to enable its transfer into target cells at target sites, efficient vector mediated transportation is required. [45,51]

Gene delivery vehicles are afflicted with certain limitations with regard to efficacy and safety and are thus subject of intensive investigations. To achieve therapeutic success, vectors with efficient gene delivery and expression capacities are indispensable. The currently applied vector systems can be classified in viral/bacterial and non-viral vectors. [9,45,47,49,51,52]

#### 3.3.1.1 Viral vectors

The natural property of viruses to invade target cells via endocytosis and to introduce their genome into the host organism's cytoplasm, and thereupon, into its nucleus renders them interesting therapeutic instruments for the utilization as carriers of genetic material. [49,56–58] Viruses consist of either single- or double-stranded deoxyribonucleic acid (DNA) or ribonucleic acid (RNA) surrounded by a protein coat (capsid), which provides protection against nucleic acid degradation through nucleases and allows facilitated attachment to host cells. The propagation of a virus relies on the insertion of its genome into a host cell to exploit the cell's machinery for

the production of viral biosynthetic and metabolic components that are needed for its transcription and replication. [49,59,60]

Presently investigated viral vectors originate from adenoviruses, adeno-associated viruses (AAV), retroviruses, herpes simplex viruses (HSV), lentiviruses, rhabdoviruses, alphaviruses, poxviruses, flaviviruses, measles viruses, Newcastle disease virus (NDV) and picornaviruses. Depending on the employed vector, gene expression profiles vary with respect to (a) transient short-term or (b) permanent long-term (e.g. due to chromosomal integration) transgene expression in host cells. [60]

The genetic engineering of viruses enables the expression of foreign transgenes as well as the broadening of viral tissue tropism and tailoring for selected therapeutic goals. [61] Modified viruses equipped with target genes, referred to as viral vectors, achieve striking gene expression performance [45] and were the first nucleic acid delivery vehicles employed in gene therapy. [52] High gene transfection efficiency of viral vectors represents an advantage over non-viral vectors, whereas on the other hand they face several challenges, such as immunogenicity [9], insertional mutagenesis [52] (carcinogenicity [58]), off-target effects [52], cytotoxicity [9], tissue tropism [42], gene-load capacity [46], and undesired clinical outcomes, such as disease or death of participants in the course of clinical trials. [52]

Recombinant viral vectors can be applied for the treatment of cancer and various other diseases. With regard to cancer therapy, viral vectors could be utilized to trigger the host immune response against tumor-associated antigens, and hence render tumor cells susceptible to the immune system. [61] For this approach autologous host cells, such as dendritic cells or T lymphocytes (antigen presenting cells), are genetically modified *ex vivo* to express tumor-specific antigens. [61] In 2004, Lizée *et al*. [62] performed a transduction of three different types of human antigen presenting cells (APC), namely “monocyte-derived dendritic cells (DC), CD40L-activated B lymphocytes, and Epstein Barr virus (EBV)-transformed B lymphocytes”. [62] Said cells were transduced by means of lentiviral vectors which expressed tyrosinase (melanoma associated antigen) or GFP (reporter gene). Tyrosinase was expressed sufficiently to elicit TAA (tumor-associated antigen)-specific T cell identification in two melanoma patients, hence, the study group concluded that the transduction of three APC types

with lentiviral vectors carrying genes of tumor antigens could effectively stimulate TAA-specific T lymphocyte recognition. [62] Tisagenlecleucel (Kymriah, Novartis; approved 2018) and axicabtagene ciloleucel (Yescarta, Gilead; approved 2017) represent two CAR-T cell-based agents which are obtained through transfection of T cells with a retrovirus vector and a lentivirus vector. Both are approved by the FDA for the treatment of particular types of B cell lymphoma and leukemia. [42,46,61]

Certain viruses naturally possess oncolytic features (e.g. reovirus, vaccinia virus, adenovirus) and preferentially infect and replicate in cancer cells, however tumor cell selectivity can even be enhanced through genetic engineering. [61,63] Oncolytic properties are attributes of replicating viruses (as outlined above), whereas non-replicating viruses are being utilized as gene delivery vectors in cancer gene therapy. [44] The application of oncolytic viruses (OVs) in cancer therapy exploits the property of wild or genetically modified viruses to specifically infect cancer cells and consequently induce cell death without the engagement of physiological tissue. [63] OVs have the capacity to directly induce oncolysis through extensive replication within tumor cells. Certain OVs additionally indirectly stimulate antitumor immunity mediated through viral replication, resulting in immunogenic cancer cell death (ICD). [8,64]

#### 3.3.1.2 Non-viral vectors

Non-viral vectors represent promising alternatives to viral vectors in light of their superiority regarding immunogenicity, safety, loading capacities and easy loading (e.g. through electrostatic interaction), stability, large-scale production, cost efficiency and design flexibility. [9,51,58] With regard to non-viral vectors, focus in this chapter will be on delivery vehicles with diameters of 1-100 nm, referred to as nanocarriers. [6] Nanocarriers provide enhanced protection to vulnerable drugs, increase the solubility of hydrophobic compounds, facilitate cell membrane permeation for substances, enable co-delivery of hydrophilic and hydrophobic substances, allow targeted drug delivery to diseased site, and hence reduce toxicity for healthy cells. [6,65] Nevertheless, viral vectors are yet advantageous in terms of transduction efficiency. [9] A major advantage of nanotherapeutics is their preferential release at tumor vicinity due to the so-called “enhanced permeability and retention (EPR) effect” [57]. The EPR effect can be explained as nanoparticles display increased blood vessel penetration and accumulation within the tumor due to its abnormal tissue structure. [46,57]

With regard to material, nanocarriers can be categorized into three classes: organic nano-formulations (e.g. liposomes, polymersomes, nanoparticles), inorganic nanoparticles (NPs) (e.g. gold NPs, quantum dots, silica NPs), and carbon-based nano-materials. [66] Some approaches will be outlined in the following.

Liposomes are composite vesicular systems exhibiting an aqueous core surrounded by a bilayer of amphiphilic lipids (e.g. phospholipids). [66,67] Due to their resemblance to biological membranes, liposomes exhibit biodegradability and biocompatibility. [66] Other advantages are their low cytotoxicity, easy generation and membrane fluidity, which can be modulated in order to improve transfection efficiency. [51,66] Nanocarriers composed of cationic lipids can be exploited for the convenient loading with anionic genetic material through intermolecular electromagnetic interactions. [9] The introduction of polyethylene glycol (PEG) into the lipid bilayer results in a reduced clearance, and thus in an enhanced malignancy bioavailability. [66,68] In 1994, Gabizon *et al.* [69] demonstrated that Doxil®, a PEG-coated liposome-based doxorubicin (DOX) formulation, showed extended plasma circulation time after injection in cancer patients. The PEGylation entails a reduced uptake of liposomes by the reticuloendothelial system, a prolonged elimination half-life and an extended accumulation at tumor sites that display the EPR effect. As a result, drug accumulation at malignant sites was increased 4- to 16-fold compared to free doxorubicin. In 1995, Doxil® was the first nano-drug to be approved by the FDA. [66–69]

Polymersomes are vesicles consisting of a solution-containing lumen encircled by a double layer membrane of synthetic block copolymers. Just like liposomes, polymersomes can be loaded with both hydrophilic agents within the central aqueous cavity and hydrophobic ones in the lipophilic membrane. Due to certain limitations faced by liposomes, such as their mechanical fragility and their sensitivity to hydrolytic cleavage of the lipid bilayer, polymersomes recently emerged as new drug delivery concepts. [66,67] Potentially advantageous features of polymersomes include their high stability, high loading capacities for hydrophobic drugs due to thick membranes, and their wide-ranging chemical flexibility which allows broad modifications in terms of fluidity, permeability and membrane assembly. [66] Surfaces of polymersomes can be equipped with active constituents, such as antibodies, proteins, carbohydrates, vitamins, etc. [70,71] However, on account of lacking investigations concerning loading

capacity of polymersomes compared to that of PEGylated liposomes, a clear superiority cannot yet be ascertained. Membrane biodegradability and its effect on compound release, plasma half-life, and stability remain insufficiently investigated. [71] For the assessment of the anti-cancer efficacy of polymersome-based systemic delivery of chemotherapeutics, Ahmed *et al.* [72] injected polymersomes equipped with a combination of paclitaxel and doxorubicin into tumor mouse models as part of a preclinical investigation in 2006. The study demonstrated prolonged tumor DOX exposure and augmented tumor regression, however, paclitaxel concentrations as well as controls with liposomal outcomes are lacking in this study. In conclusion, further evaluation of polymersomes being suitable drug delivery vehicles which display clear advantages in comparison with liposomal carriers is required. [71,72]

The wide range of currently investigated nanoparticles is extensively reviewed by Bisso *et al.* [66] and will not be further discussed within the framework of this thesis.

#### 3.3.1.3 Novel vectors

##### 3.3.1.3.1 Bacteria

Many bacteria species exhibit pathogenic and potentially carcinogenic, tumor promoting properties. Conversely, several strains have shown to selectively colonize tumors resulting in tumor clearance. [73] The bone sarcoma surgeon Dr. William B. Coley (1862-1936) observed that cancer patients with streptococcal infections experienced spontaneous tumor regression. In 1891, he introduced the concept of bacteria-based anticancer treatment by injecting live streptococcal cultures, and later, a combination of two heat-inactivated (to avoid bacteremia) bacteria strains, referred to as “Coley’s toxins”, in patients with inoperable cancers. The aim of administrating microorganisms was to induce the development of erysipelas and thereby provoke an immune response. The treatments led to cures or significant improvements in patients, which were presumably due to immunomodulatory effects of therapeutic bacteria. Dr. Coley’s investigations can thus be considered as some of the first systemic immunotherapy studies. [53,55,73–75] The only FDA-approved bacterial agent thus far is the attenuated *Mycobacterium bovis* strain Bacillus Calmette-Guerin (BCG) which is applied in patients with bladder cancer. Its therapeutic effect is presumed to be due to its immunogenic activity. [55,73,76]

Due to the increased focus on chemotherapy and radiation therapy, and other reasons, bacterial cancer therapy has played a rather subordinary role until a few decades ago. With the improved understanding of DNA technologies as well as of the tumor microenvironment, this research field experienced a certain resurgence in the mid-1990s, when the generation of less toxic and more potent bacterial strains became possible. [53,55,73–75]

The use of bacteria as antitumor therapeutics represents a promising approach to combat cancer. It has been shown that several facultative and obligate anaerobic bacteria specifically target hypoxic and necrotic regions of tumors. Furthermore, their preferential replication in tumor vicinity has been observed. [79] This tumor-selective colonization is presumably based on the anaerobic phenotype of different bacteria species. [78] However, the immunosuppressive and pathologically altered biochemical microenvironment of tumors which entails an immune-privileged and nutrient-providing niche for bacteria to thrive may also contribute to the bacterial tumor homing. [55,76]

To improve antitumor activity, bacteria can be genetically modified in numerous different ways depending on the therapeutic need. [55] Strategies of bacteria-mediated tumor-therapy (BMTT) include the exploitation of the natural bacterial toxicity to tumors, the use of genetically manipulated bacteria to express tumoricidal and immunogenic substances, tumor-associated antigens, RNA interference (RNAi) molecules, and pro-drug-cleaving products. [55,75,77] In the field of cancer research, various strains of *Bifidobacterium*, *Salmonella*, *Clostridium*, *Escherichia*, *Shigella*, *Listeria*, *Lactococcus*, *and Vibrio* have been investigated by means of animal experimentations. [53,73] Studies with whole live, genetically engineered and/or attenuated bacteria have been performed extensively. [77] Alterations of the bacterial genetic profile are crucial to reduce adverse side effects, and thus, increase safety of bacterial vectors, and, on the other hand, to enhance beneficial therapeutic effects. [55,76]

Genetically modified tumor-targeting bacteria conceived to express tumoricidal compounds and/or cytotoxic protein, tumor-associated antigens, and reporter genes have recently emerged as a novel approach in the field of cancer gene therapy. [77] Facultative or obligate anaerobic strains of the genera *Bifidobacterium*, *Salmonella*,

and *Clostridia* are the most extensively studied bacterial gene delivery vectors for the targeting of solid tumors. [28] These three species have been examined for the use as delivery vectors for suicide genes, anti-angiogenic genes, and tumor-associated antigens in tumor-bearing animal models, demonstrating partial responses to be further evaluated in humans. [77]

The most extensively investigated as well as the most efficient antitumor microbe as yet is perhaps the intracellular pathogenic strain *Salmonella enterica* serovar Typhimurium (referred to as VNP20009) due to its beneficial intrinsic characteristics. The preferential tumor accumulation and proliferation ratios of VNP20009 are above 1000/1 compared to its targeting of physiological tissue, which usually results in the inhibition of tumor growth. Additionally, *Salmonella* have the capacity to colonize large solid tumors, including hypoxic regions, and to infiltrate metastases. [53,79] The ability of Salmonella to invade cells allows the intracellular delivery of therapeutic compounds, such as RNAi or cytotoxic proteins that cannot permeate eukaryotic cell membranes. For the efficient cytosolic export of the drug, it is essential to adjust the expression of genes in order to regulate the production of the drug with regard to time and location. [79]

In 2016, Camacho *et al.* [79] have developed a *Salmonella*-based antitumor system, genetically engineered to successively produce and release the proapoptotic Cp53 peptide. Due to its rather difficult transfer into the cytosol of tumor cells, Cp53 represents a challenging agent in cancer therapy. Therefore, two separately inducible systems were incorporated in the improved *Salmonella* strain. The first system allowed an efficient production of heterologous therapeutic compounds in response to the inducer molecules acetylsalicylic acid or salicylates. The second one was based on the lambda phage lysis operon and elicited bacterial lysis upon exposure to anhydrotetracycline and the subsequent release of its content, the cytotoxic Cp53 peptide. The outcome of this study demonstrated, that 60 % of the tumor cells cultivated in cell culture models were killed with an infection range of 60-70 %, indicating that their engineered *Salmonella* is capable of producing and delivering anticancer agents into tumor cells. [79]

A further approach for the application of bacterial gene delivery systems as cancer therapeutics was performed by Osswald *et al.* [28] in 2015. The study was aimed at the assessment of the potential of multicellular tumor spheroids (MCTS) as *in vitro* models for the investigation of anaerobic bacteria to be used as gene delivery vectors. The formation of three-dimensional fluorescent spheroids was achieved by seeding cells of the colorectal carcinoma cell line HT-29 in ultra-low attachment well plates. The MCTS reached diameters of 500-1000 µm after 14 days of cultivation and displayed the relevant pathophysiological attributes of solid tumors, such as the proliferating outer cell layers and the increasing hypoxia entailing an apoptotic core with necrotic regions. Three bacteria genera, *Bifidobacterium bifidum* S17, *Salmonella typhimurium* YB1 and *Clostridium sporogenes* were assessed for their tumor-targeting capacity. [28]

*Bifidobacteria* are obligate anaerobic non-pathogenic bacteria that can be found in the intestinal microbiota of humans and are hence promising candidates for gene delivery and expression systems in cancer therapy. Their selective colonization and replication in solid tumors after intravenous, intratumoral or oral administration has been demonstrated in several studies by means of animal models. However, due to their high resistance to genetic modifications, only few strains have been manipulated to express antitumor genes. [28]

The facultative anaerobic genera *Salmonella* are, as described previously, the most frequently examined bacteria in the field of targeted cancer therapy. Osswald *et al*. generated an “obligate” anaerobic strain, referred to as *Salmonella typhimurium* YB1 based on the attenuated *S. typhimurium* SL7207. *S. typhimurium* YB1 was genetically modified to express anti-sense RNA to the mRNA of the asd gene under aerobic conditions exclusively. Asd encodes an essential enzyme for the synthesis of diaminopimelic acid (DAP) which, in turn, is required for the bacterial cell wall. The silencing of asd in aerobic regions renders *S. typhimurium* YB1 auxotrophic for DAP but allows its growth under anaerobic conditions when no complementary RNA is expressed. Essentially, *S. typhimurium* YB1 is engineered for the sake of attenuation, and at the same time displays increased accumulation and survival in poorly oxygenated areas of murine tumors, in contrast to oxygen-richer tissues. [28]

*Clostridium sporogenes* are strictly anaerobic bacteria and display spore-forming properties. Spores represent immunologically inert units and can hence safely be injected intravenously. Spores of different *Clostridia* species have shown to specifically germinate within tumors with their vegetative cells not being viable in more oxygenated murine organs. In this study, clostridial spores were investigated for their capability to target solid tumors. Therefore, MCTS were incubated with a spore preparation for seven days. [28]

The results of Osswald's study demonstrated that *Bifidobacterium* and *Salmonella* were selectively located and replicated in hypoxic regions of the spheroid core and remained viable for at least 72h following inoculation. Moreover, the clostridial spores were found to exclusively colonize and germinate in hypoxic domains of the MCTS. [28]

A further step performed by Osswald *et al.* aimed at evaluating the potential of bacteria as gene delivery vectors. For this purpose, *B. bifidum* S17 were transfected to either express a cytosine deaminase derivative [a], which converts the prodrug 5-fluorocytosin (5-FC) to the antineoplastic agent 5-fluorouracil (5-FU), or a chromate reductase [b], which converts CB1954 to DNA intercalating hydroxylamines. The co-incubation with [a] was lacking a tumor growth-inhibiting effect, suggesting that the HT-29 cell line displayed resistance to 5-FU, whereas co-cultivation with [b] resulted in a significant growth inhibition. In conclusion, it could be demonstrated that HT-29-MCTS represent an appropriate model system to evaluate obligate anaerobic bacteria/spores for their potential to target solid tumors *in vitro*. [28]

Based on the successful outcomes of above delineated and several further studies on tumor targeting bacteria, in this thesis, the potential of anaerobic methanogenic archaea to selectively target hypoxic areas of multicellular tumor spheroids (MCTS) should be investigated.

## 3.4 Archaea

### 3.4.1 Classification of archaea

Early classifications divided all living organisms - mainly based on morphology - into two major evolutionary domains, the *Prokaryota* (or prokaryotes) and the *Eukaryota* (or eukaryotes). [80,81] Prokaryotes do not possess a cell nucleus and, in the past,

primarily described bacteria, whereas eukaryotic organisms, i.e. protists, plants, fungi, and animals, contain nuclei. [82–84] In 1977, Carl Woese and coworkers, following comparative and phylogenetic analyses of nucleic acids, suggested that prokaryotes must actually be subdivided into two separate lines of descent, *Eubacteria* and *Archaebacteria*. [80–82] Due to the substantial distinctiveness of the two lineages, *Eubacteria* and *Archaebacteria* were eventually renamed to *Bacteria* and *Archaea*. [82] Today, the entirety of cellular life is categorized into the three great domains *Eukarya*, *Bacteria* and *Archaea* (*Figure 3*). [81,82]

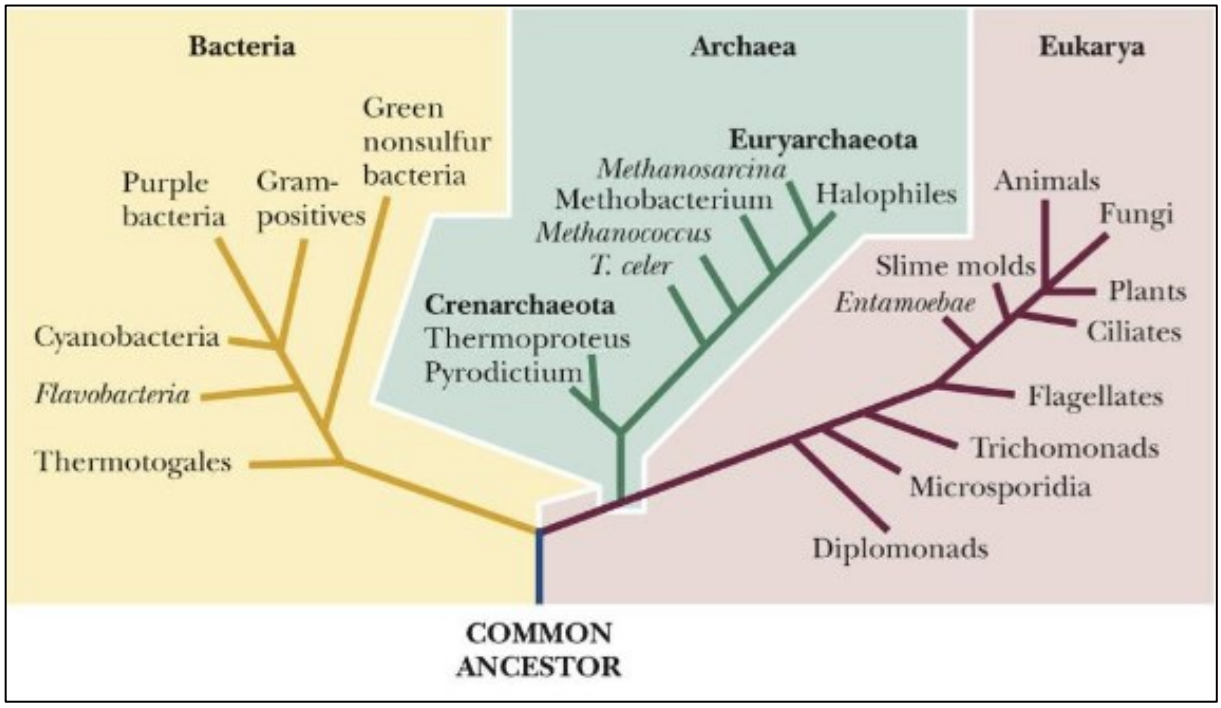


*Figure 3. The three-domain phylogenic tree of life – Archaea, Bacteria and Eukaryota. (Figure from Jayashantha, E. [84])*

Closer phylogenetic examinations in the late 1980s provided strong evidence that archaea and eukaryotes were closer related than archaea and bacteria, rendering archaea and eukaryotes sister groups in the three-domain system of life. [80,81] Some of the features that archaea and eucaryotes have in common but are lacking in bacteria are complex RNA polymerases, histones, and methionine as their start codon for translation. Moreover, archaea display several properties that are also found in eukaryotes, such as the lack of murein (peptidoglycan) in their cell walls, their transcriptional and translational apparatus, and their genomic constitution. [80] The archaea can be classified in two major phyla, the *Euryarchaeota* and the

*Crenarchaeota*, and one minor, the *Korarchaeota*. Moreover, *Thaumarchaeota* and *Nanoarchaeota* can be included as further subcategories. [82]

### 3.4.2 Habitats of archaea

Originally, archaea have been described to occur primarily in extreme environments (referred to as extremophiles), however, comprehensive research revealed that these microorganisms are widespread and exist ubiquitously, including habitats with moderate conditions for growth. Depending on the species, archaea display distinct preferences with respect to their habitats. [84–86]

Thermophiles thrive in temperatures between 50-70 °C, hyperthermophiles can even grow in temperatures above 100 °C, and acidophiles have been found to survive very low pH levels. These groups have been identified to inhabit volcanic vents, hot springs and thermal vents. [84–86] Halophiles reside in high-salinity environments, such as evaporation ponds, salt beaches and deep-sea hypersaline basins. Equally, alkaliphiles, who can survive high pH levels, have been found to inhabit these environments. [84–86] Methanogens occur in oxygen-deprived surroundings, such as coal fields, swamps, underground environments, marine sediment as well as rumens and intestinal microbiota of animals. [84–86]

Noteworthy, archaea do not necessarily imply extremophilic living conditions but equally occur in mild environments, such as soils and sewages. These archaeal species are hence referred to as mesophiles. Furthermore, psychrophiles inhabit environments with temperatures less than 20 °C, other archaeal species are resilient towards radiation, or high pressure. [84–86]

As already outlined, archaeal species have been discovered to also be abundant in the microbiota of insects and mammals, including humans, as part of the commensal flora (for details please refer to chapter 3.4.4). [85,87]

### 3.4.3 Properties of archaea

Archaea display a great diversity of morphological shapes that include perfectly regular to rather irregular spherical forms (coccus) as well as short bar-like to long needle-like rod-shaped (bacillus) formations. Moreover, species with spiral, plate, triangular or

rectangular shapes have been discovered. Single archaea display sizes from 0.1 µm to more than 15 µm, however, some species, which can be found in biofilms, form cell aggregates or filaments reaching sizes of 200 µm. Archaeal species exhibit various aggregation patterns, including the development of singular giant cells through cell fusion, long hollow tubes and “string-of-pearls” multi-species communities. [83,84]

Archaeal cell membranes possess several features that differ from other living organisms. One of those characteristics is the chirality of their membrane-forming glycerol which is a stereoisomer of that of eukaryotic or bacterial membranes. Furthermore, archaea do not use fatty acids for the assembly of membrane phospholipids but isoprenoid chains, so far, the only known organisms to do so. The linkage of the side chains to the glycerol molecules is achieved through ether bonds, which represents another specificity of archaeal membranes and is presumed to contribute to archaea’s resilience towards extreme heat or strongly alkaline or acidic environments. Most other organisms use ester linkages to link side chains to glycerol. A crucial distinguishing feature of certain archaeal species is their monolayer membrane consisting of tetraether lipids which differs fundamentally from eukaryotic or bacterial bilayer cell membranes. Lipid monolayers are, due to their stability and rigidity, extraordinarily resistant to high temperatures and are thus often found in hyperthermophilic species. Another attribute that could render archaea’s membranes more robust when exposed to high temperatures is their capability to branch their isoprenoid side chains and to form cyclopropane and cyclohexane rings. [83–87]

Archaeal cell walls also display several properties that differ from other living organisms. One such hallmark is their lack of peptidoglycan which, in the case of certain methanogenic archaea is replaced by pseudomurein, a peptidoglycan-resembling polymer. Other species were found to comprise various other complex polysaccharides. Extremely halophilic archaea, for example, possess highly sulfated polymers that contribute to cell wall stabilization by neutralizing sodium ions present in its habitats, such as hypersaline evaporation lakes or sea water. Apart from that, archaea’s cell walls are assembled of proteins that form a surface layer, referred to as “S-layer”. S-layers are paracrystalline protein arrays and serve as a protection from osmotic pressure and further as a filter that facilitates the passage of salutes with low molecular weight while obstructing it for large components (e.g. viruses). [83,84,86,87]

Beyond that, several archaeal species exhibit flagella that allow them to move. However, archaeal flagella differ significantly from those of bacteria with regard to flagellin composition and biochemical motor drive. [84]

As part of this thesis, the methanogenic *Methanococcus maripaludis* was utilized. *M. maripaludis* is an obligately anaerobic, coccoid-shaped, colony-forming, motile (thanks to its flagella), mesophilic archaeal strain that has its temperature optimum between 18 and 47 °C and its pH optimum between 6.5 and 7.4. [88]

### 3.4.4 Archaea in humans

#### 3.4.4.1 Archaea as components of the human microbiome

Several archaeal species have been detected to inhabit various ecosystems of the human body, such as the oral cavity, the respiratory tract, the skin, the vagina, and the intestine. As a result, strong focus has been placed on the exploration of the physiological role of archaea residing within the human commensalistic microbiota, which is increasingly assumed to influence its host's functionality and health. Numerous archaeal orders, such as *Methanobacteriales*, *Methanomicrobiales*, *Methanosarcinales*, *Methanoassiliicoccales*, *Halobacteriales*, *Thaumarchaeota* [89] have been identified to reside in the human microbiome. However, the majority of the human-associated species, especially those located in mouth and gut, are strains of the strictly anaerobic methanogenic order *Methanobacteriales*. [85,87,89] All methanoarchaeal orders are capable of performing methanogenesis where organic or inorganic compounds, such as fermentation products of certain bacteria (e.g. hydrogen or carbon dioxide), are converted into methane under anoxic/anaerobic conditions. [85,86] The methanogenic metabolism allows both the generation of energy for the archaeal organism and the transfer of hydrogen among distinct species which consequently enables effective and thorough breakdown of organic substrates. This process promotes the syntrophic co-existence of archaeal and bacterial species. Hence, archaea, particularly methanoarchaea, are crucial contributors to the metabolic function, and thus, to the optimum energy output of the host's microbiota. [85,87,89,90]

Investigations regarding the intestinal microbiome have hitherto primarily been dedicated to the bacterial population, such as the *Bacteroidetes* and *Firmicutes* which represent 90 % of all phyla in the human intestine. Nevertheless, several archaeal

species as well as fungi and viruses have been identified to be part of this composite community, also referred to as the “holobiont [89] concept”. *Methanobrevibacter smithii* (*M. smithii*) was found to be the predominant archaeon in the human gut, where it increases the efficiency of polysaccharide degradation by lowering the hydrogen partial pressure through methanogenesis, where hydrogen and carbon dioxide are exploited. *Methanosphaera stadtmanae* (*M. stadtmanae*) is another methanogenic strain that has been identified in human stool samples, however, its energy metabolism is restricted to the reduction of methanol in order to generate methane. More recent discoveries within the human gut are various strains of the order *Methanomassiliicoccales* which, apart from the human intestine, are presumed to also be widely distributed in the environment. [85] Additionally, it is presumed that archaea of this lineage are able to deplete trimethylamines (TMA) as part of methanogenesis. This property could be exploited for the prophylactic treatment of cardiovascular events by means of decreasing the concentration of pro-atherogenic trimethylamine-N-oxide. Equally, TMA levels of persons who suffer from trimethylaminuria could thus be decreased. [85,87,90]

Furthermore, study results from Probst *et al*. [91] (2013) propose beneficial properties of the phylum *Thaumarchaeota* found on human skin. According to their study, these archaeal representatives could be involved in the oxidation of sweat-derived ammonia compounds, and thus in the regulation of the skin pH. [85,89–91]

#### 3.4.4.2 Archaea and human disease

Besides the profitable effects of the archaea-human interdependency, archaea’s contribution to the development of various human diseases, including diverticulosis, colon cancer, diabetes, anorexia, obesity, and inflammatory bowel disease, is equally assessed. However, the obtained results often remain inconsistent due to methodological issues, such as the use of bacteria-based methods and other drawbacks. Nonetheless, infection or dysbiosis are known to be correlated with higher prevalence of methanoarchaea at distinct areas of the human body. [85,89] *Methanobrevibacter oralis* (*M. oralis*) was reported to be the most abundant species found in the oral cavity. [85] Remarkably, *M. oralis* was predominantly detected at inflamed sites of severe periodontitis as opposed to adjacent not afflicted sites. [85,89] Apart from that, *M. oralis* was shown to be present in brain abscesses. Similarly, *M.*

*smithii* was described to solely occur in the vagina of individuals suffering from vaginosis and to be lacking in healthy tissues. Beyond that, *M. smithii* was identified in patients with pneumonia, muscle abscesses, and urinary tract infections, as well as in persons suffering from refractory sinusitis in combination with *M. oralis*. [85,89] These outlined infections and dysbioses are characterized by a substantial increase of anaerobic fermentative bacteria, which coincides with an augmentation of archaea, which, in turn, could promote the excessive growth of fermentative bacteria. Hence, archaea could be contributors to described polymicrobial conditions as part of a syntrophic partnership with bacteria. Moreover, the methanoarchaea's metabolic product, methane, was shown to extend the intestinal transit time of dogs, which is presumed to be due to the interaction of methane with the enteric nervous system. This could possibly provide an explanation for the correlation of constipation with methanogens. [87,89,90]

Interestingly, despite their potential contribution to the aforementioned diseases, no per se pathogenic character of methanogenic archaea has yet been determined. This could be due to our lack of knowledge to identify archaeal pathogens as part of disease patterns or due to the actual non-pathogenicity of archaea. However, the shift from non-pathogenic archaea into pathogens cannot be ruled out. [89,92]

#### 3.4.4.2 Archaea and human immune response

Despite the favorable growth conditions that mesophilic archaea or other microorganisms find in the human body, all of those organisms are confronted with the host's epithelial defense mechanisms, i.e. the innate and the adaptive immunity. Microorganisms are defeated by the secretion of cytokines and antimicrobial peptides (AMPs). AMPs belong to the innate immune system and are released in answer to bacterial microbe-associated molecular patterns (MAMPs). [85,89,93] Hitherto, methanoarchaea's immunomodulatory activity has not been examined as extensively as that of gut-associated bacteria, most likely because no archaeal pathogen has thus far been identified. [85,94,95]

Several recent studies have provided clear indication that human-inhabiting archaea are being recognized by both the innate and the adaptive immune system and hence can initiate its activation. [85] For instance, in 2014, Bang *et al.* [94] have investigated the response of human immune cells upon the exposure to the methanogenic archaea *M.*

*smithii* and *M. stadtmanae*. Their findings demonstrated a significant pro-inflammatory response by monocyte-derived dendritic cells (moDC) towards *M. stadtmanae,* whereas the incubation with *M. smithii* only resulted in a weak immune reaction. Moreover, both archaeal strains induced the upregulation of the surface receptors CD197 and CD86, possibly indicating an additional elicitation of the adaptive immunity. Based on the outcomes of their study, Bang *et al.* outlined the potential involvement of *M. stadtmanae* in bowel pathologies and suggested "the presence of a specific archaeal-associated pattern recognition receptor in humans". [85,94]

In 2017, Vierbuchen *et al.* [96] were the first to demonstrate the explicit recognition of an archaeal strain by human cells and its specific immune stimulation at a molecular level. In their study, distinct human myeloid cells were inoculated with the methanogen *M. stadtmanae* and liposomal-complexed archaeal RNA. Both the archaeon and its RNA displayed significant stimulation of the innate immune response, with toll-like receptor 7 (TLR7) and TLR8 being the engaged pattern recognition receptors (PRRs). Additionally, these molecular interactions resulted in an alternative NLRP3 inflammasome activation which entirely depends on the involvement of TLR8 and might be unique for archaea. [89,96]

Concludingly, the delineated studies as well as other current literature suggest a strong impact of archaea on hosts and components of the microbiota. The inclusion of archaea in prospective studies concerning the microbiome is hence of great importance. Archaea's potential to interact with the human immune system and to elicit inflammation particularly emphasizes the need for further research on human-colonizing archaea. [89,94,96]

Based on the above outlined properties of particular archaea, such as their anaerobic metabolism, their broad abundance at human sites, their survival in extreme environments and their non-pathogenicity, the question arose whether archaea could, similarly as reported for anaerobic bacteria, serve as drug delivery vectors for the treatment of human disease. Hence, in this thesis, the capability of the methanogenic obligate anaerobic archaea strain *Methanococcus maripaludis* S0001 to spontaneously migrate towards the hypoxic/anoxic tumor core should be assessed.

# 4 Aim of the project

This project aimed at the investigation of multicellular tumor spheroids (MCTS) generated from 4T1 cells (murine breast cancer cells) for their suitability as *in vitro* tumor models for co-culture experiments with archaea. In order to achieve reproducible and reliable results, the first goal was to optimize spheroids with regard to various parameters, such as cell seeding number, staining methods, harvesting and embedding techniques, preparation of cryostat sections, and fixation methodologies.

Furthermore, the development of hypoxic regions and a necrotic core should be promoted in order to achieve higher resemblance to natural tumors. MCTS with the most favorable properties, such as high mechanical stability, consistent morphological shape, and steady growth rates should be identified and utilized for subsequent co-culture studies with archaea.

A further aim was to evaluate the archaea strain *Methanococcus maripaludis* S0001 with regard to its colonization pattern during incubation with MCTS. Special attention should be placed on the microorganism's ability to infiltrate inner zones of the spheroid, i.e. its ability to spontaneously target hypoxia and hence necrotic regions within MCTS. To be able to trace the archaea within spheroids, a suitable labeling dye should be determined and optimized.

# 5 Materials

## 5.1 Cell culture

### 5.1.1 Instruments

- Biological Safety Cabinet (Thermo Fisher Scientific)
- Pipette controller, accu-jet® pro (Brandtech Scientific Inc.)
- Serological pipettes 5 ml, 10 ml, 25 ml (Sarstedt)
- TC Flask T75, Stand., Vent. Cap (Sarstedt)
- TC Flask T25, Stand., Vent. Cap (Sarstedt)
- Centrifuge tubes 15 ml, 50 ml (Starlab)
- Waterbath (Linder Labortechnik)
- Eppendorf Research® plus micropipettes (Eppendorf)
- Eppendorf tubes (Nerbe plus GmbH)
- Pipette tips (Nerbe plus GmbH)
- Incubator 37 °C, 5 % $CO_2$ (Thermo Fisher Scientific)
- Centrifuge 3K30 (Sigma Laborzentrifugen GmbH)
- Corning® COSTAR® Ultra-Low Attachment 96-Well Plate (Corning Costar®)
- Nunclon™ Sphera™ Nunclon Sphera-treated 96-Well U-shaped Bottom Microplate (Thermo Scientific™)
- Parafilm®, All Purpose Laboratory Film (Pechiney Plastic Packaging)
- Hemocytometer, Neubauer Improved (Paul Marienfeld GmbH & Co. KG)
- Inverted Microscope, Motic® AE31 (Motic)
- Microscope EVOS™ FL Cell Imaging System (Thermo Scientific)
- Superfrost® Slides, cut edges (Carl Roth GmbH + Co. KG)
- Centrifuge VWR Microstar 17R (VWR International)
- Vortex Shaker (IKA®-Werke GmbH & Co. KG)
- Coverslips 24x50 mm (Carl Roth GmbH + Co. KG)
- Inverted Microscope (DM IL LED Fluo, Leica Microsystems)
- Microscope camera (DFC450C, Leica Microsystems)
- Refrigerator 4 °C (Allectric)
- Freezer -20 °C (Thermo Scientific)
- Freezer -80 °C (Thermo Scientific)
- Sterican® Stand. Gr.17 G24 x 1", Ø 0,55 x 25 mm (B. Braun Melsungen

AG)

- BD Luer-Lok™ Tip Syringe, 3 ml, disposable (Becton Dickinson & Company)
- Aluminum Foil, available in commerce

### 5.1.2 Substances and reagents

- RPMI-1640 Medium, 20 mM HEPES-supplemented (Sigma-Aldrich)
- Penicillin-Streptomycin (Sigma-Aldrich)
- Fetal Bovine Serum (FBS), heat inactivated (Sigma-Aldrich)
- L-Glutamine 200 mM (Sigma-Aldrich)
- Trypsin-EDTA Solution (Sigma-Aldrich)
- Dulbecco's Phosphate Buffered Saline (PBS) (Sigma-Aldrich)
- HOECHST 34580 (bisbenzimidazole dye) (BD Pharmingen™)
  A blue fluorescent dye for "DNA and nuclei in live or fixed cells" [97]
- Alexa Fluor™ 488 NHS Ester (Succinimidyl Ester; AF488) (Thermo Fisher Scientific)
  A green-fluorescent dye that binds covalently to primary amines, that can be found in proteins or other molecules. [98]

### 5.1.3 Cell line

- 4T1 (ATCC® CRL-2539™)
  A murine triple negative breast cancer cell line.
- 4T1-PGKiRFP720 (4T1 cells stably transduced with LV encoding for iRFP720 (Ref: Geyer et al, PMID 28874076)

## 5.2 Microorganism

| Organism | Provided by |
|---|---|
| Archaea strain *Methanococcus maripaludis* S0001 | Univ.-Prof. Christa Schleper, Dr. Simon Rittmann, and M.Sc. Barbara Reischl<br>(Archaea Biology and Ecogenomics Division - Department of Ecogenomics and Systems Biology, University of Vienna) |

## 5.3 Histology

### 5.3.1 Instruments

- Paraffin dispenser (SLEE MPS/P1, SLEE Medical GmbH)
- Table-top cooling plate, Para Cooler A (Weinkauf Medizintechnik)
- Tissue embedding cassette, 45° angle, with lid, Scientific Histosette™ I (Simport™)
- Freezer -20 °C (Thermo Scientific)
- Freezer -80 °C (Thermo Scientific)
- Eppendorf tubes (Nerbe Plus GmbH)
- Metal base molds, 7x7 (Leica Biosystems)
- Tissue Tek® O.C.T™ Compound (Sakura Finetek Europe B.V.)
- Refrigerator 4 °C (Allectric)
- Eppendorf® Research® Plus Micropipettes (Eppendorf)
- Centrifuge tubes 15 ml, 50 ml (Starlab)
- Pipette tips (Nerbe Plus GmbH)
- Aluminum foil, available in commerce
- Parafilm®, All Purpose Laboratory Film (Pechiney Plastic Packaging)
- Tissue Tek Cryomold®, Biopsy molds, flat surface 10x10x5 mm (Sakura Finetek Europe B.V)
- Tissue Tek Cryomold®, Biopsy molds, flat surface 15x15x5 mm (Sakura Finetek Europe B.V)
- Medium for embedding frozen tissue specimens.
- Cryostat, MNT (SLEE Medical GmbH)
- Microscope Slide Box, 100 Place Premium (Heathrow Scientific)
- Superfrost® plus microscope slides (Thermo Fisher Scientific)
- Coverslips 24x50 mm (Carl Roth GmbH + Co. KG)
- Coverslips 24x24 mm (Carl Roth GmbH + Co. KG)
- Brushes, available in commerce
- LPS Plasma Blade, low profile (SLEE Medical GmbH)
- Kartell™ PMP Hellendhal Staining Jar (Thermo Fisher Scientific)
- Immersion Oil Type F (Leica Microsystems)
- Paper towels, available in commerce
- Nail polish, available in commerce

- Elite PAP Pen (Cedarlane Laboratories)
- Marking pen which generates a hydrophobic barrier around the specimen.[99]
- Inverted microscope (DM IL LED Fluo, Leica Microsystems)
- Microscope camera (DFC450C, Leica Microsystems)

### 5.3.2 Substances and reagents

- Ethanol, absolute, ≥ 99 % (Thermo Fisher Scientific)
- Ethanol, 70 %, prepared through dilution of ethanol, 96% (Brenntag CEE GmbH)
- 2-Propanol/isopropanol, 99.9 % (Sigma-Aldrich)
- Xylene, > 98 %, pure, for histology (Carl Roth)
- Paraffin-polyisobutylene mixture, for tissue embedding (Paraplast®, Sigma-Aldrich)
- Erythrosin B (xanthene dye) (Sigma-Aldrich)
  A red-orange counterstain for the use in histology. [100]
- 4′,6-Diamidine-2’-phenylindol dihydrochloride (DAPI) solution, 1 mg/1 ml (Sigma-Aldrich)
  A nucleic acid blue-fluorescent dye that binds to adenine-thymine rich regions. [101]
- Paraformaldehyde, 4 % in HBS Buffer (PFA) (AppliChem GmbH)
- Dulbecco’s Phosphate Buffered Saline (PBS) (Sigma-Aldrich)
- Vectashield® Antifade Mounting Medium (Vector Laboratories)
  A medium, which minimizes loss of fluorescence of dyes. [102]

# 6 Methods and methods development

## 6.1 Cell culture

All cell culture experiments including the generation of tumor spheroids were conducted in S1 laboratories of the MMCT, Department of Pharmaceutical Chemistry, University of Vienna.

### 6.1.1 Preparation of growth medium for cells

RPMI-1640 basal medium (containing HEPES-buffer) was supplemented with 10 % (v/v) FCS, 1 % (v/v) L-Glutamine solution 200 mM, and 1 % (v/v) penicillin-streptomycin solution (Pen-Strep). For reasons of simplicity this ready to use complete medium will be referred to as 'medium' in the following.

### 6.1.2 Cultivation of 4T1-murine mammary gland carcinoma cells

4T1 wild type (4T1-wt) as well as 4T1-PGKiRFP720 cells were cultivated/incubated in T-75-cell-culture flasks in pre-warmed growth medium at 37 °C and 5 % $CO_2$ and had to be split at 80 % confluence, which was reached after approximately three to four days.

Due to the lack of appropriate imaging modalities the transduced cell line could not be used for the generation and the following imaging of MCTS. Hence, further cultivation of 4T1-PGKiRFP720 was discontinued in the course of this project and exclusively 4T1-wt cells were used for all experiments. First, the T-75 flask was taken out of the incubator. By examining the state of the cell layer inside the culture flask through the microscope (Inverted Microscope Motic® AE31, Motic) and inspecting the color of the medium (red = ok, yellow = acidic, violet = alkaline) the degree of confluence was assessed.

Initially, the old medium was removed from the flask with a serological pipette and discarded. Then, 5 ml of PBS were added to the corner of the flask which was carefully tilted in order to wash off dead cells. After removing the PBS, 2 ml detaching reagent (Trypsin-EDTA) were added to the cell layer which was then incubated for four minutes. Thereafter, the flask was taken out of the incubator and gently tapped with one hand, so the cells detached from the surface. 3 ml of medium were then added to

the cells in order to neutralize the detaching reagent and to obtain an equivalent volume as the tare-CT (centrifuge tube), the suspension was resuspended several times and subsequently pipetted into a CT-15 (holds 15 ml) and centrifuged for five minutes at 200 g. After removing the supernatant, the obtained cell pellet was resuspended in 1 ml medium and an appropriate amount of cell suspension, according to experimental determinations, was added to a new flask containing 13 ml of medium. Thereafter, the flask was incubated at 37 °C and 5 % $CO_2$.

## 6.2 Cultivation of tumor spheroids

The general workflow of MCTS formation and MCTS-archaea co-culture performed in the course of this project is demonstrated in *Figure 4.* The optimization of the outlined methodologies will be explained in detail in the following.

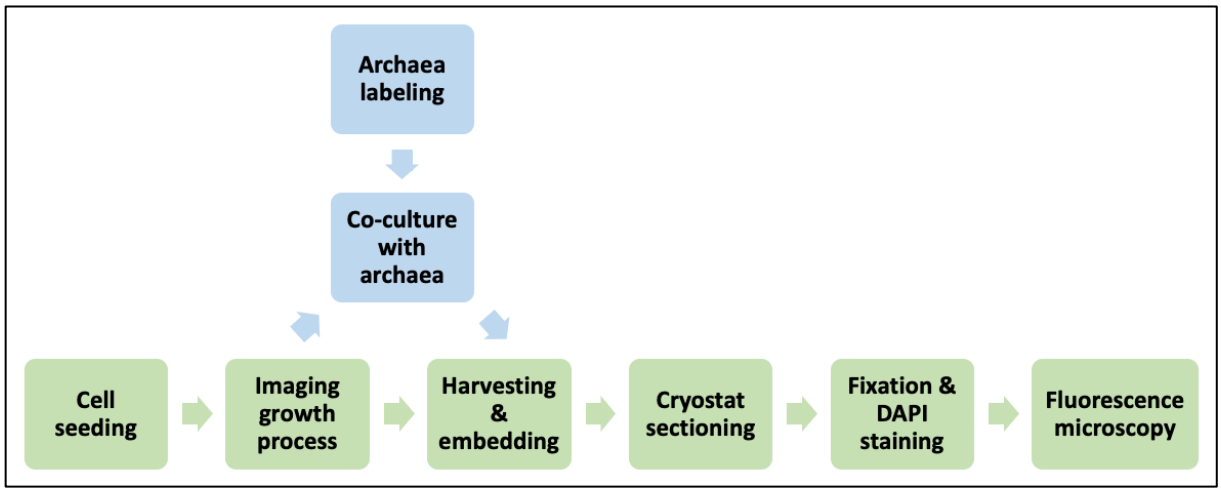


*Figure 4. Workflow for the cultivation of tumor spheroids and co-culture with archaea. Green: generation of tumor spheroids; Blue: co-culture of MCTS + archaea.*

### 6.2.1 Seeding cells in ultra-low attachment 96-well plates

For the cultivation of three-dimensional (3D) tumor spheroids - referred to as MCTS (multicellular tumor spheroids) in the following - the liquid overlay microplate method (explained in detail in chapter 3.2.2) was performed. Therefore, 4T1 cells were seeded in ultra-low attachment 96-U-well plates which promote intercellular aggregation rather than the attachment of cells to the well surface.

The culture flask containing 4T1 cells was examined for confluence and viability just as before splitting cells. After removing the old medium and washing with 5 ml PBS, 2 ml of detaching reagent were added onto the cells and incubated at 37 °C for four

minutes. When taken out of the incubator, the flask was tapped with one hand, so that cells detached from the surface. Next, the flask was flushed and filled up to a total of 5 ml with medium which was then pipetted into a CT-15 and centrifuged for five minutes at 200 g. Hereafter, the supernatant was discarded, and the pellet diluted in 1 ml medium. Due to the high cell density, the suspension was diluted to 5 ml to facilitate cell counting.

For the easy determination of the cell number, Neubauer Improved® hemocytometer was used. Therefore, a small specimen was applied to the counting chamber and cells were counted under the microscope. For obtaining the respective cell numbers in each well, a dilution series was implemented.

Since this project was mainly focused on the development and optimization of several operating procedures, MCTS were generated with varying initial cell seeding numbers to define the most suitable cell count for spheroidal tumor models to be used for co-culture with archaea. Inspired by other research groups, the range of cell counts was chosen as follows: 20,000 | 10,000 | 5,000 | 1,000 | 500 | 200 cells per 200 µl and per well. In the course of this project, the developing MCTS of various cell counts were examined for parameters like stability, size, necrotic core, etc., and thereby the ideal cell number(s) was(were) selected and reproduced. 200 µl of the respective prepared dilutions were transferred into the well plate following the pattern below (*Figure 5*). The adjacent wells were filled with 200 µl PBS in order to expose each spheroid to comparable conditions during growth.

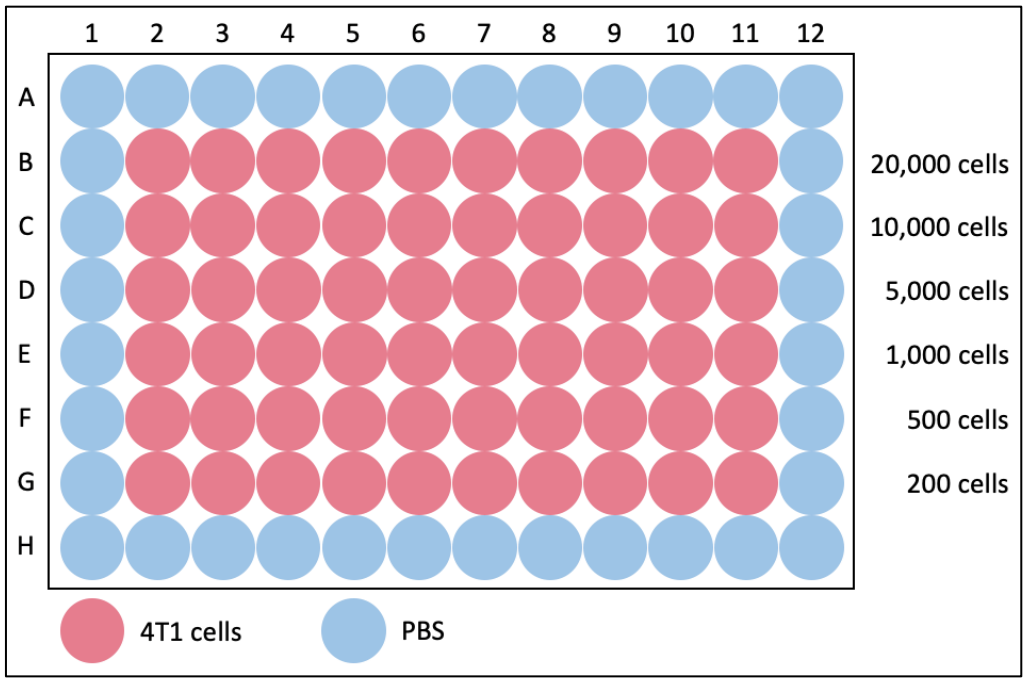


*Figure 5. Seeding pattern of 4T1-tumor spheroids.*

Subsequently, the plate was covered with a lid and incubated at 37 °C and 5 % $CO_2$. Within one to two hours after seeding the forming spheric structures became visible by eye (*Figure 6*). To allow comparison between and optimization of MCTS at different points in time during growth process the duration of MCTS cultivation varied between conducted experiments. Medium was changed every 48 hours until MCTS increased significantly in size where medium was changed every 24 hours.

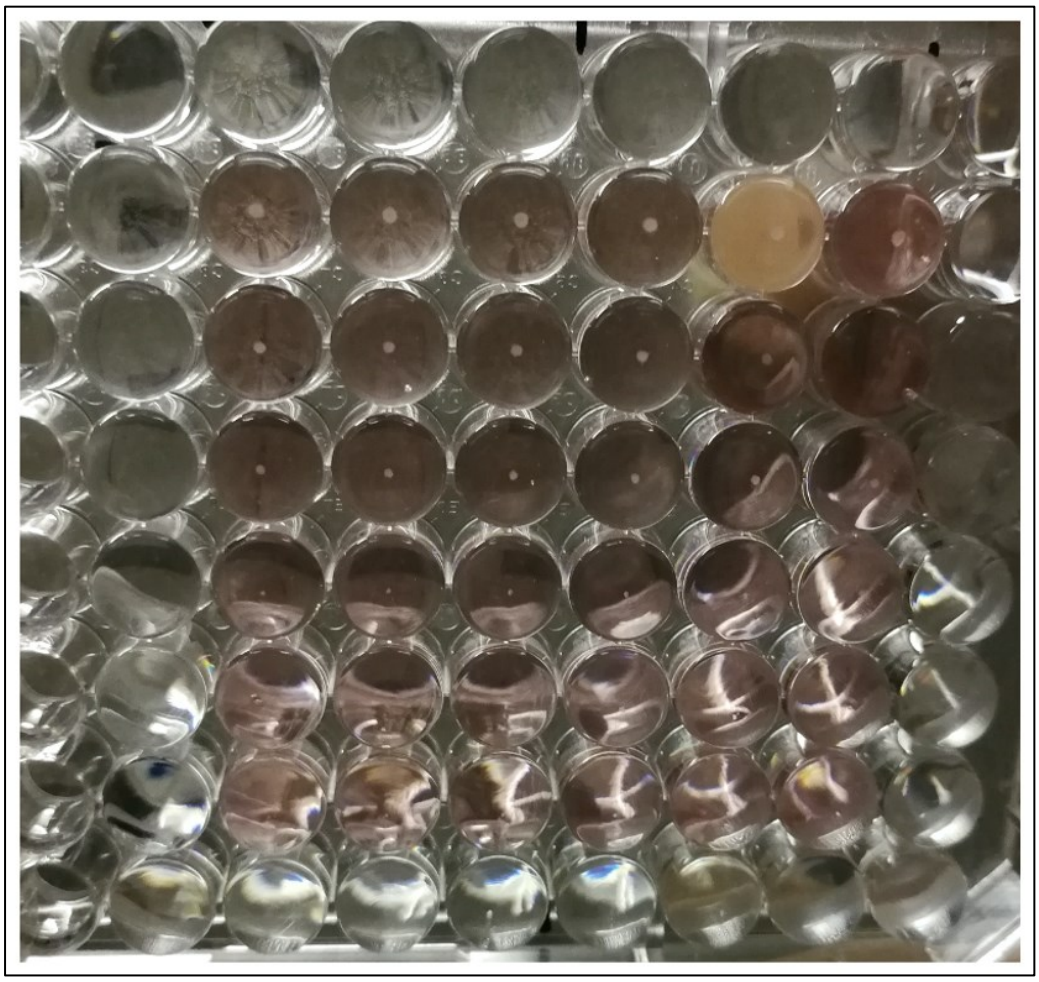

*Figure 6. Formation of spherical structures after 1-2 hours after seeding 4T1 cells in ultra-low attachment well plates.*

### 6.2.2 Imaging of tumor spheroid development

For the demonstration of the morphological development of growing MCTS, one particular spheroid of each respective cell number was followed and imaged by light microscopy. Spheroid imaging was performed every day throughout cultivation or, as soon as we had introduced MCTS-archaea co-culture experiments, until the day of inoculation. Then, fluorescence microscopy imaging of spheroid sections was initiated as described below. The respective spheroids were imaged in fourfold and tenfold magnification and the developmental progress was illustrated by arranging the pictures in rows (please refer to *Figure 11* in chapter 7.1.1).

Thus, the formation of MCTS with various cell seeding counts could be observed and characterized in view of size, shape, cell cohesion and generation of a necrotic core. The reproduction of spheroids of equal cell counts in subsequent experiments allowed

the comparison of quality among different spheroid sizes and hence, the determination of MCTS which delivered the most suitable tumor models for co-culture with archaea.

### 6.2.3 Pre-fixation of whole tumor spheroids

The fixation of cells or tissues serves to maintain the morphology of the sample and to increase its stability by deactivating any biochemical reactions. In this project, 4 % paraformaldehyde (PFA), which functions as a crosslinking (induces covalent bonds) fixative between proteins and the cytoskeleton, was used. [103] Pre-fixation is referred to as the fixation of whole tumor spheroids prior to the embedding step and should be evaluated whether or not it was a crucial step for achieving desired results.

A selection of MCTS was fixed directly within the well plate, and remaining spheroids were left without pre-fixation for comparison reasons. First, the medium of each well was carefully removed, then, spheroids were washed with PBS twice and once with PFA. 200 µl of PFA were added to each well, the well plate was covered with parafilm and aluminum foil and stored at 4 °C for 24 hours. Hereafter, the PFA was discarded, MCTS were washed with PBS three times and stored in 200 µl PBS at 4 °C in the refrigerator.

### 6.2.4 Pre-staining of tumor spheroids (Erythrosin B dye)

To be able to detect the smaller MCTS during the subsequent steps, we decided to dye the cellular structures and thereby making the spheroids visible. Inspired by numerous people on research forums discussing Erythrosin B as a suitable agent for staining spheroids, one of those delineated methods was applied. Therefore, a 0.2 % Erythrosin B in PBS solution was prepared in a CT-15. Since it was yet unclear whether this dye should be used for further experiments, the staining was conducted under sterile conditions (in laminar air flow, LAF). The MCTS were stained directly inside the well plate by removing the PBS, then adding a small amount of the dye, and incubating them for five minutes. Hereafter, the solution was discarded, the spheroids were washed twice with PBS and each well was filled up with PBS and stored at 4 °C. Although the staining was successful (*Figure 7*), this step was not performed in subsequent experiments as it had turned out to be a redundant step.

### 6.2.5 Desiccation of tumor spheroids

The suitability of paraffin wax as an embedding medium for MCTS should be evaluated. Paraffin represents a substance which is immiscible with water, hence, a preceding full desiccation of the samples needed to be performed. The well plate containing the previously PFA-fixed and stained MCTS was taken out of the incubator. After removing the PBS of each well, spheroids underwent a dehydration series with increasing alcohol concentrations to eliminate residual traces of water. The sequence started with the incubation of each spheroid in 200 µl 70 % ethanol for five minutes, continued with 200 µl 100 % ethanol for five minutes and 200 µl isopropanol for 10 minutes. To remove the alcohol, MCTS were incubated with xylene, which serves as a clearing agent, for three minutes. The desiccation of spheroids proved to be unsuccessful and represented an unnecessary step during embedding and was hence not performed in subsequent experiments.

### 6.2.6 Harvesting of tumor spheroids and embedding in paraffin wax

The smallest available metal embedding molds were placed onto the surface of the Tissue Embedding System® and a little amount of liquid paraffin (65 °C) was added. One single spheroid was transferred into one respective mold by taking it up directly with a pipette tip. Subsequently, the molds were filled up with paraffin until the attached cassette was appropriately covered, and incubated for one hour at 65 °C. In histological sample preparation, paraffin functions as a tissue penetrating agent and also replaces xylene. [104] Finally, MCTS were positioned in the center of the metal mold and placed onto the cooling plate (-25 °C) until solidified. After carefully detaching the metal mold from the paraffin block, MCTS turned out not to be embedded properly, and therefore could not be utilized for subsequent sectioning (*Figure 7)*.

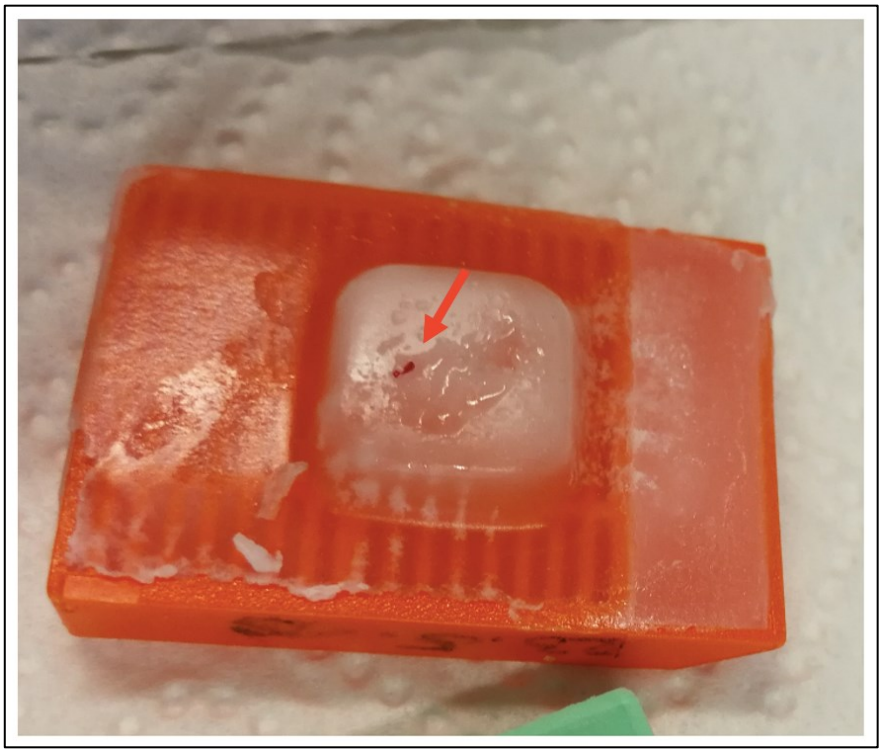

*Figure 7. Unsuccessfully embedded tumor spheroids in paraffin wax. Red arrow indicates Erythrosin B-stained MCTS.*

### 6.2.7 Optimized harvesting of tumor spheroids and embedding in Tissue Tec® O.C.T.™ Compound

Inspired by M.Sc. Debora Wernitznig's standard operating procedures (SOPs), the harvesting, embedding and cryostat sectioning of MCTS could be improved and simplified to a great extent.

Spheroid harvesting was performed after various cultivation durations (T1-T6; for more detailed information please refer to chapter 7.1.2) in order to determine the ideal time after which the spheric formations showed sufficient size but also high enough stability. During the first stage of the project though, which was focusing on the development and optimization of standard operating procedures and the practice of such, MCTS were randomly harvested after four and ten days of cultivation.

After taking the well plate out of the incubator and placing it into the LAF, three spheroids of the same cell count were transferred into one respective appropriately marked eppi by using a pipette tip. Therefore, 1,250 µl pipette tips (widest diameter) were used to avoid damaging the MCTS, especially larger sized ones. Importantly, enough medium had to be taken up with the spheroids as this turned out to be essential

to achieve favorable results, as described below. In an early experiment, it was shown that 1,250 µl Pipette tips display a wide enough aperture even for the transfer of the largest spheroids, and hence, do not need to be cut.

Three spheroids of the same cell number were collected in one Eppendorf tube (eppi) respectively. As for the preparation of MCTS embedding, one drop of the embedding medium Tissue-Tek® O.C.T.™ Compound was added to the smallest available (10x10x5 mm) and appropriately labelled plastic cryomolds.

Thereafter, one by one spheroid plus a small amount of growth medium was cautiously pipetted in the center of the cryomold containing the embedding medium. Three MCTS needed to be arranged on one horizontal level while ensuring the spheroids not be placed at the very bottom of the mold. This proved to be crucial as during the subsequent cryostat adjustment their outer layer could get damaged, as described below (*Figure 8*).

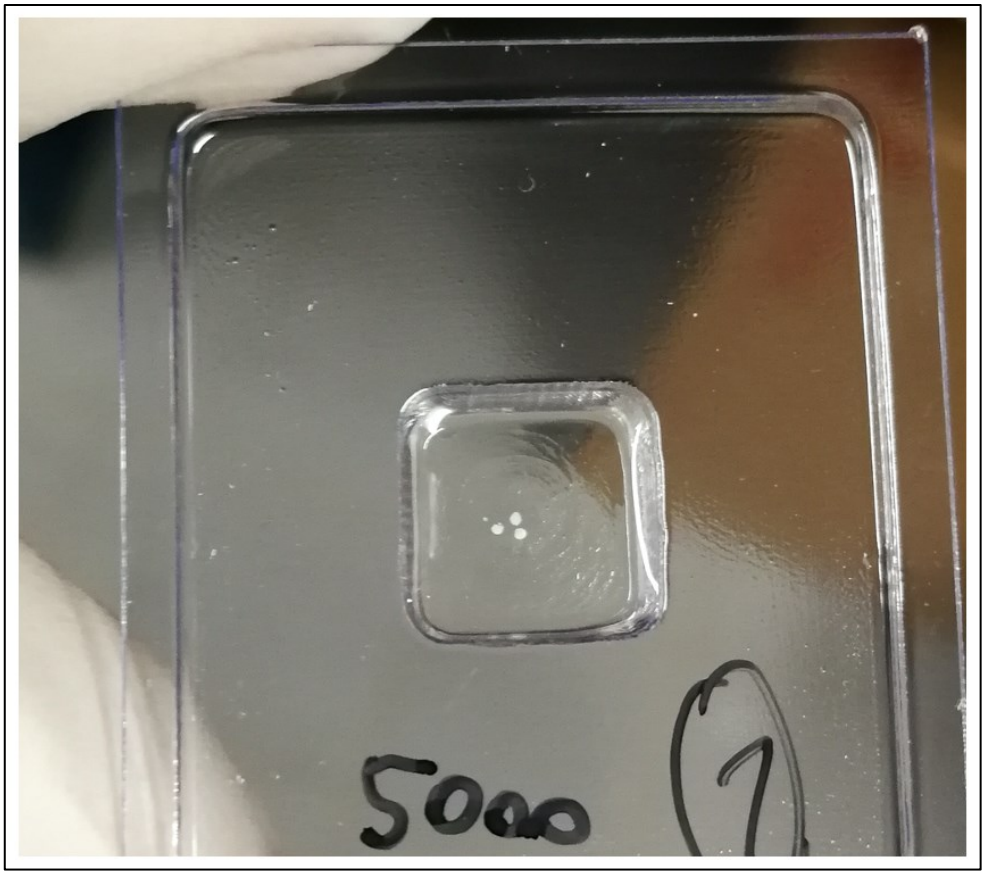


*Figure 8. Three 5k-tumor spheroids embedded on one horizontal level in a cryomold (10x10x5 mm).*

For bringing the MCTS in their ideal position, a clean pipette tip was used. Finally, Tissue-Tek® O.C.T.™ Compound was added to all molds up to the rim plus one or two drops as the block would be decreased in size when frozen.

The molds were then put into a box with lid for protection and placed into the freezer at -20 °C or at -80 °C for long-term storage in case cryostat sectioning should not be performed within three to four days after embedding. After approximately one hour, the blocks were ready to use for cryostat sectioning.

### 6.2.8 Cryostat sectioning of tumor spheroids

The cryostat was switched on at least one hour prior to the planned sectioning as it took about one hour to cool down to a temperature of -20 °C. In order to produce useable and uniform sections the settings needed to be maintained throughout all experiments. The trimming function, which delivers coarse cuts and was used for the initial approach towards embedded spheroids, was set to 10-15 µm. The cutting function, which generates fine sections of the MCTS, was set to 5 µm. The cryostat sectioning was performed by using the automatic cutting function with a defined speed of 5 mm/s downward and 22 mm/s upward.

To adjust the temperatures of MCTS blocks and the interior of the cryostat, the blocks were removed from the freezer and stored in the cryochamber for a few minutes. After acclimatization, a specimen holder was taken from the cryochamber and defrosted at room temperature. Thereafter, an appropriate blade was inserted. After adding one drop of Tissue-Tek® O.C.T.™ Compound in the center of the specimen holder, the embedded sample was cautiously pushed out of the mold and immediately mounted onto the specimen holder as evenly as possible. Then, the disc was placed in one of the holes of the quick freeze shelf® for 30 seconds until the specimen was stably attached to the disc.

After locking the handle of the manual lever in the upper position, the shaft of the disc was clamped into the specimen head by tightening the screws (*Figure 9*) The specimen plane was aligned with the cutting edge by loosening or tightening the orientation screws on the specimen head. Then, the handwheel was unlocked and turned with the set trimming function until the specimen surface approached towards the blade. The use of extremely sharp blades represented a crucial factor to achieve useable spheroid

sections. The manual sectioning and adjusting was continued until obtained sections appeared even and regular, then the automatic cutting function was initiated.

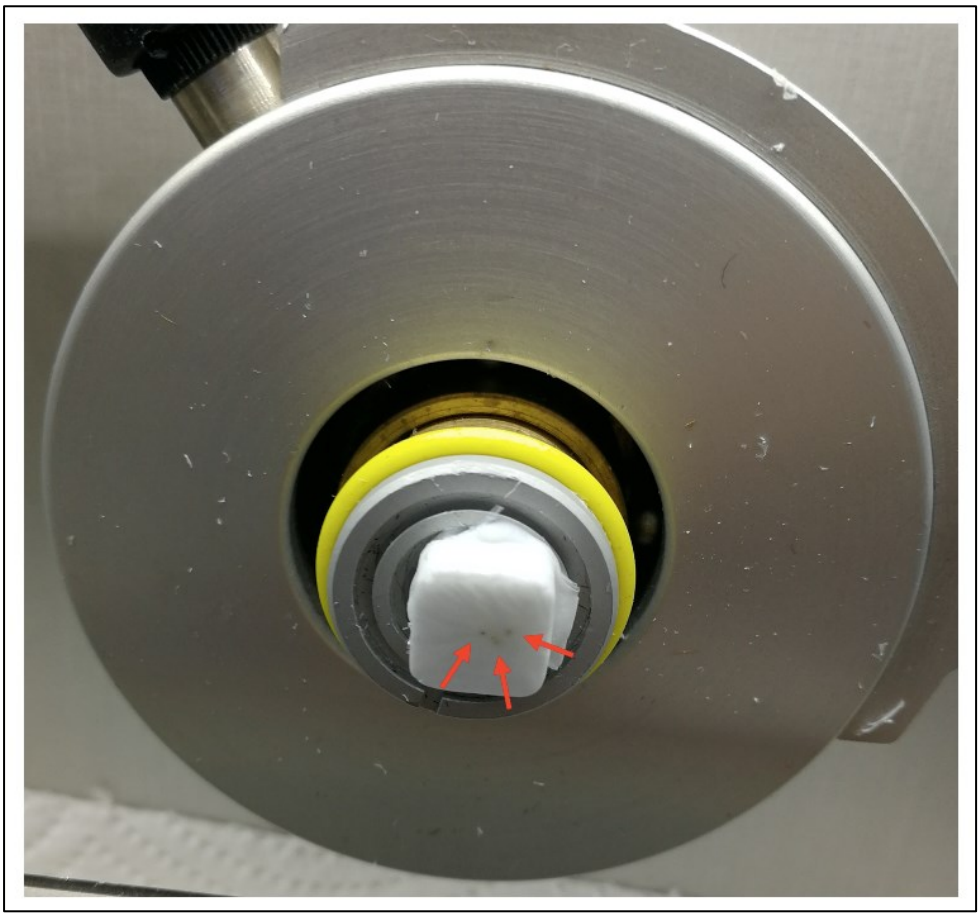

*Figure 9. Frozen cryo-matrix block containing three tumor spheroids attached to specimen disc. Red arrows indicate three single MCTS.*

The sequentially delivered sections were caught on one corner or an edge with the tip of a fine brush and transferred onto a SuperFrost® plus microscope slide. In case the section could not be lifted, it was gathered up with the microscope slide by gently pressing it onto the approaching section.

As long as the edge of the MCTS was not yet visible in the form of a tiny white dot on the slide when watched against the light, the automatic trimming was continued until dots appeared on sections. As soon as this was the case, a new microscope slide was utilized for the successive collection of all sections exhibiting the sample.

All specimen blocks were cut until no sample could be spotted on the slides anymore. The arrangement of sections on the slides followed a specific pattern in order to be

able to retrace the approximate location of all such sections within the three-dimensional spheroid (*Figure 10)*. Accordingly, after the last section containing the sample was transferred, the microscope slides were labeled ‘beginning’ or ‘inner’ or ‘end’ by determining their probable origin within the MCTS. Subsequently, the microscope slides were placed into slide boxes by arranging them correspondingly to their sectioning order. This order was maintained throughout all subsequent experiments. To avoid the detachment of the samples from the slides or modifications in their shape, the box was stored in the freezer at -20 °C for short-term storage (four to five days) or at -80 °C for prolonged storage.

*Figure 10. 5k-tumor spheroid sections arranged in a successive order on a microscope slide.*

To evaluate the reproducibility of results until this point and also for practice purposes, the preceding experiments were repeated by harvesting MCTS of the same plate at a later time.

### 6.2.9 Fixation of tumor spheroid sections and nuclear staining with DAPI

For the visualization of cancer cells under the microscope, the prepared MCTS sections were stained with the fluorescent cell nuclei dye DAPI. DAPI binds to regions in the DNA displaying adenine and thymine and hence stains cell nuclei. DAPI is capable to permeate through intact cell membranes and therefore dyes live and fixed cells. [101] Since archaea possess a ring chromosome, DAPI also stains archaeal cells, which, however, did not influence the evaluation of the fluorescence images later on.

For the sake of preservation and increase of mechanical stability of spheroid sections, a histological fixation was performed prior to the staining procedure. Also, to avoid washing off the cryosections during the staining process, this fixation was inevitable. Therefore, the slide box was taken out of the freezer and placed under the laboratory hood. The microscope slides containing the spheroid sections were placed on a paper towel and thawed at room temperature. A staining jar was filled with a 4 % PFA solution wherein spheroid section-containing slides were placed and incubated for 30 minutes. Subsequently, after discarding the PFA solution, the jar was filled with PBS. The PBS was discarded, and the jar was filled with PBS again to wash off the PFA solution. After repeating this washing step for one more time, the jar was filled up with PBS in order not to allow the slides to dry up. By holding the microscope slides against the light, it was ensured that the MCTS sections were not flushed off the slides. This fixation step will be referred to as post-fixation as it was performed after spheroid embedding.

Another preparation step for the staining with DAPI was the encircling of single or grouped spheroid sections with a hydrophobic pen (Elite PAP® Pen). By doing so, the staining solution could be used economically and specifically at the precise area of interest. The spheroid sections were clearly visible as small white dots when held against the light and therefore could easily be detected. After applying the circles, the slides needed to be placed back into the PBS-containing jar to avoid letting them dry up.

MCTS sections were dyed with a 2 µg/mL DAPI in PBS solution, which was prepared by adding 2 µl of the DAPI stock solution (1 mg/ml) to 998 µl PBS. For the staining of the sections of one slide, approximately 1.5 ml DAPI solution were needed, hence, the appropriate amount was prepared. Equally as for the other fluorescent dyes, the

staining procedure ideally had to be conducted with the exclusion of light due to DAPI's light sensitivity. Then, after placing one by one microscope slides on paper towels, drops of the DAPI solution were added to the encircled spheroid sections with a pipette. To minimize evaporation and exposure to light, the slides were incubated in lightproof boxes for 20-30 minutes.

Afterwards, the slides were put back into PBS filled containers to remove the excess stain and subsequently washed with PBS five times. Again, until the slides were being processed, they were consistently kept in PBS to avoid dehydration. Consecutively, the slides were removed from the jar and carefully dabbed onto paper towel to remove the liquid. For the preservation of DAPI's fluorescence, one to two drops of mounting medium were added to each slide and covered with a cover slip. To achieve homogeneous spreading of the medium, the coverslip was pressed down from top to bottom with a pipette tip. The excessive mounting medium was removed and conclusively, the coverslip was sealed with nail polish. Until fluorescence imaging, the slides were placed into opaque slide boxes and stored at 4 °C. The subsequent fluorescence imaging will be discussed in chapter 6.3.6.

## 6.3 Co-culture of tumor spheroids and archaea

This project was conducted based on the collaboration of different departments (for detailed information please refer to chapter 5.2). All MCTS-archaea co-culture experiments were performed in laboratories of the MMCT, Department of Pharmaceutical Chemistry, University of Vienna.

To provide and maintain anaerobic conditions, archaea were preserved in an anaerobic serum bottle equipped with a rubber stopper, suspended in culture medium. The respective concentrations of cells per milliliter were determined by M.Sc. B. Reischl by means of optical density- (OD-) measurement and communicated.

### 6.3.1 Preparation of specific concentrations of archaea

The provided archaea culture came in lower concentrations than required for the inoculation of MCTS, and hence had to be increased. Initially, the needed amount of archaea was calculated depending on the required number of MCTS to be inoculated when using 20 µl per spheroid. To achieve a tenfold higher concentration, 2 x 1 ml of the suspension were extracted from the serum bottle by using a syringe and needle

and transferred into two respective eppis. Strict attention needed to be placed on securing the syringe in its proper position given the pressurized environment in the bottle. This was also important for safety reasons. The two eppis were then placed in the centrifuge for five minutes at 6,800 g to obtain a cell pellet.

After removing the eppis from the centrifuge and inspecting them by holding them against the light, no pellet could be identified at first. For subsequent experiments the archaea cell pellet was clearly visible due to higher concentrations. As there was the possibility of having a cell pellet which could not be spotted by the naked eye, the pellet was assumed on the bottom of the tube. Carefully, the supernatant archaea culture medium was removed with a pipette and discarded. To wash off the archaea growth medium, 100 µl PBS were added to the two eppis respectively, the pellet was resuspended and the 2 x 100 µl combined in one eppi. By extracting 20 µl from this suspension and diluting it with 180 µl PBS, two concentrations with cell numbers differing by a factor of 10 were prepared for comparison reasons.

### 6.3.2 Staining of archaea with HOECHST

In search of methods to label archaea for the subsequent identification among DAPI-stained cancer cells, archaea were dyed with blue-fluorescent HOECHST stain, a live and dead cell dye which binds to thymine-adenine-rich regions in the minor groove of DNA. [97] Therefore, a solution of 5 µg/ml HOECHST in PBS was prepared. The archaea cell pellet, which was prepared as described previously, was resuspended in 50 µl PBS. Then, 50 µl of the HOECHST dye were added to the eppi containing the archaea and thoroughly mixed by pipetting up and down. The eppi was wrapped in aluminum foil to avoid exposing the light-sensitive HOECHST stain to light, and subsequently, the eppi was left for incubation for 30 minutes.

Thereafter, the suspension was centrifuged for five minutes at 8,000 g, the supernatant was discarded. The centrifugation was repeated three times whereby 100 µl PBS were used respectively to resuspend the cell pellet. Finally, two concentrations were prepared for comparison reasons. HOECHST-labeling of archaea, however, did not yield expected results as archaea could not be identified among DAPI-labeled cancer cells at later fluorescence imaging (*Appendix Compl. Figure 25*).

### 6.3.3 Staining of archaea with Alexa Fluor® 488 (AF488)

As the identification of archaeal cells among cancer cells proved to be impossible when using HOECHST stain for archaea and DAPI for MCTS sections, a different staining method needed to be chosen. Alexa Fluor 488® (AF488) is a green-fluorescent dye containing a succinimidyl ester which binds covalently to primary amines which can be found in proteins as well as in other molecules. [98]

The staining of archaea with AF488 succinimidyl ester was conducted in a similar way as priorly described for the HOECHST dye, however different concentrations of the dye were applied. As this project was performed to optimize the various parameters to create ideal three-dimensional cancer research models for the co-culture with archaea, parameters such as concentrations of agents, cell seeding numbers, etc., were altered for consecutive experiments depending on the observations that were made.

For the labeling of archaea with AF488, 5 µl of the dye were added to 150 µl archaea suspension followed by a quick mixing on the vortex. This concentration was determined empirically and maintained throughout all experiments. To ensure significant results, an equal amount of archaea suspension was left unstained for comparison purposes. As before, for the protection of the light-sensitive dye, the eppi was wrapped in aluminum foil and thereafter placed on the shaker for 4 hours for incubation. The suspension was mixed on the vortex every hour. After the expiration of the incubation time, the eppi was centrifuged for five minutes, and the supernatant was removed. Thereafter, the pellet was resuspended in 150 µl PBS and centrifuged again. This “washing” step was repeated two times to remove the surplus of AF488 dye molecules in the suspension. Subsequently, the pellet was resuspended in 150 µl PBS. The obtained archaea suspension was used for co-culture experiments with MCTS.

To evaluate the potential of AF488 to stain the archaea surface proteins and thus to be a suitable dye for their identification, a small sample of the archaea suspension (approximately 10 µl) was transferred onto a microscope slide, sealed with nail polish and checked under the microscope. Equally, the unlabeled (AF488-untreated) archaea suspension was examined for the presence of a potential autofluorescence signal by fluorescence microscopy.

### 6.3.4 Inoculation of tumor spheroids with archaea

For the inoculation of MCTS, the well plate was removed from the incubator, placed in the LAF and the lid was removed. Due to the developmental character of this project, the inoculation was conducted at various points in time (e.g. day 6|7|8 etc. after seeding; for detailed information please refer to chapter 7.2.2). After resuspending, 40 µl of the prepared archaea suspensions were pipetted to each spheroid-containing well respectively, following a specific pattern. Every well contained one spheroid of the particular cell seeding number. However, a certain number of MCTS were left without archaea inoculation for control purposes.

Hence, MCTS were either inoculated with AF488-stained archaea (referred to as AA in the following), unlabeled archaea (UA) or were not treated with archaea (UT).

*Table 2. Abbreviations and their meanings.*

| **Abbreviation** | **Meaning** |
|---|---|
| AA | MCTS + AF488-dyed archaea |
| AU | MCTS + undyed archaea |
| UT | Untreated MCTS |

Due to the required anaerobic environment of the archaea, it was crucial to work at a faster pace as soon as the archaea got exposed to atmospheric oxygen. Also, after the last spheroid was inoculated, the well plate needed to be sealed tightly with parafilm to provide an anaerobic setting. In addition, the plate was wrapped in aluminum foil to avoid loss of fluorescence intensity of AF488. Finally, the well plate was placed in the incubator at 37 °C.

### 6.3.5 Preparation of spheroid sections for imaging

#### Harvesting of tumor spheroids at different timepoints, embedding, cryostat sectioning, histological fixation, and DAPI staining of tumor spheroids

As for the harvesting of the cultured archaea-inoculated MCTS, specific points in time were selected (T1-T6; for more detailed information please refer to chapter 7.1.2). The procedure of harvesting, embedding, cryostat sectioning, histological fixation, and DAPI staining of the MCTS was performed in an analogous manner as described in chapters 6.2.7, 6.2.8, and 6.2.9.

### 6.3.6 Imaging of tumor spheroid sections by fluorescence microscopy

To assess the archaea's potential to infiltrate MCTS, the slides containing spheroid sections were examined under the fluorescence microscope. Pictures were taken in twenty- and fortyfold magnification by means of the Leica Application Suite (LAS) X software. The fortyfold objective was utilized with immersion oil to achieve higher resolutions. To obtain fluorescent images, MCTS sections were excited with light of respective wavelengths by using green (excitation of AF488) and blue filters (excitation of DAPI). Also, brightfield images were taken for the later assembly of pictures. The subsequent merging of the various images taken of one particular spheroid section provided the basis of interpretation of the archaea's potential to migrate towards the center of the spheroid.

# 7 Results and discussion

## 7.1 Cultivation of tumor spheroids

**Optimization of 4T1-tumor spheroids**

The generation of three-dimensional 4T1 MCTS of defined cell counts was performed by seeding respective cell suspensions in ultra-low attachment 96-U-well plates. In order to determine the cell seeding number(s) yielding spheroids with the most suitable properties for co-culture with archaea, the following cell counts were selected: 20,000 | 10,000 | 5,000 | 1,000 | 500 | 200 cells per well. The aim of generating spheroids of various sizes was to identify those exhibiting high stability, development of a necrotic core, appropriate size and durability. Regardless of the number of cells seeded, within one to two hours, spheroidal formations had established and reached sizes large enough to be visible to the eye (*Figure 6*).

### 7.1.1 Imaging of tumor spheroid development

The morphological development of MCTS was pursued by imaging one representative spheroid of each cell number by light microscopy every day throughout the entire cultivation time or until the day of archaea inoculation. Pictures were taken in four- and tenfold magnification to assess spheroid size and shape, cell cohesion, necrotic core formation and time-dependent development. Spheroids of respective cell counts were followed over extended periods of time in order to assess the optimal stage for harvesting. *Figure 11* displays a representational selection of MCTS imaged by means of light microscopy at distinct points in time during growth process. An illustration of different tumor spheroids can be found in the attached *Appendix* (*Compl. Figure 23*).

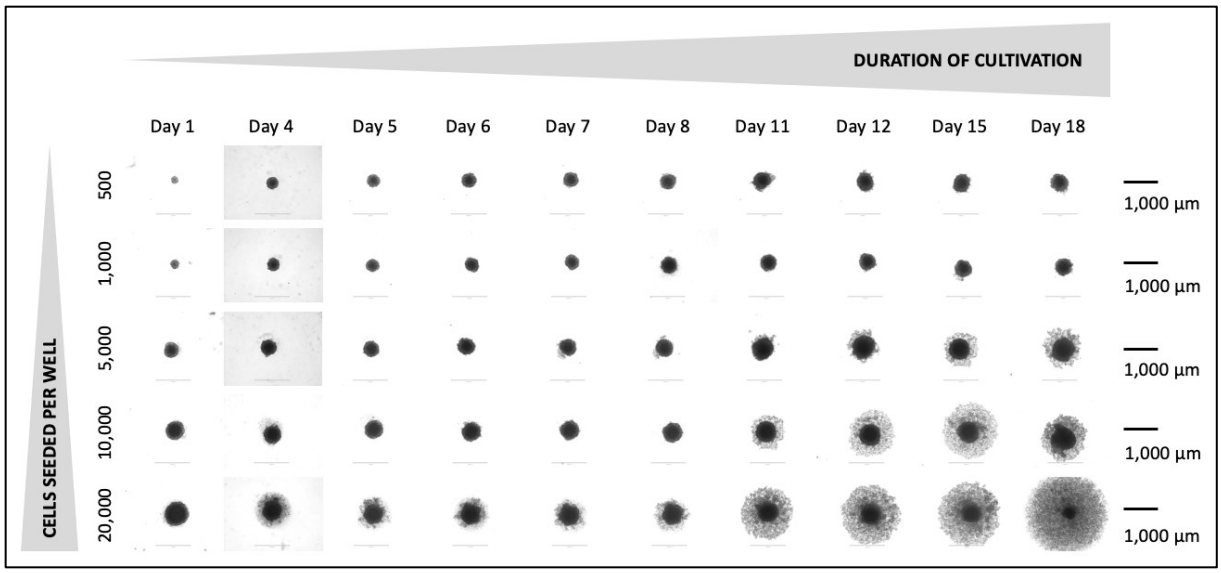


*Figure 11. Illustration of the morphological development of selected, representative 4T1-tumor spheroids over a period of 18 days. Spheroids of the following cell seeding numbers are portrayed in 4x magnification visualized by light microscopy: 20,000; 10,000; 5,000; 1,000; 500. (For further details regarding spheroid generation and imaging please refer to chapter 6.2 and Table 3). Scale bar: 1,000 µm.*

For simplification, MCTS derived from 20,000 seeded cells will be referred to as 20k-MCTS, MCTS from 10,000 cells to as 10k-MCTS, etc. The circular and relatively regular cell formations that are demonstrated in *Figure 11* let us draw the conclusion that cells had organized in a spheroidal cluster rather than being attached to the plate surface. Spheroids of all cell seeding numbers experienced alterations in morphology during incubation time. 20k-MCTS exhibited constant increase in diameter far beyond 1,000 µm from day 11 onwards, probably due to the strong loosening of cells in the outer zone. Presumably, the overall loss of cell density entailed a substantial decrease in stability. The lack of stability particularly became evident during the harvesting of the spheroid. Comparatively, 10k-MCTS remained fairly compact up until day 8 when outer cell layers started to become more loosely assembled. Nevertheless, the inner core appeared to endure in its density throughout the entire cultivation time. 10k-spheroids reached diameters larger than 1,000 µm on day 11 but remained below the size of 20k-MCTS. 5k-MCTS developed similarly to 10k-MCTS, however, they displayed less cell dispersal, hence, higher overall compactness and higher relative increase in diameter which slightly exceeded the 1,000 µm. 1k-MCTS and 500 cell-MCTS both displayed inconsistent growth with considerable gain in size up until day 4 and a rather moderate growth thereafter. Both reached diameters of around 500 µm at the end of cultivation time.

Initially, spheroids of all cell seeding numbers were used for MCTS-archaea co-culture experiments. However, as can be observed in *Figure 11 & Appendix* Compl*. Figure 23*, 5k- and 10k-MCTS appear to be the most suitable tumor models due to uniform and constant increase in diameter, invariable central density, and consistent stability and growth. Hence, 5k-and 10k-MCTS were used for final experiments. Eventually, 5k-MCTS were considered the models with the most preferable features, such as structural cohesion (*Figure 11*), mechanical stability, and development of a necrotic core (*Figure 13*) and were exclusively used for the concluding experiment.

### 7.1.2 Optimized harvesting of tumor spheroids and embedding in Tissue Tec® O.C.T.™ Compound

Successfully cultivated MCTS were harvested after different incubation durations, namely 24 h, 48 h, 72 h, 96 h, 120 h, or 168 h after cell seeding. The various incubation periods were aimed at the identification of the optimal harvesting time in order to obtain spheroids with both sufficient size and stability. Additionally, due to its relevance for co-culture with archaea, the time-dependent development of a necrotic core was examined.

Spheroid harvesting was performed using wide diameter pipette tips in order not to damage the three-dimensional structure. Selected MCTS of all sizes were harvested and transferred into respective eppis successfully without the spheroidal shape sustaining damage. The subsequent transfer into Tissue-Tek® O.C.T.™ Compound-containing cryomolds (10x10x5 mm or 15x15x5 mm) was optimized by following specific work- and time-saving procedures. After several cryostat sectioning trials and errors it could be shown that the procedure could be facilitated to a great extent by using the smallest available cryomolds (10x10x5 mm) since MCTS could be detected much easier within the smaller volume. Furthermore, taking the time for the precise positioning of the spheroids in the mold during embedding (on one horizontal level) (*Figure 8*) had crucial importance for saving time during the sectioning process as well as for obtaining more informative results.

### 7.1.3 Cryostat sectioning of tumor spheroids

To improve the quality of delivered spheroid sections, several procedures during cryostat sectioning needed to be optimized as already described in chapter 6.2.8 to

some extent. The usability of sections depended strongly on a slow and uniform operation of the cryostat by using the automatic cutting function which allowed consistent results. Moreover, quite frequently, the section quality was affected by the blunting of the knife which then could be shifted to one side or the other to change the cutting position. Ultimately though, the blade needed to be exchanged from time to time as an extremely sharp blade proved to be essential for gaining sections of good quality. As soon as the knife became dull, the sections crumpled up and got lost rather than sliding over the blade evenly and unfolded. Also, the material residues that accumulated through the process needed to be swept off the knife carefully with a brush to ensure clean sections. Another crucial factor to facilitate later experiments was the immediate arrangement of sections on the slide following a particular pattern (*Figure 10*) in order to be able to retrace the approximate location of all such sections within the three-dimensional spheroid as well as to identify a potential necrotic core. Eventually, cryostat sectioning was optimized to successfully produce spheroid sections with homogenous size and quality to be used for further experiments.

### 7.1.4 Fixation of tumor spheroid sections and nuclear staining with DAPI

Both pre-fixation (prior to embedding) and post-fixation (fixation of MCTS sections) methodologies were performed in order to identify the optimal procedure to preserve the spheroid morphology. It became apparent that pre-fixation represented an optional step for the maintenance of the mechanical and morphological stability of the spheroid sections, whereas post-fixation proved to be indispensable for sustaining the section structure and its adhesion to the slide during the staining process. These observations suggest that post-fixation represents an inevitable step prior to histological staining procedures of spheroid sections. The subsequent staining of MCTS sections with DAPI allowed a clear visualization of cancer cells during fluorescence imaging, and hence, is a suitable dye for 4T1 cells.

**Visualization of necrotic core in tumor spheroids**

To evaluate the three-dimensional assembly of differently sized MCTS, sections were stained with the fluorescent cell nuclei dye DAPI and imaged by fluorescence microscopy.

*Figure 12* demonstrates an array of successively obtained spheroid sections derived from one 5k-spheroid which was incubated for 168 h. As can be seen, the spheroid

reached a diameter of approximately 500 µm which represents the size at which MCTS develop hypoxic and necrotic regions within their core. [31] The red arrow indicates the spatial direction from outer zones of the spheroid towards its center. Hence, the picture in the top left corner displays a section derived from the outer third of the spheroid, the subsequent images originate from spheroid zones further towards the center, and the picture in the bottom left corner shows a section derived from the equatorial inner spheroid zone. As exemplified here, the closer to the center the less fixable histological structures can be identified, suggesting the presence of a hypoxic and necrotic core starting roughly 150 µm below the spheroid surface.

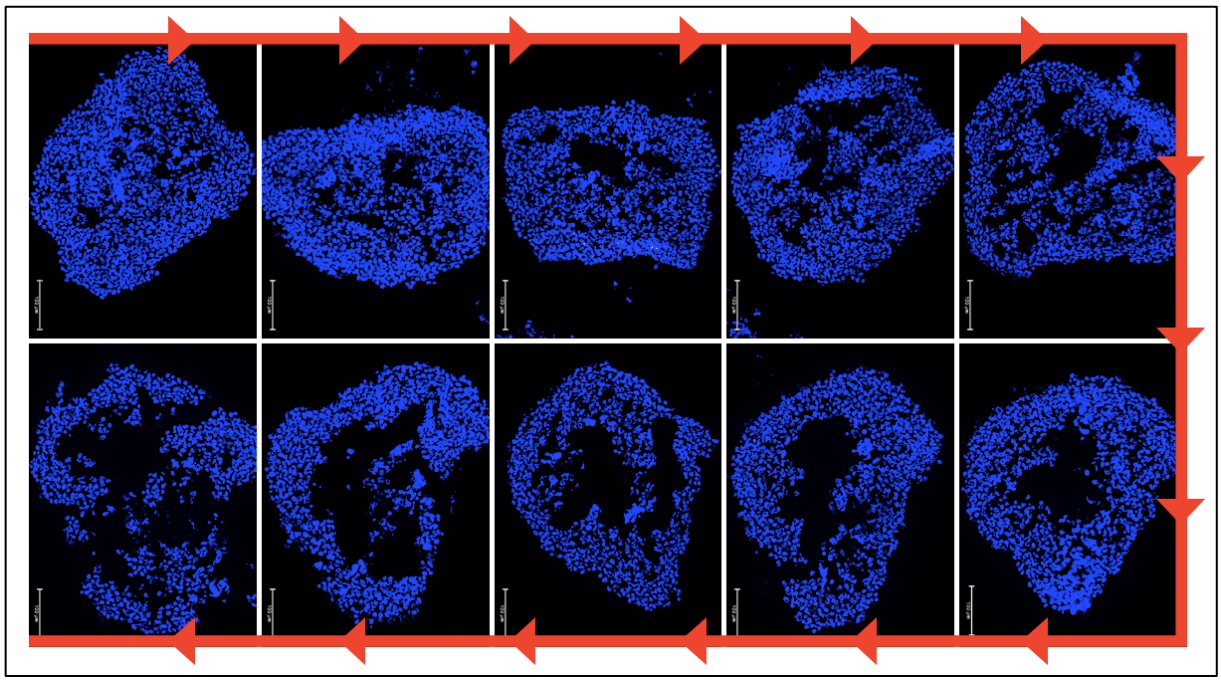

*Figure 12. Array of consecutive sections derived from one 5k-4T1-spheroid exhibiting necrotic regions. Images were taken in 20x magnification. (For further details regarding spheroid generation and imaging please refer to chapter 6.2 and Table 3). The red arrow indicates the spatial direction from outer spheroid layers towards its center. Scalebar: 100 µm.*

*Figure 13* displays a comparison of the time-dependent development of hypoxic and necrotic areas in 5k-MCTS and 10k-MCTS. 5k-MCTS exhibit diameters below 400 µm without presence of necrotic regions after 24 hours as well as after 48 hours of incubation. 10k-MCTS reached sizes larger than 400 µm after 24 hours, however, no necrotic center had formed either. After 96 hours, both 5k-MCTS and 10k-MCTS show significant increase in diameter and overall loosening of cell cohesion. Nonetheless, no necrotic core had formed until this point. After 120 hours of cultivation, 5k-MCTS equally show no development of central necrotic zones, whereas 10k-MCTS exhibit

slight signs of a necrotic core. Eventually, 168 hours after cell seeding, both 5k-MCTS and 10k-MCTS appeared to have established the characteristic zones with gradually diminishing amounts of cells towards the center and a total lack of structures within the core, recognizable by the fainting fluorescence signal towards the center and its eventual extinction.

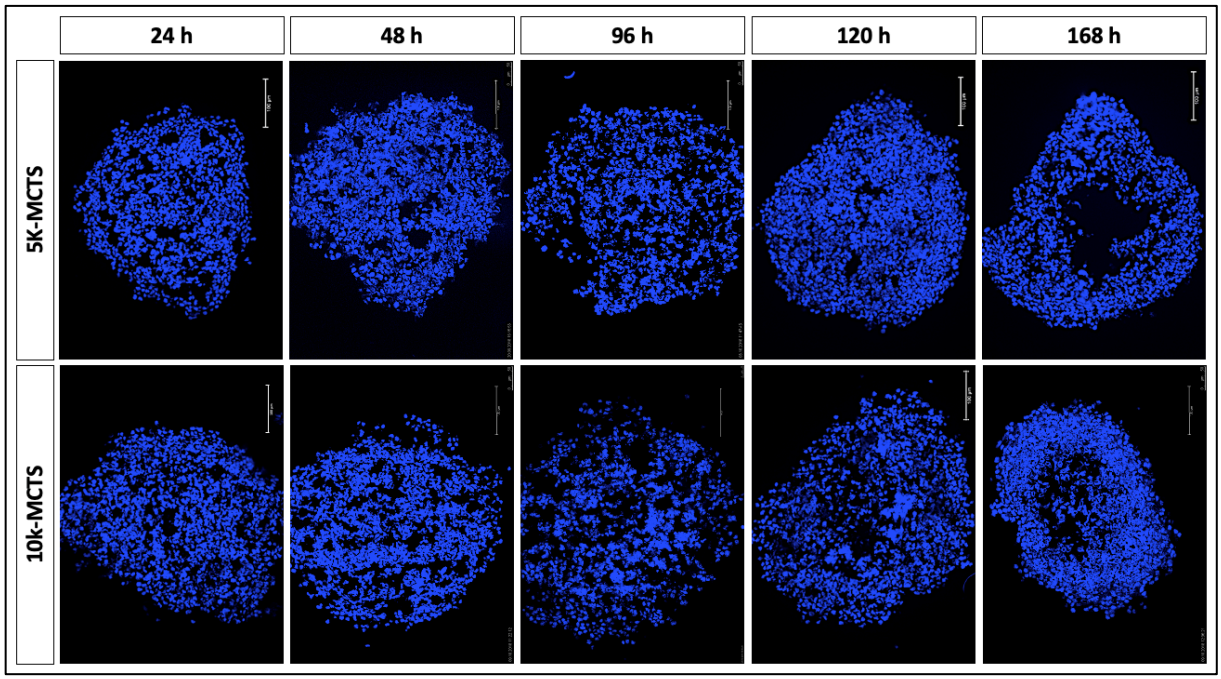


*Figure 13. Time-dependent formation of hypoxic and necrotic regions within MCTS of two different cell seeding numbers. 5k-MCTS and 10k-MCTS were cultivated for 24 h, 48 h, 96 h, 120 h, and 168 h. Images were taken in 20x magnification. (For further details regarding spheroid generation and imaging please refer to chapter 6.2 and Table 3). Scale bar: 100 µm.*

According to the results of the MCTS section imaging, both 5k- and 10k-MCTS formed a necrotic core when cultivated for periods longer than 120 hours. Hypoxic and necrotic regions were, in previous literature, found to occur in spheroids larger than 400 µm [31] which correlates with the results of this experiment. This observation suggests that the cultivation of MCTS should exceed 120 h in order to promote the formation of a necrotic core.

## 7.2 Co-culture of tumor spheroids and archaea

Once the cultivation of suitable 4T1 MCTS had succeeded, the second phase of the project, i.e. the involvement of archaea, was initiated. For the inoculation of MCTS with archaea, it had to be ensured that spheroids displayed uniform and reproducible morphology in order to achieve significant results among performed experiments. MCTS of various cell seeding numbers (20,000 | 10,000 | 5,000 | 1,000 | 500 cells per 200 µl and per well) were generated and imaged under the light microscope in fourfold and tenfold magnification every day from the day of cell seeding in ultra-low attachment 96-well plates. In order to detect archaea within MCTS sections, an effective archaea-labeling method needed to be determined prior to the inoculation of MCTS with archaea.

### 7.2.1 Labeling of archaea

**Optimization of archaea labeling**

In an initial experiment, when archaea-containing MCTS sections were solely labeled with DAPI, it could be observed that a distinction between cancer cells and archaea was impossible due to insufficient objective resolution. Despite the unequal dimensions of cancer and archaeal cells, the fluorescence signals could not clearly be assigned to the distinct types of cells (*Appendix Compl. Figure 24*). Similarly, no promising outcomes were achieved by pre-labeling archaea with HOECHST and MCTS sections with DAPI as archaea could equally not be identified within the spheroid section (*Appendix Compl. Figure 25*). Hence, a different archaea-labeling dye needed to be chosen. Alexa Fluor 488 (AF488), a green fluorescent dye, enabled an efficient staining of archaeal cells and was used for archaea-labeling in all following experiments.

*Figure 14* shows a suspension of AF488-stained archaea imaged by fluorescence microscopy. The non-uniformity of visible structures suggests that archaea have partially formed cell clusters, which is a known property of *Methanococcus maripaludis* S0001. [88] Thus, small green spherical dots presumably represent single archaeal cells, as *M. maripaludis* (coccus) displays coccoid morphology (red arrows), whereas larger green formations could indicate archaeal cell aggregations (blue arrows), since *M. maripaludis* is a colony-forming strain.

For control purposes, AF488-unlabeled archaea were equally examined for the presence of potential autofluorescence, which proved not to apply (*Appendix Compl. Figure 26*).

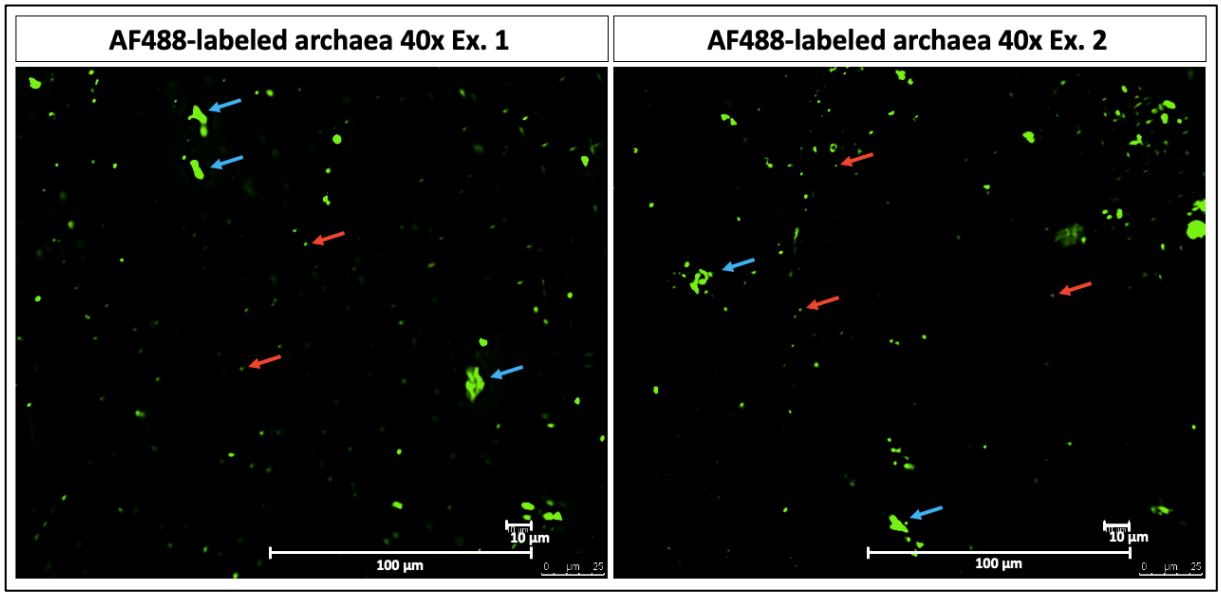


*Figure 14. Archaea labeled with AF488 emitting green fluorescence shown in two examples. Images were taken by fluorescence microscopy in 40x magnification. (For further details regarding archaea labeling and imaging please refer to chapter 6.3.3 and Table 3). Blue arrows indicate possible archaea cell clusters, red arrows indicate single spherically shaped archaeal cells. Scale bars: 100 µm and 10 µm.*

### 7.2.2 Inoculation of tumor spheroids with archaea

After successfully labeling the archaea, co-culture experiments of MCTS and archaea were started. Following the initial optimization phase, three MCTS-archaea co-culture experiments with partly same and partly differing parameters were conducted. An overview is shown in *Table 3.*

*Table 3. Compilation of parameters of three significant archaea-MCTS co-culture experiments (Exp.). MCTS = multicellular tumor spheroids; AA = MCTS + AF488-dyed archaea; AU = MCTS + undyed archaea; UT = Untreated MCTS; AF488 = Alexa Fluor 488; DAPI = 4',6-Diamidin-2-phenylindol BF = bright field microscopy; FL = fluorescence microscopy; PFA = paraformaldehyde.*

| **Parameters** | **Archaea-in-MCTS co-culture Exp. 1** | **Archaea-in-MCTS co-culture Exp. 2** | **Archaea-in-MCTS co-culture Exp. 3** |
|---|---|---|---|
| *Cell seeding numbers for MCTS cultivation* | 20,000 \| 10,000 \| 5,000 \| 1,000 \| 500 | 10,000 \| 5,000 | 5,000 |
| *Overall cultivation time* | 11 days | 14 days | 13 days |
| *Time of archaea inoculation* | day 6 | day 8 | day 7 |
| *Concentration of archaea suspension* | $9x10^8$ archaea/ml | $9x10^8$ archaea/ml | $8x10^6$ archaea/ml |
| *Archaea-MCTS co-culture* | MCTS + AF488-dyed archaea (AA)<br><br>Control: Untreated MCTS | MCTS + AF488-dyed archaea (AA)<br><br>MCTS + undyed archaea (AU)<br><br>Control: Untreated MCTS | MCTS + AF488-dyed archaea (AA)<br><br>MCTS + undyed archaea (AU)<br><br>Control: Untreated MCTS |
| *Archaea labeling* | Pre-staining with AF488 dye | Pre-staining with AF488 dye | Pre-staining with AF488 dye |
| *Volume of archaea suspension added to MCTS* | 40 µl (i.e. $3.6x10^7$ archaea/spheroid) | 40 µl (i.e. $3.6x10^7$ archaea/spheroid) | 40 µl (i.e. $3.2x10^5$ archaea/spheroid) |
| *Co-culture conditions* | Coverage of well plate with parafilm & aluminum foil Incubator: 37 °C | Coverage of well plate with parafilm & aluminum foil Incubator: 37 °C | Coverage of well plate with parafilm & aluminum foil Incubator: 37 °C |
| *Duration of archaea-MCTS co-culture* | 48 h<br>96 h<br>120 h | 24 h<br>120 h<br>168 h | 48 h<br>120 h<br>168 h |
| *Fixation* | PFA 4 % post-fixation | PFA 4 % post-fixation | PFA 4 % post-fixation |

| | | | |
|---|---|---|---|
| *MCTS cell labeling* | DAPI | DAPI | DAPI |
| *Imaging* | MCTS: BF 4x\|10x<br>Sections: FL<br>20x\|40x | MCTS: BF 4x\|10x<br>Sections: FL<br>20x\|40x | MCTS: BF 4x\|10x<br>Sections: FL<br>20x\|40x |

**Archaea-MCTS co-culture Exp. 1**

To assess the ideal cell seeding number(s) for the cultivation of 4T1-MCTS that are suitable for the inoculation with archaea, an array of various selected cell counts, i.e. 20,000 | 10,000 | 5,000 | 1,000 | 500 cells per well, was prepared. Spheroids of all cell seeding numbers were imaged every day by light microscopy in fourfold and tenfold magnification until the day of inoculation with archaea. MCTS were incubated for 11 days at the longest and inoculated with the archaea strain *Methanococcus maripaludis* S0001 on day six of cultivation. Growth medium was changed every 48 hours during the first seven days and every 24 hours from day eight. 20k-MCTS reached a diameter of around 1,000 µm, however this comparatively large size was majorly due to the loosening of the outer cell layers (*Figure 11*). 10k-MCTS exhibited sizes of around 700 µm, 5k-MCTS reached 600 µm, 1k-MCTS reached 500 µm, and 500-MCTS displayed a diameter of around 400 µm on day 6. MCTS of all cell seeding numbers exhibited sufficient sizes to potentially develop hypoxic areas and a necrotic core. Hence, all spheroids were used for MCTS-archaea co-culture.

On day 6, four MCTS of each cell seeding number were treated with AF488-labeled archaea (AA) and some MCTS were left archaea-untreated (UT) for control purposes. The obtained archaea suspension contained $9x10^7$ archaea/ml and was concentrated tenfold in order to comprise $9x10^8$ archaea/ml. Subsequently, the higher concentrated archaea suspension was incubated with 2.7 µl AF488/100 µl. After staining the archaea with AF488 dye, archaeal fluorescence emission was confirmed by fluorescence microscopy (*Figure 14*). Spheroids of all cell seeding numbers were respectively inoculated with the prepared archaea suspension by adding 40 µl (i.e. 36 M archaea/spheroid) to the wells containing single spheroids, and several MCTS were left untreated.

After providing optimal incubation conditions for the anaerobic and fluorescently labeled archaea strain by excluding light and oxygen, MCTS and archaea were

incubated for various periods of time. Respectively, MCTS were harvested 48 hours, 96 hours, and 120 hours after inoculation in order to evaluate whether archaeal infiltration of spheroids represented a time-dependent process. Moreover, the period of time whereupon archaea migrated towards the MCTS core should be evaluated. The subsequent embedding, cryostat sectioning, fixation, DAPI staining, and fluorescence imaging were performed following the optimized operating procedures as described in chapters 6.2.7, 6.2.8, 6.2.9, and 6.3.6. These procedures were not altered after the introduction of archaea to experimentations.

*Figure 15* shows fluorescence images of central sections of archaea-infiltrated 5k-MCTS after co-culture for 48 hours, 96 hours, and 120 hours. The aim of following MCTS-archaea co-culture over time was to evaluate the archaea's capability to progressively migrate towards the MCTS core over time. Images were taken in 20x (top row) and 40x magnification (bottom row). The labeling of archaea with AF488 and DAPI staining of MCTS sections allowed a clear differentiation of archaeal cells and cancer cells by means of fluorescence microscopy. Green fluorescence indicates the presence of archaea, whereas blue fluorescence shows MCTS-forming cancer cells. With high probability, the emission of green light originated from archaeal cells due to the presence of small green dots about the size of single archaea (red arrows). Moreover, archaea-untreated MCTS (UT) (*Figure 15)* and MCTS inoculated with AF488-unlabeled archaea (AU) in later experiments did not emit any green fluorescence after excitement with the respective wavelength which provides additional evidence for archaea being associated with the emission of green fluorescence. Due to high consistency in morphology and efficient archaeal colonization, 5k-MCTS were chosen for representative demonstration of archaeal spheroid infiltration in *Figure 15*.

As recognizable in *Figure 15*, archaeal infiltration can be observed in all presented sections. As previously outlined, the used archaea strain *Methanococcus maripaludis* has the property of aggregating into cell clusters [88] which, presumably, here appears as larger green formations (white arrows), whereas small green dots, most probably, represent single archaeal cells (red arrows).

After 48 hours of MCTS-archaea co-culture, archaea appear to have invaded the spheroid's outer layer to a certain extent. Noticeably, archaea seem to have accumulated at restricted sites rather than distributing uniformly over the entire spheroid. This behavior has been observed frequently throughout the conducted experiments.

96 hours of MCTS-archaea co-culture resulted in enhanced green fluorescence at sites closer towards the spheroid core. Again, archaea are mainly visible in confined areas, however, their dissemination seems to have increased to a significant extent. Compared to 48 hour-co-culture, the results indicate further archaeal advance towards the spheroid center over time. Furthermore, a larger number of smaller green fluorescent formations suggest that archaeal aggregation has loosened to some degree compared to the outcomes of 48 hour-co-culture.

120 hours after inoculation of MCTS with archaea, green fluorescence increased substantially when compared to 96 hour-co-culture. The remarkable raise of archaeal cells within MCTS let us draw two possible hypotheses: archaea could have proliferated massively within spheroids, especially during the 24 hours between this and the previous harvesting or the majority of archaea could have been lingering in supernatant culture medium and only have started to infiltrate spheroids after an extended period of 120 hours. Another crucial development after 120 hours is the strong approach of archaea towards the spheroid core. Just as observed for 48 hour- and 96-hour-cultivation, archaeal aggregation and accumulation is still recognizable (white arrows), however, the closer proximity of green fluorescence to the spheroid center is clearly visible.

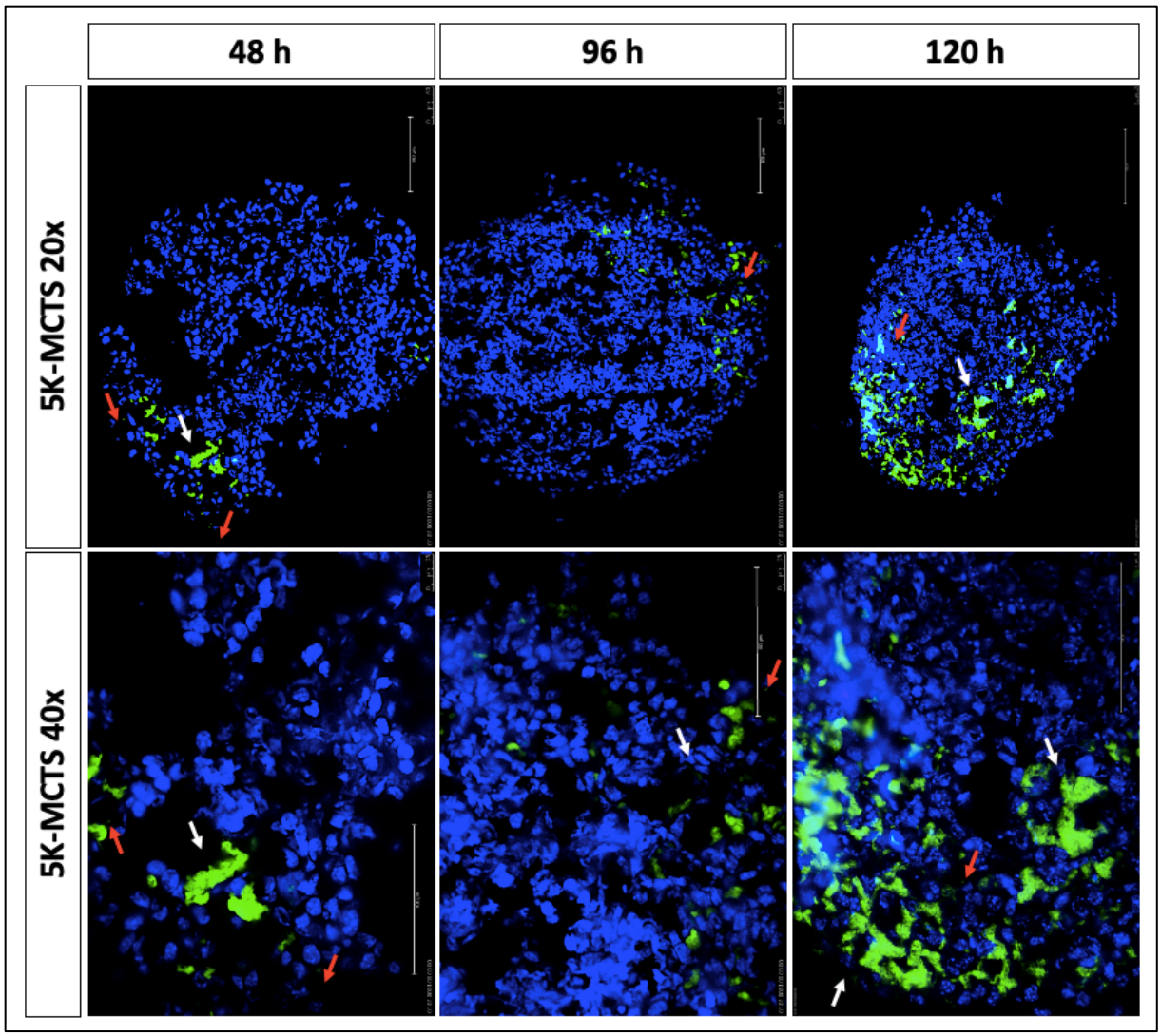


*Figure 15. Fluorescence microscopic images of sections derived from AF488-archaea-infiltrated 5k-MCTS (AA) after 48h, 96 h, and 120 h in 20x and 40x magnification. (For further details regarding spheroid generation and imaging please refer to chapter 6.2 and Table 3). Green emission: AF488-labeled archaea; blue emission: DAPI-stained cancer cell nuclei; white arrows indicate possible archaea clusters; red arrows indicate single archaea. Scale bar 20x: 100 µm; scale bar 40x: 100 µm.*

In order to investigate possible green autofluorescence of 4T1 cells or other components, archaea-untreated spheroids (UT) were cultivated in the same well plate, hence on the same terms, and derived sections were excited with equal wavelengths. *Figure 16* demonstrates the obtained imaging results of sections of archaea-untreated MCTS (UT) after 48 hours, 96 hours, and 120 hours of cultivation. No green fluorescent signal is recognizable in any of the samples taken. Thus, it can be assumed that green fluorescence specifically derived from AF488-labeled archaea.

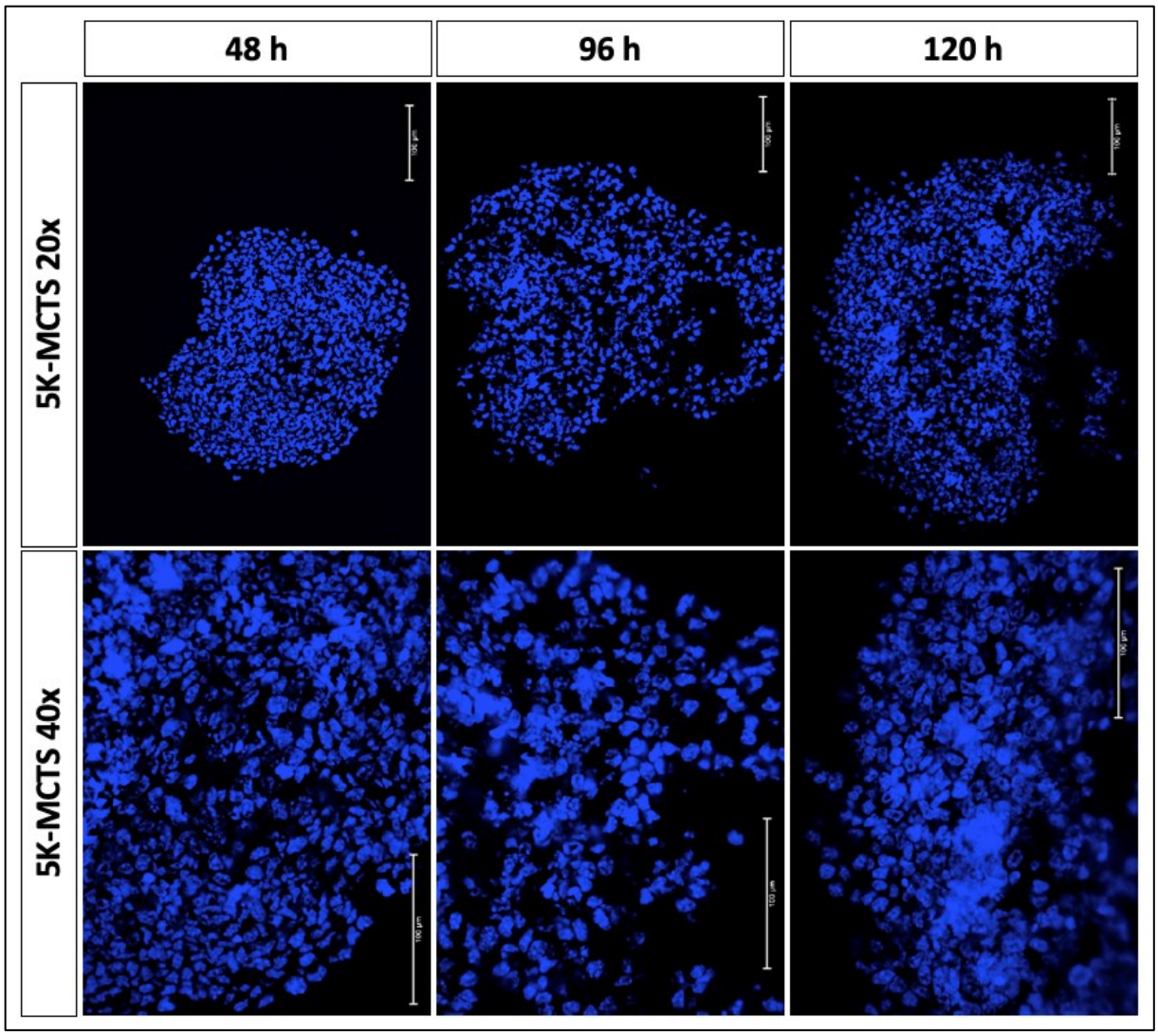


*Figure 16. Fluorescence microscopic images of sections derived from archaea-untreated 5k-MCTS (UT) after 48h, 96 h, and 120 h in 20x and 40x magnification. (For further details regarding spheroid generation and imaging please refer to chapter 6.2 and Table 3). Blue emission: DAPI-stained cancer cell nuclei. Scale bar 20x: 100 µm; scale bar 40x: 100 µm.*

On the basis of the outlined results obtained in this experiment, it could be demonstrated that the utilized archaea strain *Methanococcus maripaludis* can successfully be labeled with a concentration of 2.7 µl AF488/100 µl archaea suspension. It could be shown that the strain indeed is able to infiltrate 4T1-MCTS. As clearly visible in *Figure 15*, the advance of archaea towards the spheroid center as well as their distribution and proliferation within spheroids appears to be a time-dependent process. After 48 hours of MCTS-archaea co-culture, archaea can mainly be found in peripheral zones of the spheroid and, presumably, form cell aggregations as fluorescence images exhibit large green formations. Archaea are still predominantly located in outer spheroid layers after 96 hour-co-culture. However, compared to the 48

hour-culture, archaea seem to have proceeded inward to a certain extent. Moreover, smaller green fluorescent structures can be identified, suggesting that archaeal cell accumulations have dissipated comparatively. MCTS harvested after 120 hours of co-culture with archaea display the overall highest green fluorescence signal in relation to 48 hours and 96 hours. The obtained images (*Figure 15*) suggest a significantly higher number of archaea within the spheroid after 120 hours of co-culture, and, most importantly, a closer proximity to the spheroid core.

Due to the strong time-dependency of archaeal spheroid infiltration, more prolonged co-culture durations should be introduced in order to investigate the further development of archaea-colonization of 4T1-MCTS. Moreover, MCTS with the most suitable initial cell seeding number should be defined to investigate archaeal infiltration of spheroids at a more comparable level.

**Archaea-MCTS co-culture Exp. 2**

The aim of the second experiment was to apply equal MCTS-archaea co-culture conditions as for the first experiment in order to evaluate the reproducibility of the demonstrated results. However, harvesting times were altered to a certain degree to investigate archaeal colonization of spheroids over an extended time frame. The array of cell seeding numbers for the generation of MCTS was cut down to only 5k- and 10k-spheroids due to significantly higher consistency regarding their stability and archaeal colonization (*Figure 11 & Appendix Compl. Figure 23*). Moreover, MCTS were cultivated for seven days and inoculated with archaea on day 8 (in Exp. 1, MCTS were inoculated with archaea on day 6). On day 6 (inoculation time of Exp. 1), 10k-MCTS reached diameters of around 700 µm, 5k-MCTS displayed sizes of around 600 µm. These diameters are comparable to those of 5k- and 10k-MCTS generated in Exp. 1. On day 8 (inoculation with archaea), 5k-spheroids reached sizes of around 700 µm, 10k-MCTS displayed diameters of around 750 µm. Sections of MCTS with a high initial cell seeding number (20,000 cells) displayed loose and disintegrating structures - quite frequently even devoid of spherical shape. Due to this lack of internal cellular cohesion, 20k-MCTS appeared to be inappropriate tumor models for co-culture with archaea and were, consequently, not used for subsequent experiments. Sections of lower cell seeding numbers (1,000 and 500 cells) exhibited only a minor increase in diameter

over cultivation time which seemed to resemble the behavior of natural tumors insufficiently. Hence, 1k- and 500-MCTS were not employed for further experiments.

In this experiment, twelve 5k- and twelve 10k-MCTS were treated with AF488-labeled archaea (AA) after eight days of cultivation, the same amount of MCTS was co-cultured with AF488-unlabeled archaea (AU) in order to investigate possible green autofluorescence. Just like in the previous experiment, some MCTS were left archaea-untreated (UT) for control purposes and cultivated for equal durations as AA and AU. An archaea suspension containing $9x10^7$ archaea/ml was concentrated to $9x10^8$ archaea/ml. A small sample of archaea suspension was stained with AF488 and examined for emission of green fluorescence. Subsequently, 40 µl (i.e. $3.6x10^7$ archaea/spheroid) of the suspension containing AF488-labeled archaea or AF488-unlabeled archaea were added to respective spheroid-comprising wells. In order to define the time frame of effective archaeal spheroid penetration, a shorter cultivation period of 24 hours for MCTS-archaea co-culture was included in this experiment. To investigate archaeal behavior within MCTS after more extended co-culture periods, spheroids were additionally harvested after prolonged cultivation of 168 hours. The ensuing procedures for preparation of MCTS sections were performed analogously as outlined in Exp. 1.

*Figure 17* displays central sections of 10k-MCTS co-cultured with AF488-labeld archaea for 24 hours, 120 hours and 168 hours. Sections were imaged by fluorescence microscopy in 20x and 40x magnification. Noteworthy, when compared to archaeal infiltration results after 48 hours from Exp. 1, green fluorescent archaea appear to aggregate to a lesser extent after 24 hours of MCTS-archaea co-culture and are distributed more widely over the spheroid. However, archaea are also predominantly located in peripheral spheroid zones. After 120 hours of co-culture, archaea exhibit comparatively less deep penetration of the 10k-spheroid as it was observed for 5k-MCTS after equal cultivation time in the first experiment. Moreover, the amount of overall green fluorescence and the presence of large green structures is considerably lower than in 120 hour-5k-MCTS section from Exp.1.

A remarkable increase of green fluorescence can be observed after 168 hours of MCTS-archaea co-culture, suggesting major archaeal proliferation within the spheroid

or penetration of additional archaea that had lingered in the supernatant growth medium until this point. Similar to the 120 h-5k-spheroid from the previous experiment, large green formations, indicating archaeal aggregation, can be detected. Archaea seem to have migrated towards the spheroid center to a great extent, however, the actual core had still not been colonized. Interestingly, two apparent groups of cell accumulations can be found, both approximately located at equidistance around the spheroid core.

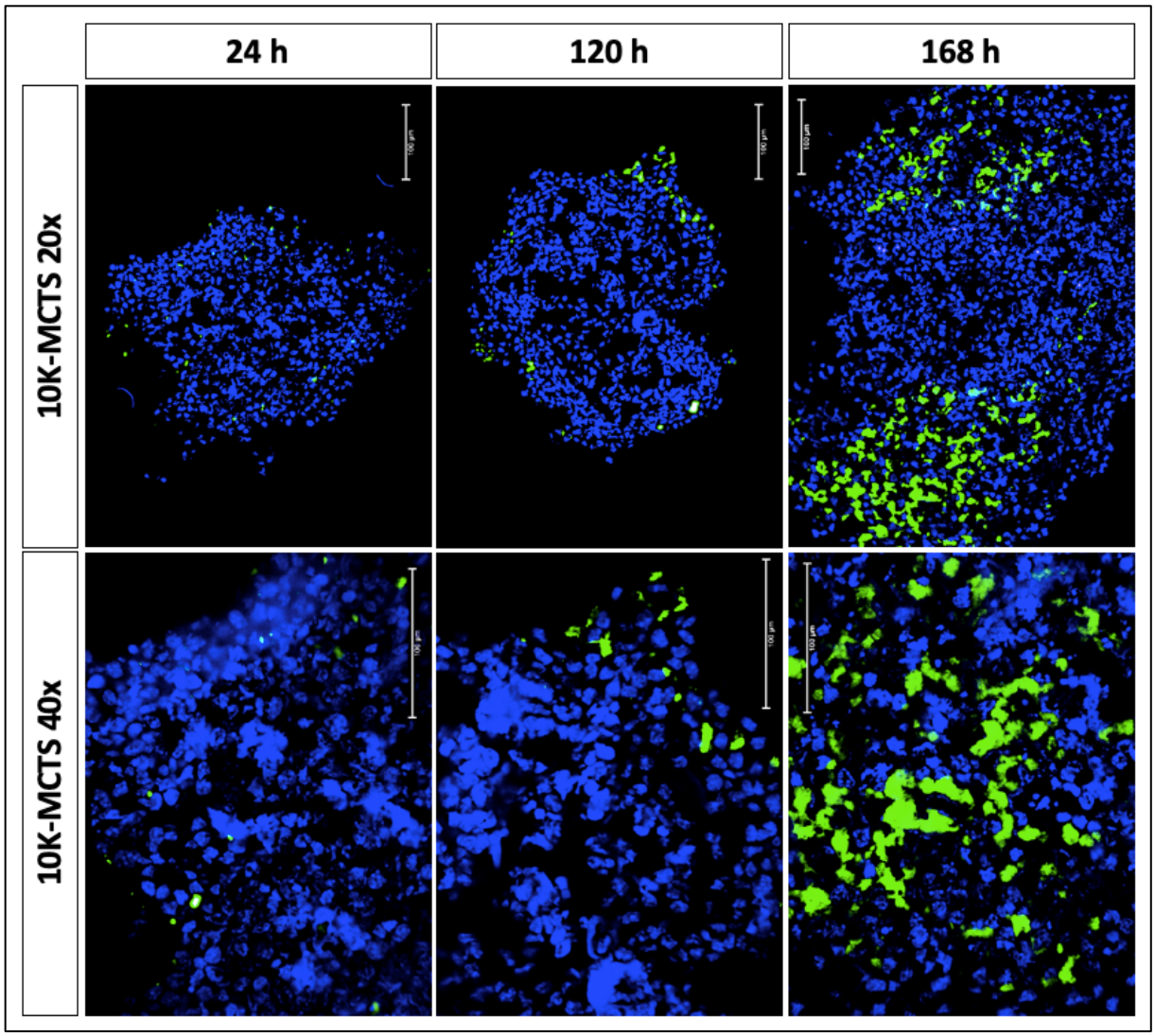


*Figure 17. Fluorescence microscopic images of sections derived from AF488-archaea-infiltrated 10k-MCTS (AA) after 24h, 120 h, and 168 h in 20x and 40x magnification. (For further details regarding spheroid generation and imaging please refer to chapter 6.2 and Table 3). Green emission: AF488-labeled archaea; blue emission: DAPI-stained cancer cell nuclei. Scale bar 20x: 100 µm; scale bar 40x: 100 µm.*

As demonstrated in *Figure 18*, archaeal colonization of 5k-MCTS after 24 hours resembles that of 10k-MCTS (*Figure 17*) to a fair extent as archaea are located in the

outer spheroid layers and occur as small green fluorescent dots. However, the section derived from 5k-spheroid co-cultured with archaea for 120 hours exhibits green fluorescence considerably more inward, surrounding the spheroid core. Remarkable results were obtained after co-culturing 5k-MCTS and archaea for 168 hours. The section was derived from the center of the sample, and therefore represents the interior of the spheroid. Hence, the presence of extensive green fluorescence indicates a broad archaeal colonization of the majority of the spheroid's body. Furthermore, when compared to spheroids harvested after 120 hours, the area exhibiting green fluorescence seems to have more than quadrupled, suggesting a strong increase of archaeal presence within the spheroid.

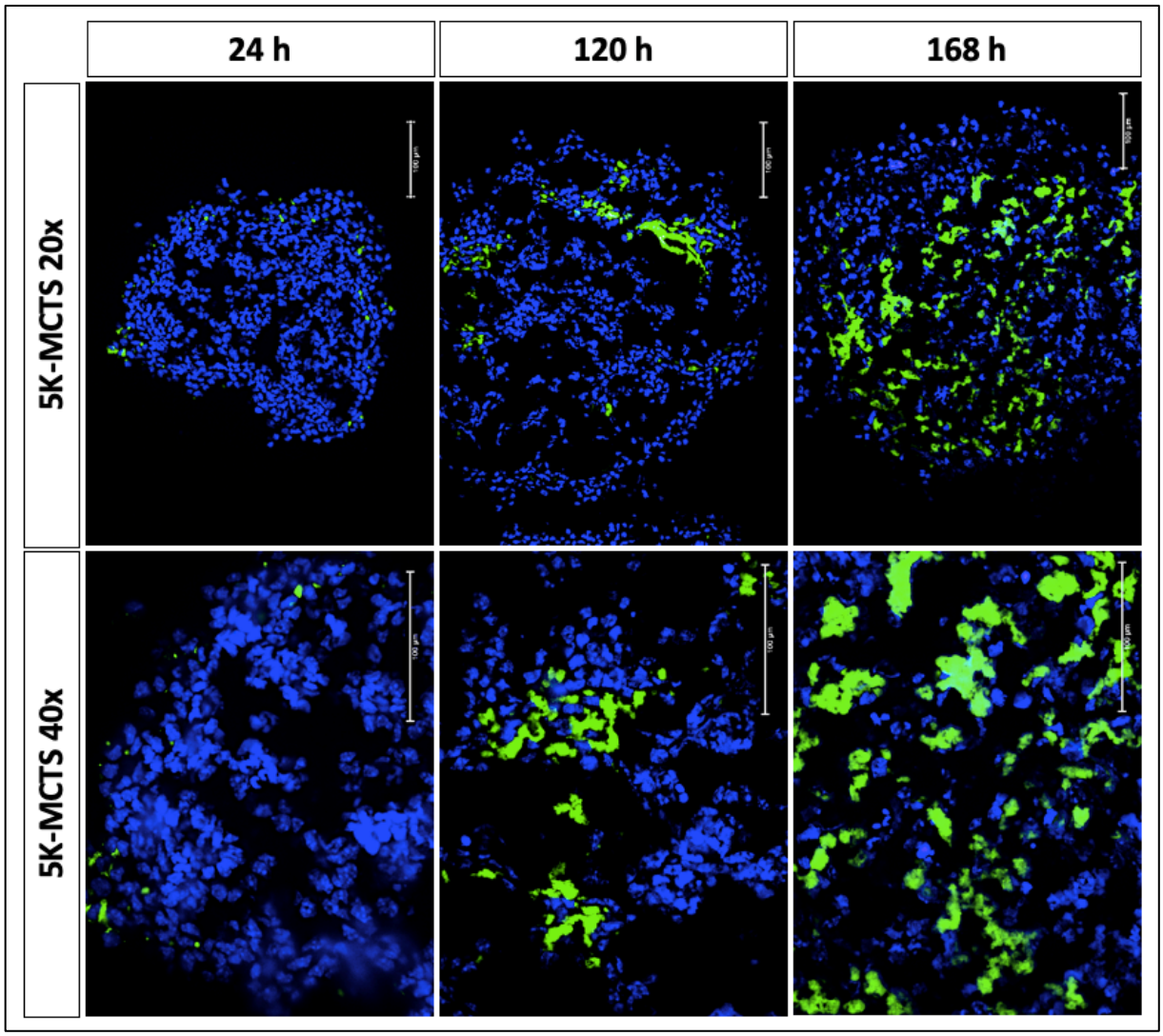


*Figure 18. Fluorescence microscopic images of sections derived from AF488-archaea-infiltrated 5k-MCTS (AA) after 24h, 120 h, and 168 h in 20x and 40x magnification. (For further details regarding spheroid generation and imaging please refer to chapter 6.2 and Table 3). Green emission: AF488-labeled archaea; blue emission: DAPI-stained cancer cell nuclei. Scale bar 20x: 100 µm; scale bar 40x: 100 µm.*

To investigate archaea for potential autofluorescence, MCTS of respective cell seeding numbers were inoculated with AF488-unlabeled archaea (AU) and imaged by fluorescence microscopy at the AF488 excitation wavelength. *Figure 19* displays 10k-spheroid sections inoculated with AU-archaea harvested after 24 hours, 120 hours, and 168 hours in 20x and 40x magnification. As can be seen in *Figure 19*, no green fluorescence can be detected in any of the 10k-AU-MCTS sections, suggesting that *Methanococcus maripaludis* does not emit any autofluorescence after excitation with the equal wavelength used for AF488-labeled archaea.

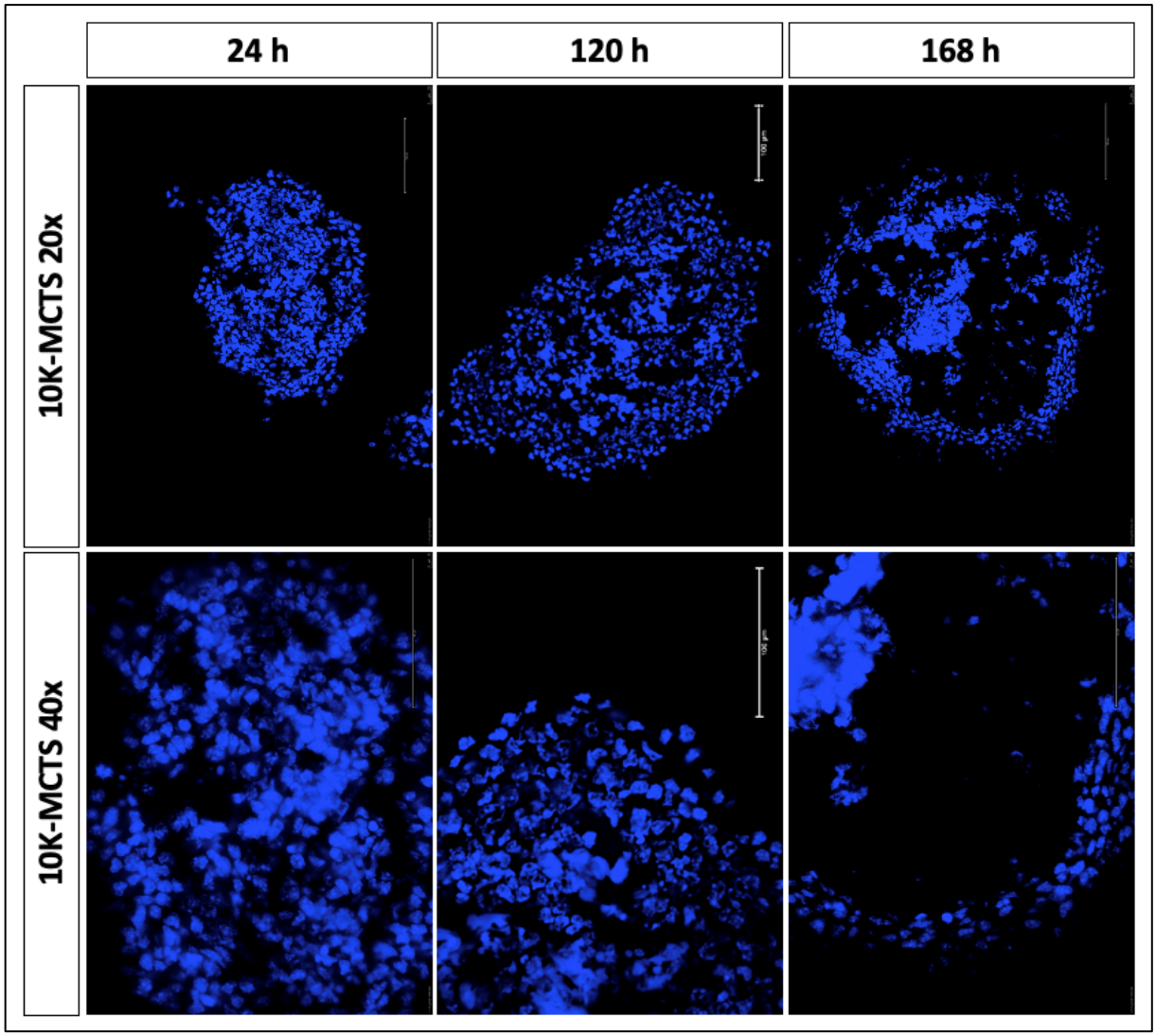


*Figure 19. Fluorescence microscopic images of sections derived from 10k-MCTS + unlabeled archaea (AU) after 24 h, 120 h, and 168 h in 20x and 40x magnification. (For further details regarding spheroid generation and imaging please refer to chapter 6.2 and Table 3). Blue emission: DAPI-stained cancer cell nuclei. Scale bar 20x: 100 µm; scale bar 40x: 100 µm.*

Surprisingly, 5k-MCTS co-cultured with AF488-unlabeled archaea revealed several green fluorescent structures after 168 hours of cultivation, as demonstrated in *Figure 20*. The appearance of the green formations resembles those observed in AA-MCTS sections to a great extent, hence it was presumed that the signal emanates from AF488-stained archaea. The occurrence of green fluorescence in AU-MCTS sections can, most probably, be explained by a contamination of AU-MCTS with AF488-labeled archaea, since AA-MCTS and AU-MCTS were cultivated in the same well plate. A contamination could have been caused by an overflow of supernatant AA-archaea suspension into wells of AU-MCTS early after inoculation during the movement of the well plate. Noteworthy, AU-MCTS harvested after 168 hours and AA-MCTS have been cultivated in adjacent wells, hence a spillover cannot be ruled out and represents the most plausible explanation for green fluorescent formations in AU-MCTS sections.

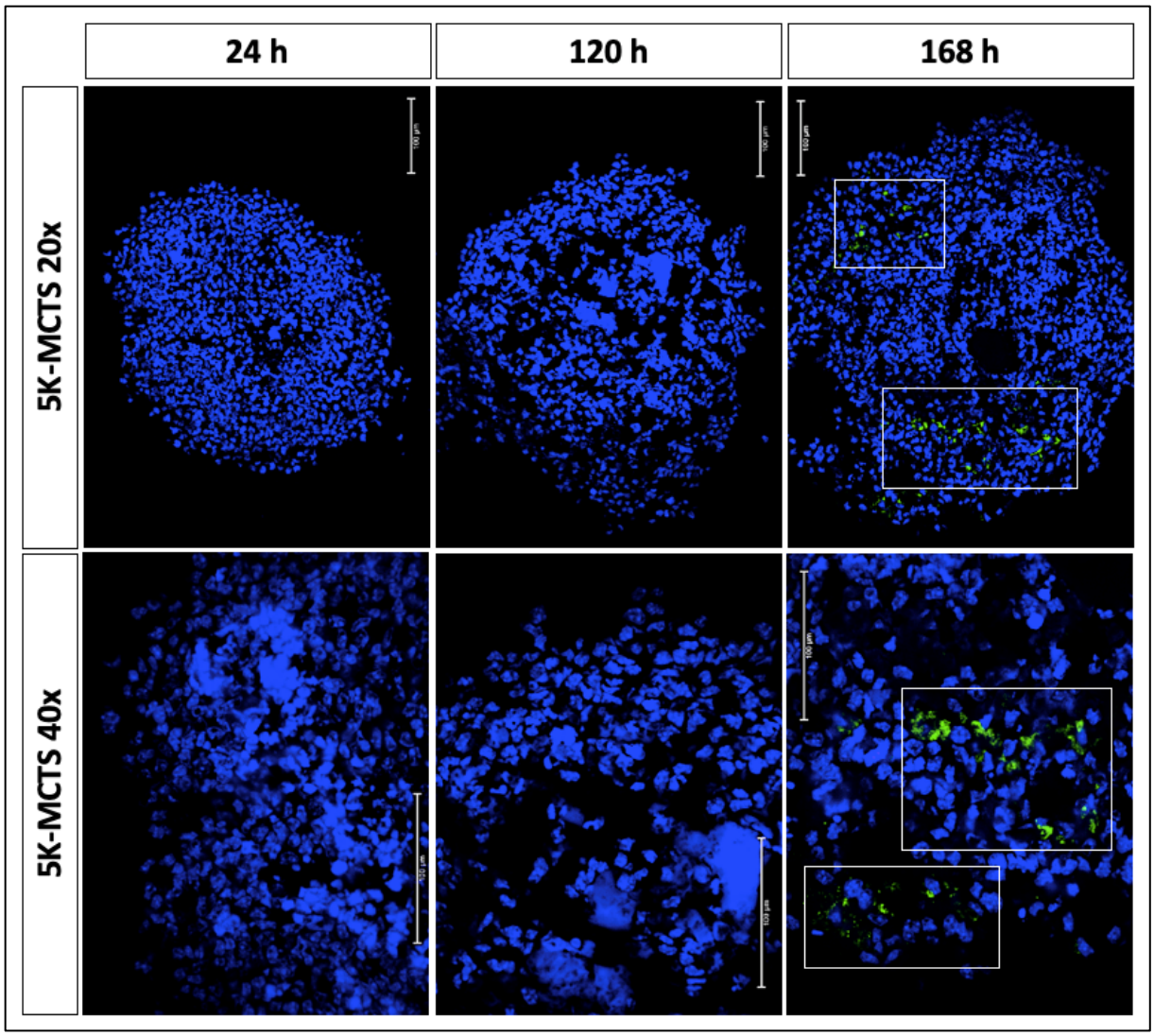


*Figure 20. Fluorescence microscopic images of sections derived from 5k-MCTS + unlabeled archaea (AU) after 24 h, 120 h, and 168 h in 20x and 40x magnification. (For further details regarding spheroid generation and imaging please refer to chapter 6.2 and Table 3). Blue emission: DAPI-stained cancer cell nuclei; white boxes indicate occurrence of green fluorescence. Scale bar 20x: 100 µm; scale bar 40x: 100 µm.*

The outlined imaging results of Exp. 2 indicate that the archaea strain *Methanococcus maripaludis* had followed similar behavior patterns during co-culture experiments with MCTS as observed in Exp. 1 which was performed under the same cultivation conditions as Exp. 2. Green fluorescent archaea are almost exclusively located in peripheral spheroid zones at first harvesting after 24 hours and appear to occur as single archaeal cells or small-sized cell aggregations in both 10k- and 5k-MCTS. When compared to 48 hours-cultivation from Exp. 1 (*Figure 15*), significantly less green fluorescent structures and less and smaller archaeal accumulations can be identified, suggesting that archaeal aggregation within MCTS represents a time-dependent

process. Moreover, green dots are spread widely over the entire spheroidal profile, indicating that archaeal cohesion had taken place only to a minor extent after 24 hours of co-culture.

After 120 hours, archaeal infiltration of spheroids differs between 10k- and 5k-MCTS to a certain degree. 10k-spheroids display occurrence of archaea in less deep zones, whereas 5k-MCTS show a further inward (towards the spheroid center), annular archaeal colonization. This non-uniform archaeal penetration of two spheroids with varying cell seeding numbers after equal cultivation periods could be due to different morphological compositions of respective MCTS, such as varying looseness of cellular cohesion. However, the results obtained from 120 hour-cultivated MCTS in Exp. 1 did not deliver analogous outcomes. Archaea appear to have migrated much closer towards the 5k-MCTS center after 120 hours in the first experiment (*Figure 15*), whereas the 5k-spheroid from Exp. 2 displays only slight progression of archaea towards the core. This could be due to inconsistent concentrations of the archaea suspension used for Exp. 1 and Exp. 2. For both experiments the same archaea culture batch was used, however, it cannot be ruled out that the archaea concentration had not remained constant (due to cell death of archaea) in the interim between inoculation of Exp. 1 and Exp. 2.

168 hours of MCTS-archaea co-culture resulted in a tremendous increase of archaeal colonization of the spheroid in both 5k- and 10k-MCTS, however, the expansion of green fluorescence is found to be considerably higher in the 5k-spheroid. The comparatively high amount of visible green fluorescence could be due to extensive archaeal proliferation within the spheroids during the time between 120 hours and 168 hours of co-culture or to the invasion of high amounts of archaea into the spheroid during said time frame. In 5k-MCTS, archaea had distributed over the entire spheroid, including the core, suggesting that 168 hours of co-culture represents an adequate duration to observe archaeal colonization of the spheroid core. The occurrence of green fluorescence in 5k-MCTS inoculated with AF488-unlabeled archaea (*Figure 20*) after 168 hours of co-culture can, most likely, be traced back to imprecise handling of the well plate early after archaea inoculation. None of the subsequently imaged AU-MCTS exhibited green fluorescence after excitement with the equal wavelength, hence

it can be presumed that this case is based on spillage of AF488-labeled archaea into AU-MCTS.

Due to the overall higher mechanical stability of 5k-MCTS sections as well as their more consistent and reproducible results between samples compared to 10k-MCTS (*Figure 11& Appendix Compl. Figure 23*), exclusively 5k-MCTS were selected for cultivation in the course of the final experiment.

**Archaea-MCTS co-culture Exp. 3**

For the final experiment, solely 5k-MCTS were generated and utilized for MCTS-archaea co-culture due to their more solid properties and higher reproducibility of archaeal colonization patterns. On day 7, the day of inoculation with archaea, spheroids had reached diameters of around 600 µm which correlates with the results of Exp. 1 and Exp. 2. Since MCTS harvested after 24 hours of co-culturing with archaea did not display significant archaeal migration towards the spheroid center, this early harvesting time was not included in this experiment. Instead, 48 hour-MCTS-archaea co-culture should be reinvestigated in order to assess its relevance for archaeal infiltration of spheroids. The other two harvesting times (120 hours and 168 hours) were reproduced from Exp. 2. Noteworthy, archaeal inoculation was performed on day 7 in this experiment, whereas in Exp. 1, MCTS were inoculated on day 6, in Exp. 2 on day 8.

After eight days of cultivation, 18 5k-MCTS were treated with AF488-labeled archaea (AA), 12 5k-MCTS were inoculated with AF488-unlabeled archaea (AU), and some MCTS were not co-cultured with archaea for control purposes. The aim of the final experiment was to reproduce promising results of previous experiments, therefore, a concentration of $9x10^8$ archaea/ml should be prepared for MCTS-archaea co-culture. Due to an initially incorrectly determined cell count of the obtained archaea stock suspension, which only came to light after the inoculation, the prepared archaea concentration comprised only $8x10^6$ archaea/ml, as it was calculated in retrospect. Nonetheless, the results of this experiment, i.e. MCTS colonization of a lower number of archaea, represent an unexpected but valuable contribution to this project, and hence should be demonstrated in this context. Archaea were labeled with 2.7 µl AF488/100 µl and archaeal fluorescence emission was confirmed by fluorescence microscopy. For inoculation, 40 µl (i.e. $3.2x10^5$ archaea/spheroid) of the respective

archaea suspensions were added to MCTS and cultivated for 48 hours, 120 hours, or 168 hours. For comparison, in Exp. 1 and Exp. 2 respective MCTS were co-cultured with $3.6x10^7$ archaea, hence the concentrations, approximately, differ by a factor 100.

*Figure 21* demonstrates the results of 48 hour-, 120 hour-, and 168 hour-co-culture of MCTS and archaea in 20x and 40x magnification. When compared to the results of previous experiments, clearly less green fluorescence can be detected in MCTS sections obtained during Exp. 3, indicating lower presence of archaea within the spheroid. Therefore, images of archaea-infiltrated MCTS sections cannot be compared directly to images obtained during Exp. 1 and Exp. 2, however, similar archaeal behavior patterns for the colonization of MCTS can nevertheless be observed.

After 48 hours of co-culture, few green fluorescent dots can be found exclusively in peripheral layers of the spheroid, suggesting that only a small number of archaea had penetrated the spheroid until this point. This marginal invasion of archaea into the MCTS appears similar to the 24 hour-10k section shown in *Figure 17*, where only a small amount of green fluorescent dots can be recognized as well. However, a closer inspection on the 48 hour-section from Exp. 3 (*Figure 21*) and the 48 hour-section from Exp. 1 (*Figure 15*) reveals that these MCTS exhibit larger green formations compared to the 24 h-sections from Exp. 2. These observations could indicate that archaea start to form larger cell clusters after more than 24 hours of MCTS-archaea co-culture.

Interestingly, MCTS harvested after 120 hours show only minor increase of visible green fluorescence despite the extended cultivation time by 72 hours. These results suggest that archaea in comparatively lower concentrations require even more prolonged incubation time in order to be abundant at high rates within MCTS. However, archaeal migration towards the spheroid core appears not to be fully impeded by lower numbers of archaea as more green fluorescent structures can be found in slightly more inward spheroid zones. The archaea's location within the section can indeed be compared to results of 120 hour-5k-MCTS sections from Exp. 2 (*Figure 18*), although different archaea concentrations had been applied.

A comparatively stronger increase of green fluorescence can be observed in sections from MCTS co-cultured with archaea for 168 hours. As recognizable in *Figure 21*, the

amount of visible archaea represents only a fraction of observed archaea abundance in 168 hour-MCTS from Exp. 2 (*Figure 17 & Figure 18*), however, these results prove that archaea are anyway able to survive and proliferate within MCTS or increasingly invade MCTS even when present in lower numbers. Remarkably, archaea are located at much further distance from the spheroid center when compared with sections from MCTS that had been cultivated for equal durations (Exp. 2). This could indicate that lower concentrations of archaea require longer co-culture periods in order to proceed closer to the spheroid core. Furthermore, when compared to results of previous experiments, a considerably lower presence of large green fluorescent formations within MCTS sections throughout all co-culture durations can be observed.

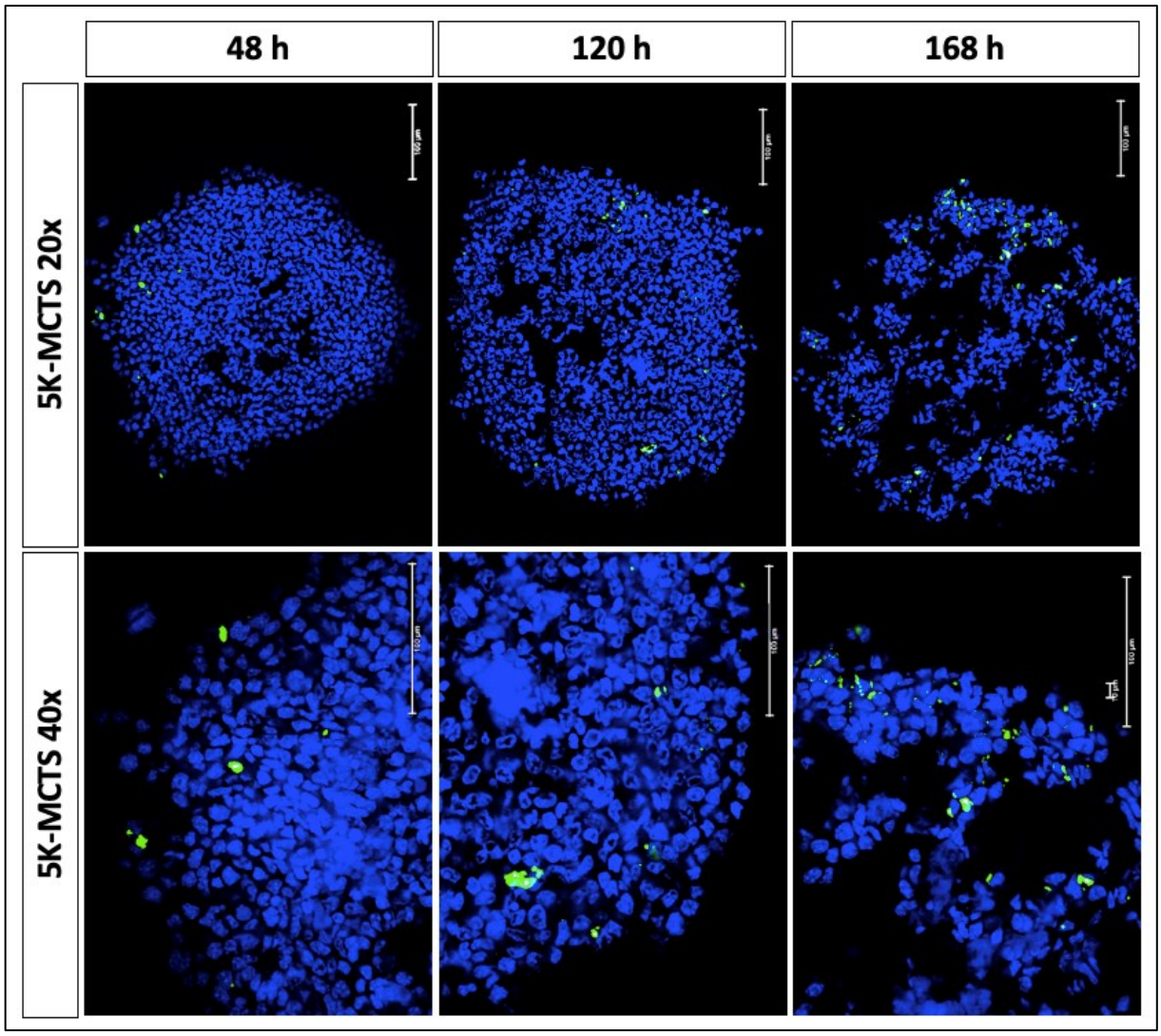


*Figure 21. Fluorescence microscopic images of sections derived from AF488-archaea-infiltrated 5k-MCTS (AA) after 48 h, 120 h, and 168 h in 20x and 40x magnification. (For further details regarding spheroid generation and imaging please refer to chapter 6.2 and Table 3). Green emission: AF488-labeled archaea; blue emission: DAPI-stained cancer cell nuclei. Scale bar 20x: 100 µm; scale bar 40x: 100 µm.*

To evaluate whether AF488-unlabeled archaea emit any autofluorescence, respective AU-MCTS were imaged after 48 hours, 120 hours, and 168 hours by fluorescence microcopy at AF488 excitation wavelength in 20x and 40x magnification (*Figure 22*). Due to the occurrence of green fluorescence in AU-MCTS in Exp. 2 (*Figure 20*), several AU-MCTS were examined for potential autofluorescence. None of the imaged sections displayed any green fluorescence at said wavelength which provides further indication for the hypothesis that AU-MCTS must have been contaminated with AF488-labeled archaea.

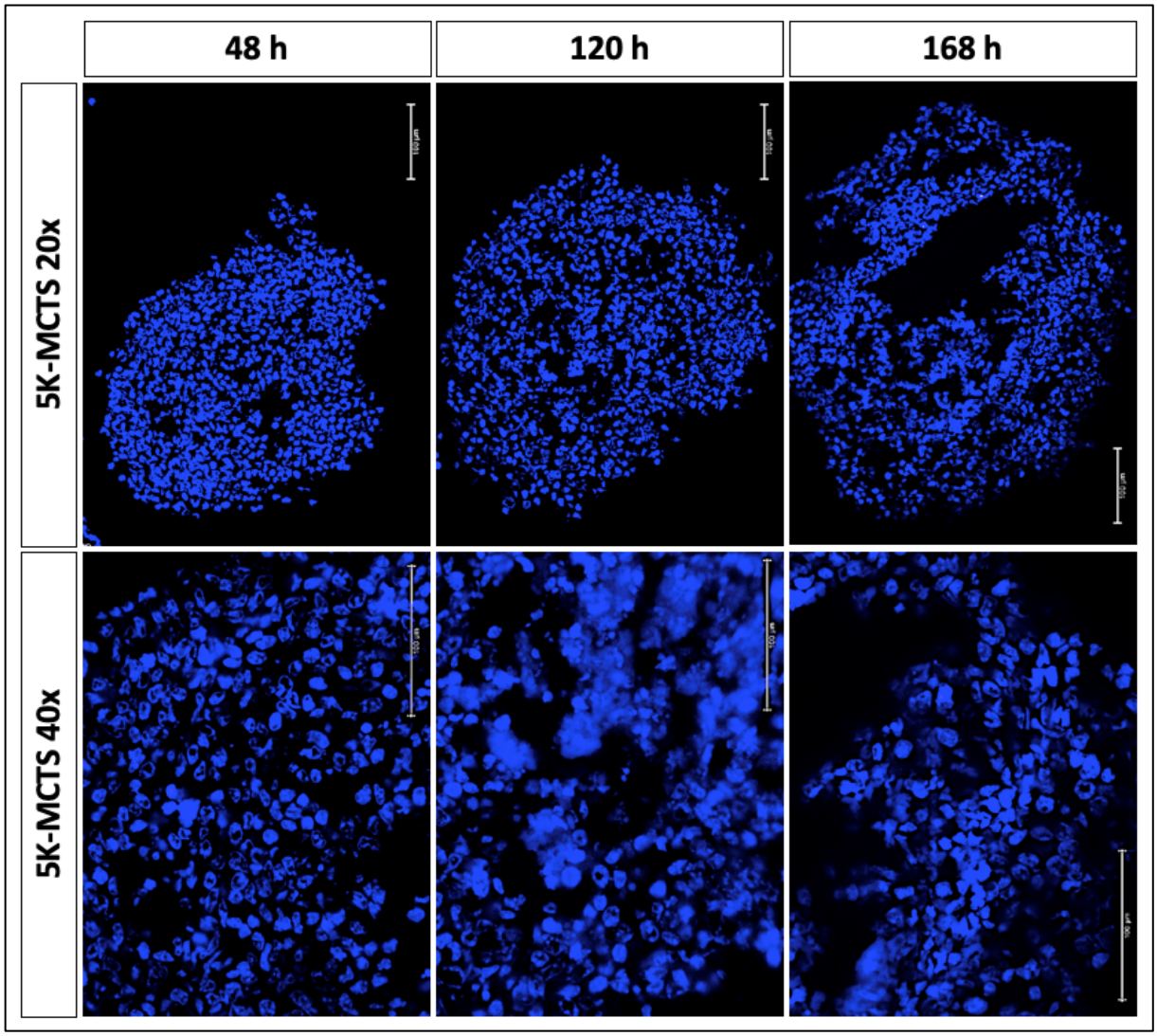


*Figure 22. Fluorescence microscopic images of sections derived from 5k-MCTS + unlabeled archaea (AU) after 48 h, 120 h, and 168 h in 20x and 40x magnification. (For further details regarding spheroid generation and imaging please refer to chapter 6.2 and Table 3). Blue emission: DAPI-stained cancer cell nuclei. Scale bar 20x: 100 µm; scale bar 40x: 100 µm.*

The results of Exp. 3 delivered essential additional information about archaeal behavior within MCTS. Despite the substantially lower number of archaea added to MCTS, archaea exhibited similar colonization patterns during co-culture with spheroids as observed in previous experiments. It could be shown that archaea had proceeded at a substantially slower pace in direction of the spheroid core when compared to results of equal co-culture durations obtained during Exp. 1 (*Figure 15*) and Exp. 2 (*Figure 17 & Figure 18)*. After 48 hours of MCTS-archaea co-culture, few green fluorescent structures are identifiable in outer spheroid zones, suggesting that archaea had not migrated significantly towards the MCTS center until this point. Besides this, larger archaeal aggregations seem to build up only after more than 24 hours of MCTS-archaea co-culture, as it can be recognized by comparison of 24 hour-sections (*Figure 17 & Figure 18*) and 48 hour-sections (*Figure 15 & Figure 21*).

The extended cultivation period of 72 hours between 24 hour-MCTS-archaea co-culture and 120 hours-co-culture displayed only a minor increase of green fluorescence and only slightly more inwardly located archaea. Supposedly, archaea in lower numbers require longer co-culture durations in order to proceed closer to the spheroid core. Moreover, noticeably smaller archaeal cell clusters can be detected in obtained images, suggesting that the formation of larger cell aggregations also depends on the quantity of archaea present during co-culture with MCTS.

Sections from MCTS harvested after 168 hours of co-culture with archaea display a comparatively marginal archaeal colonization when compared to 168 hour-sections from previous experiments. These results are not surprising, taking into account the archaeal concentration difference between performed experiments (factor 100). Nevertheless, the results indicate that archaea had proliferated within MCTS or that an increased number of archaea had penetrated the spheroid over time.

The three conducted experiments delivered several interesting findings with regard to co-culture of MCTS and archaea. First off, it could be confirmed that Alexa Fluor 488 (AF488) represents a suitable labeling dye for the used archaea strain *Methanococcus maripaludis*. Moreover, in the course of Exp. 1 and Exp. 3, it could be observed that archaea seem to form larger cell clusters only after more than 24 hours of co-culture with MCTS. The archaeal colonization of spheroids appears to be a time- and

concentration-dependent process. Presumably due to their strict obligate anaerobic character of *Methanococcaceae* [88], the used archaea strain spontaneously chases hypoxic and necrotic regions within MCTS. The longer the periods of MCTS-archaea co-culture and the higher the number of inoculated archaea, the more efficient the archaeal colonization of the spheroid, i.e. higher abundance of archaea within the MCTS section and higher proximity of archaea to the spheroid core. The MCTS size and morphology represent further factors that determine the rate of archaeal migration towards the spheroid core. Based on the evaluation of MCTS of various initial cell seeding numbers, it can be concluded that 5k-MCTS are superior to other investigated spheroid models regarding mechanical stability, archaeal progression towards the core, reproducibility of morphological shape, and consistency of archaeal colonization patterns and should, hence, be included in prospective investigations. The expansion of single archaea or archaeal cell clusters towards the spheroid core or even its colonization could only be observed after 168 hours of co-culture. Hence, a period of 168 hours represents the minimum time for MCTS-archaea co-culture to achieve archaeal colonization of the spheroid core. However, these results were only obtained when MCTS were inoculated with comparatively high archaea concentrations ($3.6x10^7$ archaea/spheroid).

For prospective studies, the determination of the prepared archaea suspension to be used for MCTS-archaea co-culture experiments should be performed shortly prior to inoculation in order to obtain correlating data. Moreover, the number of archaea per MCTS should be sufficiently high (≥ $3.6x10^7$) and the duration for MCTS-archaea co-culture should be 168 hours or longer to achieve promising colonization results.

# 8 Conclusion

On the basis of obtained results of all performed experiments, MCTS composed of 4T1 cells appear to represent appropriate *in vitro* tumor models for the investigation of archaeal targeting of hypoxic and/or necrotic regions in tumors. MCTS with optimal properties, such as mechanical stability, consistency of growth development, reproducibility of morphological shape, and promising archaeal colonization outcomes, were achieved by spheroids generated from 5,000 4T1 cells per well.

Furthermore, the demonstrated data provides evidence that the used archaea strain *Methanococcus maripaludis* S0001 represents a microorganism that is capable of infiltrating 4T1-MCTS. The archaeal migration towards the MCTS center seems to be a time-dependent process as could be shown through fluorescence microscopy. After comparatively shorter time frames of MCTS-archaea co-culture, such as 24 hours and 48 hours, MCTS did not display colonization by archaea in close proximity to the spheroid core. Only spheroids harvested after 168 hours of co-culture with archaea exhibited high archaeal abundance, frequently including the center of the spheroid.

In order to learn more about archaeal behavior patterns within MCTS after even more extended durations of cultivation, an interesting approach would be to include longer co-culture time frames (> 168 hours). An additional factor which determines archaeal MCTS infiltration rates is the concentration of archaea applied to respective spheroids. Higher archaea concentrations yielded considerably higher archaeal progression and abundance, partly including the spheroid center, whereas co-culture with lower numbers of archaea resulted in only peripheral archaeal colonization of the spheroid.

# 9 Appendix

## 9.1 Complementary figures

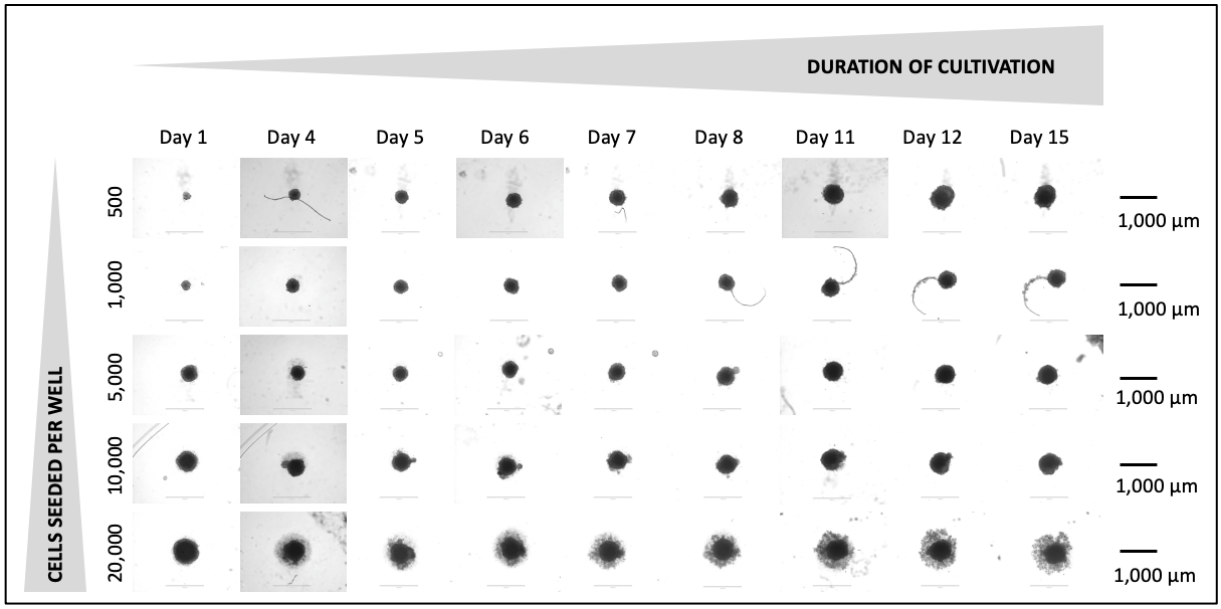


*Compl. Figure 23. Illustration of the morphological development of selected, representative 4T1-tumor spheroids over a period of 15 days. Spheroids of the following cell seeding numbers are portrayed in 4x magnification visualized by light microscopy: 20,000; 10,000; 5,000; 1,000; 500. (For further details regarding spheroid generation and imaging please refer to chapter 6.2). Scale bar: 1,000 µm.*

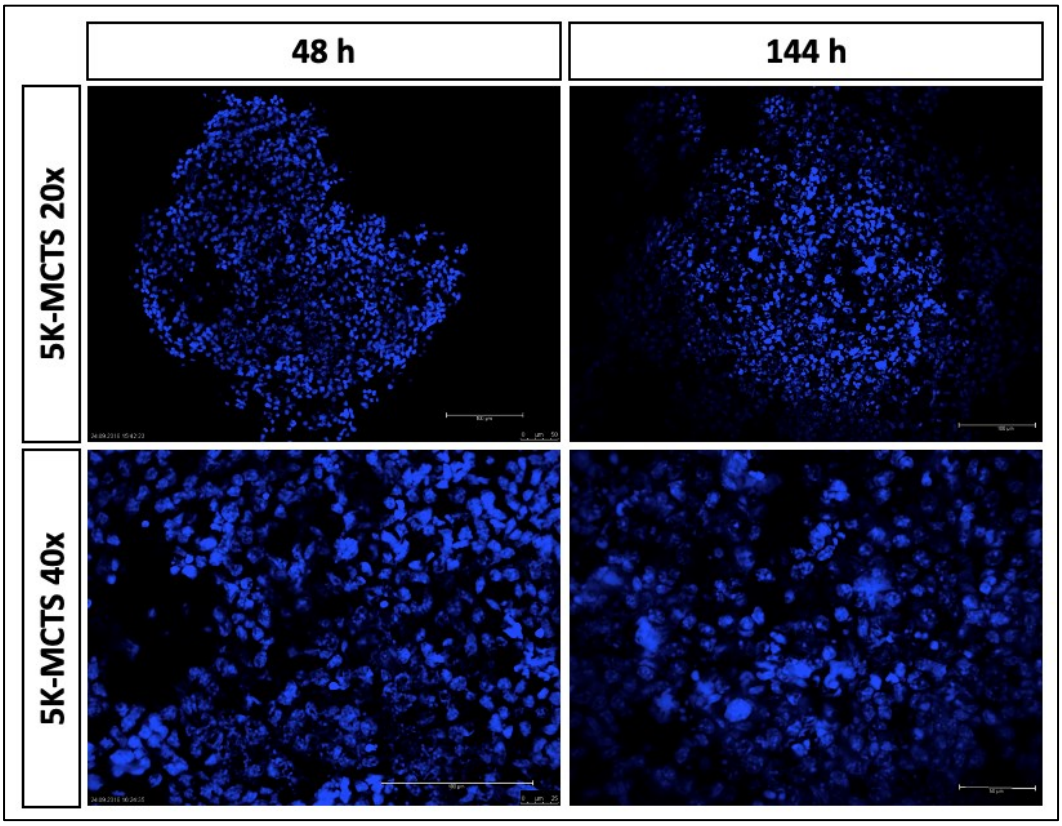


*Compl. Figure 24. Fluorescence microscopic images of DAPI-stained sections derived from 5k-MCTS + archaea after 48 h and 144 h in 20x and 40x magnification. (For further details regarding spheroid generation and imaging please refer to chapter 6.2 and Table 3). Blue emission: DAPI-stained cancer cell nuclei (+ potentially archaea). Scale bar 20x: 100 µm; scale bar 40x: 100 µm.*

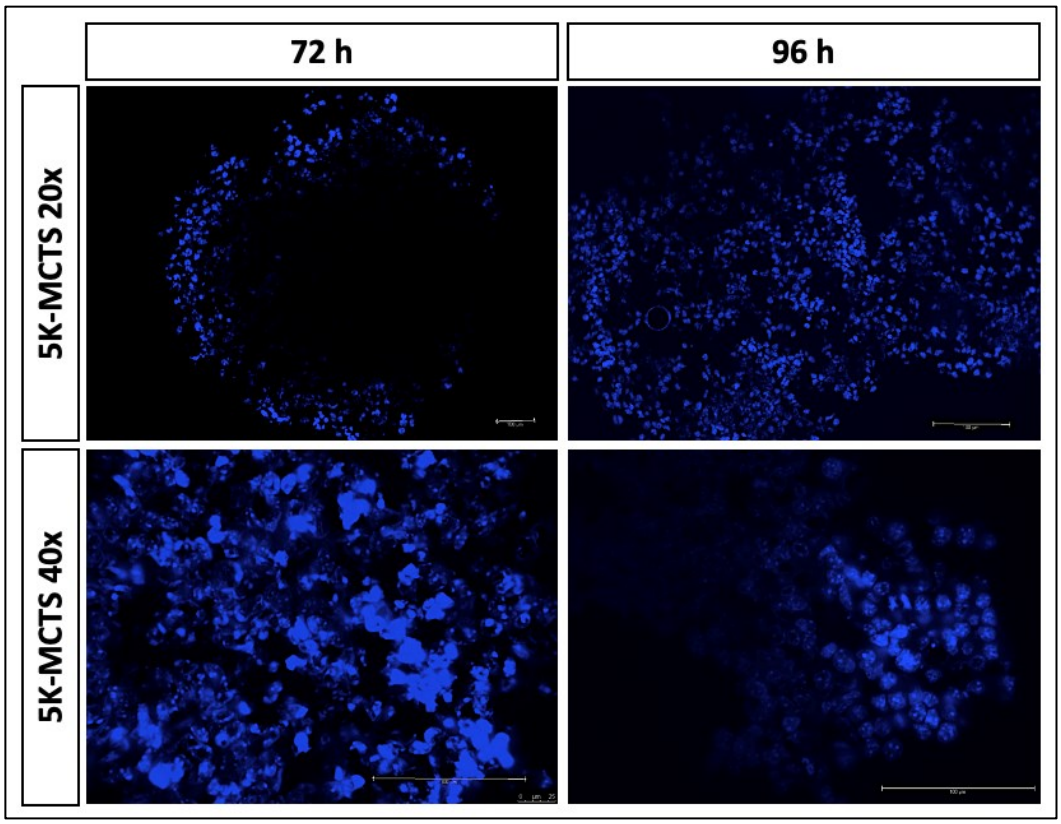


*Compl. Figure 25. Fluorescence microscopic images of sections derived from 5k-MCTS + HOECHST-labeled archaea after 72 h and 96 h in 20x and 40x magnification. (For further details regarding spheroid generation and imaging please refer to chapter 6.2 and Table 3). Blue emission: DAPI-stained cancer cell nuclei (+ potentially HOECHST-labeled archaea. Scale bar 20x: 100 µm; scale bar 40x: 100 µm.*


*Compl. Figure 26. AF488-unlabeled archaea without emission of green fluorescence. Images were taken by fluorescence microscopy in 20x and 40x magnification. (For further details regarding archaea labeling and imaging please refer to chapter 6.3.3 and Table 3). Scale bars: 100 µm.*

## 9.2 List of abbreviations

| | |
|---|---|
| 10k | Ten thousand |
| 1k | One thousand |
| 20k | Twenty thousand |
| 2D | Two-dimensional |
| 3D | Three-dimensional |
| 5-FU | 5-fluorocytosin |
| 5k | Five thousand |
| AA | MCTS + AF488-dyed archaea |
| AAV | adeno-associated viruses |
| Alexa Fluor 488 | AF488 |
| AMPs | antimicrobial peptides |
| APC | antigen presenting cells |
| AU | MCTS + undyed archaea |
| B. bifidum | Bifidobacterium bifidum |
| BCG | Bacillus Calmette-Guerin |
| BMTT | bacteria-mediated tumor-therapy |
| CAR-T | chimeric antigen receptor T cell |
| Cas | CRISPR associated |
| CD40L | cluster of differentiation 40L |
| Compl. | Complementary |
| Conc. | Concentration |
| CRISPR | Clustered Regularly Interspaced Short Palindromic Repeats |
| CT | centrifuge tube |
| DAP | diaminopimelic acid |
| DAPI | 4′,6-Diamidin-2-phenylindol |
| DC | dendritic cells |
| DNA | deoxyribonucleic acid |
| DOX | doxorubicin |
| e.g. | “for example” (exempli gratia) |
| EBV | Epstein Barr virus |
| ECM | Extracellular matrix |

| | |
|---|---|
| eppis | eppendorf tubes |
| EPR | enhanced permeability and retention |
| Exp. | Experiment |
| FBS | Fetal Bovine Serum |
| FDA | Food and Drug Administration |
| FGF-2 | fibroblast growth factor-2 |
| gp100 | glycoprotein 100 |
| HEPES | 4-(2-hydroxyethyl)-1-piperazineethanesulfonic acid |
| HSV | herpes simplex viruses |
| HTS | High Throughput Screening |
| i.e. | “that is” (id est) |
| IFN | interferon |
| IL | interleukin |
| LAF | Laminar Air Flow |
| M. maripaludis | Methanococcus maripaludis |
| M. oralis | Methanobrevibacter oralis |
| M. smithii | Methanobrevibacter smithii |
| M. stadtmanae | Methanosphaera stadtmanae |
| MAMPs | microbe-associated molecular patterns |
| MCTS | Multicellular tumor spheroids |
| MDR1 | multi-drug resistance 1 |
| miRNA | micro RNA |
| moDC | monocyte-derived dendritic cells |
| mRNA | messenger RNA |
| NDV | Newcastle disease virus |
| NF-κB | nuclear factor 'kappa-light-chain-enhancer' of activated B-cells |
| NP | nanoparticle |
| OD | optical density |
| ODN | oligodeoxynucleotides |
| OV | oncolytic viruses |
| PBS | Dulbecco's phosphate buffered saline |
| PEG | polyethylene glycol |
| Pen-Strep | penicillin-streptomycin |

| | |
|---|---|
| PFA | paraformaldehyde |
| pHEMA | poly-2-hydroxyethyl methacrylate |
| PRR | pattern recognition receptors |
| PSA | prostate specific antigen |
| PTEN | phosphatase and tensin homolog |
| RNA | ribonucleic acid |
| RNAi | RNA interference |
| RPMI-1640 | Rosswell Park Memorial Institute 1640 |
| S. typhimurium | Salmonella typhimurium |
| shRNA | Short hairpin RNA |
| siRNA | small interfering RNA |
| SOP | standard operating procedure |
| STAT3 | Signal transducer and activator of transcription 3 |
| TAA | tumor-associated antigen |
| TALEN | transcription activator-like effector nuclease |
| TLR | toll-like receptor |
| TMA | trimethylamines |
| TME | Tumor microenvironment |
| TNF | tumor necrosis factor |
| TP53 | tumor protein p53 |
| TSP-1 | thrombospondin 1 |
| UT | Untreated MCTS |
| VEGF | vascular endothelial growth factor |
| wt | wild type |
| ZFN | zinc-finger nuclease |

# 10 References


1. Bray F, Ferlay J, Soerjomataram I, Siegel RL, Torre LA, Jemal A. Global Cancer Statistics 2018: GLOBOCAN Estimates of Incidence and Mortality Worldwide for 36 Cancers in 185 Countries. *CA CANCER J CLIN*. 2018;0. doi:10.3322/caac.21492
2. Wang JJ, Lei KF, Han F. Tumor microenvironment: Recent advances in various cancer treatments. *Eur Rev Med Pharmacol Sci*. 2018;22(12):3855-3864. doi:10.26355/eurrev-201806-15270
3. Lortet-Tieulent J, Georges D, Bray F, Vaccarella S. Profiling global cancer incidence and mortality by socioeconomic development. *Int J Cancer*. 2020;147(11):3029-3036. doi:10.1002/ijc.33114
4. Yang L, Shi P, Zhao G, et al. *Targeting Cancer Stem Cell Pathways for Cancer Therapy*. Vol 5. Springer US; 2020. doi:10.1038/s41392-020-0110-5
5. Sun Y. Translational horizons in the tumor microenvironment: Harnessing breakthroughs and targeting cures. *Med Res Rev*. 2015;35(2):408-436. doi:10.1002/med.21338
6. Zaimy MA, Saffarzadeh N, Mohammadi A, et al. New methods in the diagnosis of cancer and gene therapy of cancer based on nanoparticles. *Cancer Gene Ther*. 2017;24(6):233-243. doi:10.1038/cgt.2017.16
7. Batlle E, Clevers H. Cancer stem cells revisited. *Nat Med*. 2017;23(10):1124-1134. doi:10.1038/nm.4409
8. Sun W, Shi Q, Zhang H, Yang K, Ke Y, Wang Y QL, Sun W, Shi Q, et al. Advances in the techniques and methodologies of cancer gene therapy. *Discov Med*. 2017;27(146):45-55. http://www.ncbi.nlm.nih.gov/pubmed/30721651. Accessed December 4, 2020.
9. Shim G, Kim D, Le Q-V, Park GT, Kwon T, Oh Y-K. Nonviral Delivery Systems For Cancer Gene Therapy: Strategies And Challenges. *Curr Gene Ther*. 2018;18(1):3-20. doi:10.2174/1566523218666180119121949
10. Nunes AS, Barros AS, Costa EC, Moreira AF, Correia IJ. 3D tumor spheroids as in vitro models to mimic in vivo human solid tumors resistance to therapeutic drugs. *Biotechnol Bioeng*. 2018;116(1):206-226. doi:10.1002/bit.26845
11. Bowers HJ, Fannin EE, Thomas A, Weis JA. Characterization of multicellular breast tumor spheroids using image data-driven biophysical mathematical

modeling. *Sci Rep*. 2020;10(1):1-12. doi:10.1038/s41598-020-68324-4

12. Galuschka C, Proynova R, Roth B, Augustin HG, Muller-Decker K. Models in translational oncology: A public resource database for preclinical cancer research. *Cancer Res*. 2017;77(10):2557-2563. doi:10.1158/0008-5472.CAN-16-3099
13. Porter RJ, Murray GI, McLean MH. Current concepts in tumour-derived organoids. *Br J Cancer*. 2020;123(8):1209-1218. doi:10.1038/s41416-020-0993-5
14. Fang Y, Eglen RM. Three-Dimensional Cell Cultures in Drug Discovery and Development. *SLAS Discov*. 2017;22(5):456-472. doi:10.1177/1087057117696795
15. Ham SL, Joshi R, Thakuri PS, Tavana H. Liquid-based three-dimensional tumor models for cancer research and drug discovery. *Exp Biol Med*. 2016;241(9):939-954. doi:10.1177/1535370216643772
16. Breslin S, O'Driscoll L. The relevance of using 3D cell cultures, in addition to 2D monolayer cultures, when evaluating breast cancer drug sensitivity and resistance. *Oncotarget*. 2016;7(29):45745-45756. doi:10.18632/oncotarget.9935
17. Costa EC, Moreira AF, de Melo-Diogo D, Gaspar VM, Carvalho MP, Correia IJ. 3D tumor spheroids: an overview on the tools and techniques used for their analysis. *Biotechnol Adv*. 2016;34(8):1427-1441. doi:10.1016/j.biotechadv.2016.11.002
18. Antoni D, Burckel H, Josset E, Noel G. Three-dimensional cell culture: A breakthrough in vivo. *Int J Mol Sci*. 2015;16(3):5517-5527. doi:10.3390/ijms16035517
19. Teicher BA, Herman TS, Holden SA, et al. Tumor resistance to alkylating agents conferred by mechanisms operative only in vivo. *Science (80- )*. 1990;247(4949):1457-1461. doi:10.1126/science.2108497
20. Elliott NT, Yuan F. A review of three-dimensional in vitro tissue models for drug discovery and transport studies. *J Pharm Sci*. 2011;100(1):59-74. doi:10.1002/jps.22257
21. Kobayashi H, Man S, Graham CH, Kapitain SJ, Teicher BA, Kerbel RS. Acquired multicellular-mediated resistance to alkylating agents in cancer. *Proc Natl Acad Sci U S A*. 1993;90(8):3294-3298. doi:10.1073/pnas.90.8.3294

22. Guillaume L, Rigal L, Fehrenbach J, Severac C, Ducommun B, Lobjois V. Characterization of the physical properties of tumor-derived spheroids reveals critical insights for pre-clinical studies. *Sci Rep*. 2019;9(1):1-9. doi:10.1038/s41598-019-43090-0
23. Lazzari G, Couvreur P, Mura S. Multicellular tumor spheroids: A relevant 3D model for the: In vitro preclinical investigation of polymer nanomedicines. *Polym Chem*. 2017;8(34):4947-4969. doi:10.1039/c7py00559h
24. Sutherland RM, Inch WR, McCredie JA, Kruuv J. A multi-component radiation survival curve using an in vitro tumour model. *Int J Radiat Biol*. 1970;18(5):491-495. doi:10.1080/09553007014551401
25. Zanoni M, Piccinini F, Arienti C, et al. 3D tumor spheroid models for in vitro therapeutic screening: a systematic approach to enhance the biological relevance of data obtained. *Sci Rep*. 2016;6(1):19103. doi:10.1038/srep19103
26. Balkwill FR, Capasso M, Hagemann T. The tumor microenvironment at a glance. *J Cell Sci*. 2012;125(23):5591-5596. doi:10.1242/jcs.116392
27. Nath S, Devi GR. Three-dimensional culture systems in cancer research: Focus on tumor spheroid model. *Pharmacol Ther*. 2016;163:94-108. doi:10.1016/j.pharmthera.2016.03.013
28. Osswald A, Sun Z, Grimm V, et al. Three-dimensional tumor spheroids for in vitro analysis of bacteria as gene delivery vectors in tumor therapy. *Microb Cell Fact*. 2015;14(1):1-12. doi:10.1186/s12934-015-0383-5
29. Ho WY, Yeap SK, Ho CL, Rahim RA, Alitheen NB. Development of Multicellular Tumor Spheroid (MCTS) Culture from Breast Cancer Cell and a High Throughput Screening Method Using the MTT Assay. Mehta K, ed. *PLoS One*. 2012;7(9):e44640. doi:10.1371/journal.pone.0044640
30. Hirschhaeuser F, Menne H, Dittfeld C, West J, Mueller-Klieser W, Kunz-Schughart LA. Multicellular tumor spheroids: An underestimated tool is catching up again. *J Biotechnol*. 2010;148(1):3-15. doi:10.1016/j.jbiotec.2010.01.012
31. Mehta G, Hsiao AY, Ingram M, Luker GD, Takayama S. Opportunities and challenges for use of tumor spheroids as models to test drug delivery and efficacy. *J Control Release*. 2012;164(2):192-204. doi:10.1016/j.jconrel.2012.04.045
32. Ferreira LP, Gaspar VM, Mano JF. Design of spherically structured 3D in vitro

tumor models -Advances and prospects. *Acta Biomater*. 2018;75:11-34. doi:10.1016/j.actbio.2018.05.034

33. Rodrigues T, Kundu B, Silva-Correia J, et al. Emerging tumor spheroids technologies for 3D in vitro cancer modeling. *Pharmacol Ther*. 2018;184:201-211. doi:10.1016/j.pharmthera.2017.10.018
34. Rodenhizer D, Dean T, D'Arcangelo E, McGuigan AP. The Current Landscape of 3D In Vitro Tumor Models: What Cancer Hallmarks Are Accessible for Drug Discovery? *Adv Healthc Mater*. 2018;7(8):1701174. doi:10.1002/adhm.201701174
35. Ghosh S, Spagnoli GC, Martin I, et al. Three-dimensional culture of melanoma cells profoundly affects gene expression profile: A high density oligonucleotide array study. *J Cell Physiol*. 2005;204(2):522-531. doi:10.1002/jcp.20320
36. Zanoni M, Pignatta S, Arienti C, Bonafè M, Tesei A. Anticancer drug discovery using multicellular tumor spheroid models. *Expert Opin Drug Discov*. 2019;14(3):289-301. doi:10.1080/17460441.2019.1570129
37. Leek R, Grimes DR, Harris AL, McIntyre A. Methods: Using three-dimensional culture (spheroids) as an in vitro model of tumour hypoxia. *Adv Exp Med Biol*. 2016;899:167-196. doi:10.1007/978-3-319-26666-4_10
38. Lin RZ, Chang HY. Recent advances in three-dimensional multicellular spheroid culture for biomedical research. *Biotechnol J*. 2008;3(9-10):1172-1184. doi:10.1002/biot.200700228
39. Velasco V, Shariati SA, Esfandyarpour R. Microtechnology-based methods for organoid models. *Microsystems Nanoeng*. 2020;6(1):76. doi:10.1038/s41378-020-00185-3
40. Upreti M, Jamshidi-Parsian A, Koonce NA, et al. Tumor-Endothelial Cell Three-dimensional Spheroids: New Aspects to Enhance Radiation and Drug Therapeutics. *Transl Oncol*. 2011;4(6):365-376. doi:10.1593/tlo.11187
41. High KA, Roncarolo MG. Gene Therapy. *N Engl J Med*. 2019;381(5):455-464. doi:10.1056/NEJMra1706910
42. Cring MR, Sheffield VC. Gene therapy and gene correction: targets, progress, and challenges for treating human diseases. *Gene Ther*. October 2020. doi:10.1038/s41434-020-00197-8
43. Thorne B, Takeya R, Vitelli F, Swanson X. Gene therapy. In: *Advances in Biochemical Engineering/Biotechnology*. Vol 165. Springer Science and

Business Media Deutschland GmbH; 2018:351-399. doi:10.1007/10_2016_53

44. Chaurasiya S, Fong Y. Viroimmunotherapy for breast cancer: promises, problems and future directions. *Cancer Gene Ther*. December 2020. doi:10.1038/s41417-020-00265-6
45. Zhou Z, Liu X, Zhu D, et al. Nonviral cancer gene therapy: Delivery cascade and vector nanoproperty integration. *Adv Drug Deliv Rev*. 2017;115:115-154. doi:10.1016/j.addr.2017.07.021
46. Roma-rodrigues C, Rivas-garcía L, Baptista P V., Fernandes AR. Gene therapy in cancer treatment: Why go nano? *Pharmaceutics*. 2020;12(3):233. doi:10.3390/pharmaceutics12030233
47. Pahle J, Walther W. Vectors and strategies for nonviral cancer gene therapy. *Expert Opin Biol Ther*. 2016;16(4):443-461. doi:10.1517/14712598.2016.1134480
48. Wang D, Wang K, Cai Y. An overview of development in gene therapeutics in China. *Gene Ther*. 2020;27(7-8):338-348. doi:10.1038/s41434-020-0163-7
49. Amer MH. Gene therapy for cancer: present status and future perspective. *Mol Cell Ther*. 2014;2(1):27. doi:10.1186/2052-8426-2-27
50. Ji W, Sun B, Su C. Targeting microRNAs in cancer gene therapy. *Genes (Basel)*. 2017;8(1). doi:10.3390/genes8010021
51. Patil S, Gao YG, Lin X, et al. The development of functional non-viral vectors for gene delivery. *Int J Mol Sci*. 2019;20(21):5491. doi:10.3390/ijms20215491
52. Goswami R, Subramanian G, Silayeva L, et al. Gene Therapy Leaves a Vicious Cycle. *Front Oncol*. 2019;9(APR). doi:10.3389/fonc.2019.00297
53. Kramer MG, Masner M, Ferreira FA, Hoffman RM. Bacterial therapy of cancer: Promises, limitations, and insights for future directions. *Front Microbiol*. 2018;9(JAN). doi:10.3389/fmicb.2018.00016
54. Nguyen VH, Min JJ. Salmonella-Mediated Cancer Therapy: Roles and Potential. *Nucl Med Mol Imaging (2010)*. 2017;51(2):118-126. doi:10.1007/s13139-016-0415-z
55. Zhou S, Gravekamp C, Bermudes D, Liu K. Tumour-targeting bacteria engineered to fight cancer. *Nat Rev Cancer*. 2018;18(12):727-743. doi:10.1038/s41568-018-0070-z
56. Milone MC, O'Doherty U. Clinical use of lentiviral vectors. *Leukemia*. 2018;32(7):1529-1541. doi:10.1038/s41375-018-0106-0

57. McErlean EM, McCrudden CM, McCarthy HO. Delivery of nucleic acids for cancer gene therapy: Overcoming extra-and intra-cellular barriers. *Ther Deliv*. 2016;7(9):619-637. doi:10.4155/tde-2016-0049
58. Hidai C, Kitano H. Nonviral Gene Therapy for Cancer: A Review. *Diseases*. 2018;6(3):57. doi:10.3390/diseases6030057
59. Tsagris EM, de Alba ÁEM, Gozmanova M, Kalantidis K. Viroids. *Cell Microbiol*. 2008;10(11):2168-2179. doi:10.1111/j.1462-5822.2008.01231.x
60. Lundstrom K. Viral Vectors in Gene Therapy. *Diseases*. 2018;6(2):42. doi:10.3390/diseases6020042
61. Chulpanova DS, Solovyeva V V., Kitaeva K V., Dunham SP, Khaiboullina SF, Rizvanov AA. Recombinant viruses for cancer therapy. *Biomedicines*. 2018;6(4):94. doi:10.3390/biomedicines6040094
62. Lizée G, Gonzales MI, Topalian SL. Lentivirus vector-mediated expression of tumor-associated epitopes by human antigen presenting cells. *Hum Gene Ther*. 2004;15(4):393-404. doi:10.1089/104303404322959542
63. Fu LQ, Wang SB, Cai MH, et al. Recent advances in oncolytic virus-based cancer therapy. *Virus Res*. 2019;270:197675. doi:10.1016/j.virusres.2019.197675
64. Guo ZS, Liu Z, Bartlett DL. Oncolytic immunotherapy: Dying the right way is a key to eliciting potent antitumor immunity. *Front Oncol*. 2014;4 APR. doi:10.3389/fonc.2014.00074
65. Dang Y, Guan J. Nanoparticle-based drug delivery systems for cancer therapy. *Smart Mater Med*. 2020;1:10-19. doi:10.1016/j.smaim.2020.04.001
66. Bisso S, Leroux JC. Nanopharmaceuticals: A focus on their clinical translatability. *Int J Pharm*. 2020;578:119098. doi:10.1016/j.ijpharm.2020.119098
67. Siepmann J, Faham A, Clas SD, et al. Lipids and polymers in pharmaceutical technology: Lifelong companions. *Int J Pharm*. 2019;558:128-142. doi:10.1016/j.ijpharm.2018.12.080
68. Bhaw-Luximon A, Goonoo N, Jhurry D. Nanotherapeutics promises for colorectal cancer and pancreatic ductal adenocarcinoma. In: *Nanobiomaterials in Cancer Therapy: Applications of Nanobiomaterials*. Elsevier Inc.; 2016:147-201. doi:10.1016/B978-0-323-42863-7.00006-2
69. Gabizon A, Catane R, Uziely B, et al. Prolonged Circulation Time and

Enhanced Accumulation in Malignant Exudates of Doxorubicin Encapsulated in Polyethylene-glycol Coated Liposomes. *Am Assoc Cancer Res*. 1994;154:987-992. https://cancerres.aacrjournals.org/content/54/4/987. Accessed February 1, 2021.

70. LoPresti C, Lomas H, Massignani M, Smart T, Battaglia G. Polymersomes: Nature inspired nanometer sized compartments. *J Mater Chem*. 2009;19(22):3576-3590. doi:10.1039/b818869f
71. Matoori S, Leroux JC. Twenty-five years of polymersomes: Lost in translation? *Mater Horizons*. 2020;7(5):1297-1309. doi:10.1039/c9mh01669d
72. Ahmed F, Pakunlu RI, Brannan A, Bates F, Minko T, Discher DE. Biodegradable polymersomes loaded with both paclitaxel and doxorubicin permeate and shrink tumors, inducing apoptosis in proportion to accumulated drug. *J Control Release*. 2006;116(2 SPEC. ISS.):150-158. doi:10.1016/j.jconrel.2006.07.012
73. Yaghoubi A, Khazaei M, Hasanian SM, Avan A, Cho WC, Soleimanpour S. Bacteriotherapy in breast cancer. *Int J Mol Sci*. 2019;20(23):5880. doi:10.3390/ijms20235880
74. McCarthy EF. The toxins of William B. Coley and the treatment of bone and soft-tissue sarcomas. *Iowa Orthop J*. 2006;26:154-158. https://www.ncbi.nlm.nih.gov/pmc/articles/PMC1888599/.
75. Felgner S, Pawar V, Kocijancic D, Erhardt M, Weiss S. Tumour-targeting bacteria-based cancer therapies for increased specificity and improved outcome. *Microb Biotechnol*. 2017;10(5):1074-1078. doi:10.1111/1751-7915.12787
76. Song S, Vuai MS, Zhong M. The role of bacteria in cancer therapy - Enemies in the past, but allies at present. *Infect Agent Cancer*. 2018;13(1):9. doi:10.1186/s13027-018-0180-y
77. Sedighi M, Zahedi Bialvaei A, Hamblin MR, et al. Therapeutic bacteria to combat cancer; current advances, challenges, and opportunities. *Cancer Med*. 2019;8(6):3167-3181. doi:10.1002/cam4.2148
78. Lee CH. Engineering bacteria toward tumor targeting for cancer treatment: Current state and perspectives. *Appl Microbiol Biotechnol*. 2012;93(2):517-523. doi:10.1007/s00253-011-3695-3
79. Camacho EM, Mesa-Pereira B, Medina C, Flores A, Santero E. Engineering

Salmonella as intracellular factory for effective killing of tumour cells. *Sci Rep*. 2016;6(March):1-12. doi:10.1038/srep30591

80. Baker BJ, De Anda V, Seitz KW, Dombrowski N, Santoro AE, Lloyd KG. Diversity, ecology and evolution of Archaea. *Nat Microbiol*. 2020;5(7):887-900. doi:10.1038/s41564-020-0715-z
81. Eme L, Spang A, Lombard J, Stairs CW, Ettema TJG. Archaea and the origin of eukaryotes. *Nat Rev Microbiol*. 2017;15(12):711-723. doi:10.1038/nrmicro.2017.133
82. Niederberger T. Archaea. Encyclopaedia Britannica. https://www.britannica.com/science/archaea. Published 2020. Accessed March 8, 2021.
83. Chamikara P. Morphology, Physiology, biochemistry & Diversity of domain Archaea. 2016;(03). doi:10.13140/RG.2.2.32683.95523
84. Jayashantha E. Archaea Morphology, Physiology, Biochemistry and Applications. 2015;(04). doi:10.13140/RG.2.1.4382.9281.
85. Bang C, Schmitz RA. Archaea associated with human surfaces: Not to be underestimated. *FEMS Microbiol Rev*. 2015;39(5):631-648. doi:10.1093/femsre/fuv010
86. Gong P, Lei P, Wang S, Zeng A, Lou H. Post-translational modifications aid archaeal survival. *Biomolecules*. 2020;10(4):1-18. doi:10.3390/biom10040584
87. Nkamga VD, Henrissat B, Drancourt M. Archaea: Essential inhabitants of the human digestive microbiota. *Hum Microbiome J*. 2017;3:1-8. doi:10.1016/j.humic.2016.11.005
88. Rosenberg E, De Long EF, Lory S, Stackebrandt E, Thompson F. The prokaryotes: Other major lineages of bacteria and the archaea. *Prokaryotes Other Major Lineages Bact Archaea*. 2014:1-1028. doi:10.1007/978-3-642-38954-2
89. Borrel G, Brugère JF, Gribaldo S, Schmitz RA, Moissl-Eichinger C. The host-associated archaeome. *Nat Rev Microbiol*. 2020;18(11):622-636. doi:10.1038/s41579-020-0407-y
90. Moissl-Eichinger C, Pausan M, Taffner J, Berg G, Bang C, Schmitz RA. Archaea Are Interactive Components of Complex Microbiomes. *Trends Microbiol*. 2018;26(1):70-85. doi:10.1016/j.tim.2017.07.004
91. Probst AJ, Auerbach AK, Moissl-Eichinger C. Archaea on Human Skin. *PLoS*

*One*. 2013;8(6). doi:10.1371/journal.pone.0065388

92. Eckburg PB, Lepp PW, Relman DA. Archaea and their potential role in human disease. *Infect Immun*. 2003;71(2):591-596. doi:10.1128/IAI.71.2.591-596.2003
93. Bang C, Schilhabel A, Weidenbach K, et al. Effects of antimicrobial peptides on methanogenic archaea. *Antimicrob Agents Chemother*. 2012;56(8):4123-4130. doi:10.1128/AAC.00661-12
94. Bang C, Weidenbach K, Gutsmann T, Heine H, Schmitz RA. The intestinal archaea Methanosphaera stadtmanae and Methanobrevibacter smithii activate human dendritic cells. *PLoS One*. 2014;9(6):1-9. doi:10.1371/journal.pone.0099411
95. Chaudhary PP, Conway PL, Schlundt J. Methanogens in humans: potentially beneficial or harmful for health. *Appl Microbiol Biotechnol*. 2018;102(7):3095-3104. doi:10.1007/s00253-018-8871-2
96. Vierbuchen T, Bang C, Rosigkeit H, Schmitz RA, Heine H. The human-associated archaeon Methanosphaera stadtmanae is recognized through its RNA and induces TLR8-dependent NLRP3 inflammasome activation. *Front Immunol*. 2017;8(NOV):1-13. doi:10.3389/fimmu.2017.01535
97. Hoechst,34580,RUO - 565877 | BD Biosciences-US. https://www.bdbiosciences.com/us/applications/research/cell-and-tissue-microscopy/kits-buffers-and-stains/hoechst-34580/p/565877. Accessed April 16, 2021.
98. Alexa Fluor™ 488 NHS Ester (Succinimidyl Ester). https://www.thermofisher.com/order/catalog/product/A20000#/A20000. Accessed November 22, 2020.
99. Product Listing - PAP PEN/LIQUID BLOCKER Slide Marker - Cedarlane. https://www.cedarlanelabs.com/products/listing/pap_pen_slide_marker?lob=Reagents. Accessed November 28, 2020.
100. Erythrosin B Dye content >= 95 % | 15905-32-5 | Sigma-Aldrich. https://www.sigmaaldrich.com/catalog/product/aldrich/200964?lang=en&region=CA. Accessed April 18, 2021.
101. 4′,6-Diamidino-2-phenyl-indol -dihydrochlorid for nucleic acid staining | Sigma-Aldrich. https://www.sigmaaldrich.com/catalog/product/sigma/d9542?lang=de&region=AT. Accessed November 27, 2020.

102. VECTASHIELD Antifade Mounting Media (IF) | Vector Labs. https://vectorlabs.com/browse/vectashield-antifade-mounting-media. Accessed November 28, 2020.
103. Reipert S, Kotisch H, Wysoudil B, Wiche G. Rapid microwave fixation of cell monolayers preserves microtubule- associated cell structures. *J Histochem Cytochem*. 2008;56(7):697-709. doi:10.1369/jhc.7A7370.2008
104. Wick MR. The hematoxylin and eosin stain in anatomic pathology—An often-neglected focus of quality assurance in the laboratory. *Semin Diagn Pathol*. 2019;36(5):303-311. doi:10.1053/j.semdp.2019.06.003